UNIVERSITY OF CALIFORNIA
at Los Angeles

Optimization of Phase Change Heat Transfer in Biporous Media

A dissertation submitted in partial satisfaction of the requirements for the degree Doctor of Philosophy in Mechanical Engineering

Sean William Reilly

2013

ABSTRACT OF THE DISSERTATION

A Model of Phase Change Heat Transfer in Biporous Media

By

Sean William Reilly

Doctor of Philosophy in Mechanical Engineering

University of California, Los Angeles, 2013

Professor Ivan Catton, Chair

As the heat transfer demands placed on small electronics devices increase, the demand for efficient evaporators for heat pipes and spreaders will increase in kind. Sintered copper porous media have found many uses in the electronics cooling industry as they effectively transfer energy while maintaining low heater side temperatures. Evaporator wicks of this type transfer heat through sensible and latent heat as the liquid evaporates. A biporous wick is particularly effective for this application as there are two distinct size distributions of pores; small pores to provide ample capillary pressure in order to drive flow through the wick and large pores to provide high permeability for escaping vapor.

This dissertation is focused on the methods by which one can enhance and optimize the performance of biporous material. This includes changes to the geometry and a predictive model which can be used to predict dryout phenomenon in wicks. The experimental work consists of investigations carried out by the author on a variety of different wicks. These wicks' construction and purposes are detailed. Measurements of their peak effective heat transfer

coefficients are presented and used as a basis for determining the most effective geometries in terms of heat transfer. Furthermore, the physics and motivations behind their geometries are also detailed.

The modeling proposed in this work was inspired by the work by Kovalev [18], which used a pore size distribution in order to determine the most probable pore size at a given position. The model distinguishes phases by choosing a "cutoff" pore size, above which all pores were assumed to be filled with vapor and below which they are filled with liquid. For a given wick thickness and working fluid, this 1-D model predicts a temperature difference across the wick for a given input heat flux as well as other thermophysical properties. The modeling detailed in this work is compared to experimental data collected on biporous evaporators at UCLA for validation. The correlation of thermophysical properties such as phase permeabilities and a volumetric heat transfer coefficient to the pore size distribution are also explained.

The experimental and simulation based methods discussed in this thesis are used as a basis to optimize sintered particle, biporous evaporators. Using the information gained in this thesis research effort, a methodology by which one could optimize a biporous wick for particular applications is explained as well as suggestions of future work needed to extend the foundations laid in this effort.

DOCTORAL COMMITTEE

The dissertation of Sean William Reilly is approved

Yongho Sungtaek Ju

Adrienne Lavine

Gerassimos Orkoulas

Ivan Catton, chair

DEDICATION

I would like to dedicate this thesis to all of my parents and to my wonderful girlfriend, Jenna Zimmer, because without them, none of this would have been possible.

TABLE OF CONTENTS

LIST OF FIGURES

LIST OF TABLES

LIST OF SYMBOLS

List of letters

D – Cluster size dimension (μm)

d – Particle size dimension (μm)

f – Pore size distribution

G – Vapor flux ($kg/m^2/s$)

h_{fg} – enthalpy of vaporization of working fluid (J/kg/K)

K – permeability (m^2)

k_{eff} – effective thermal conductivity of the biporous medium ($W/m/^oK$)

P – Pressure (Pa)

q –heat flux (W/cm^2)

R* - cutoff pore radius (m)

r – pore radius (m)

T- Temperature (^oK)

v – Velocity (m/s)

z – Position in wick (m)

Greek Symbols

α – volumetric heat transfer coefficient ($W/m^3/K$)

δ – Thickness of a particular medium layer (μm)

ϕ – Cumulative distribution function of pore sizes

μ - viscosity (Pa*s)

κ - relative permeability (m^2)

λ – relaxation parameter

ρ – Density (kg/m^3)

σ – Surface tension (N*m)

θ – T_d - T_v (^oK)

Subscripts

c – capillary pressure

d – solid portion of the wick

eff – “effective”, used to describe the effective thermal conductivity of biporous material

h – evaporation

l – Liquid

n – normal to wick surface

S- Surface of solid wick structure

v – Vapor

w – Wall

ACKNOWLEDGMENTS

I would like to thank my advisor, Professor Ivan Catton, for giving me the opportunity to pursue my PhD and for all of his guidance and support. I would like to additionally thank Ladan Amouzegar, Armin Karimi, Mike Stubblebine, Jake Supowit, Qi Yao, David Geb, George DeMoulin, and Krsto Sbutega for all their help in finishing my research. I would like to acknowledge the support for this work under DARPA BAA07-36 Thermal Ground Plane (TGP) with Dr. Tom Kenny and Dr. Avram Bar-Cohen as Program managers.

VITA/BIOGRAPHICAL

2007	B.S. in Mechanical Engineering
	Virginia Polytechnic Institute and State University
	Blacksburg, Virginia
2010	M.S. in Mechanical Engineering
	University of California at Los Angeles
	Los Angeles, California
2012-2013	Teaching Assistant
	University of California at Los Angeles
	Los Angeles, California

Publications

JOURNAL ARTICLES

1. **S. Reilly**, I. Catton 2011. "Utilization of Advanced Working Fluids with Biporous Evaporators". ASME Journal of Thermal Engineering and Engineering Applications, TSEA-11-1014.
2. **S. Reilly**, L. Amouzegar, I. Catton 2010. "Advances in Biporous Wick Design and Testing for Thermal Ground Planes". Frontiers in Heat Pipes Journal 1, 013001 (2010).

CONFERENCE PROCEEDINGS

1. A. Hersh, M. Jones, **S. Reilly**, "Grazing Flow Wedge Resonator Impedance Model". Proceedings of the 2012 AIAA Aeroacoustics Conference, Colorado Springs, CO, USA.
2. **S. Reilly**, I. Catton 2012. "Utilization of pore-size distributions to predict performance of Biporous Wick evaporators". HT2012-58443, Proceedings of the 2012 ASME Summer Heat Transfer Conference, San Juan, Puerto Rico, USA**.**

3. **Reilly, Sean,** Tao, T., Catton, I. 2011. "Use of Inorganic Aqueous Solutions for Passivation of Heat Transfer Devices". Proceedings of the 10th International Heat Pipe Symposium, Taipei, Taiwan.

4. **Reilly, Sean,** Catton, I. 2010. "Utilization of Advanced Working Fluids in Heat Pipes". Proceedings of the ASME/JSME 2011 Joint Heat Transfer Conference, Honolulu, HI.

5. Amouzegar, Ladan, **Reilly, S.**, Catton, I. 2010. *"Investigating the Performance of Bi-Porous Disk-Shaped Wick with the Restricted Vapor Space Via Developing an Electric Analogue Method"*. Proceedings of the ASME/JSME 2011 Joint Heat Transfer Conference, Honolulu, HI.

6. **Reilly, Sean**, Amouzegar, L., Catton, I. 2010. " Comparison of Vacuum Chamber Tested Biporous Wicks with Thermal Ground Plane Testing". Proceedings of 2010 ASME IHTC, Washington D.C.

7. **Reilly, Sean**, Catton, I. 2009. "Characterization of Vapor Escape Restriction Biporous Wicks with Monolayers for Thermal Ground Plane Optimization". Proceedings of the 2009 ASME IMECE, Lake Buena Vista, FL.

8. **Reilly, Sean**, Catton, I. 2009. "Improving Biporous Heat Transfer by Addition of Monoporous Interface Layer". Proceedings of 2009 ASME SHTC., San Francisco, CA

Patents

1. Inorganic Aqueous Solution for use in Heat Pipes – Full Patent Pending R268_69267
2. Autonomous Thermal Connector – Full Patent Pending 61/648,459

Presentations

1. "*Evaporation Heat Transfer Enhancement*". Invited Seminar, NASA Jet Propulsion Laboratory, Pasadena CA, May 10, 2013
2. "*Use of Inorganic Aqueous Solutions in Performance Enhanced Heat Pipes*". Invited Workshop, DARPA/MTO Thermal Management Technologies, Washington D.C., January 24, 2013
3. *"Characterization and Use of a Novel Inorganic Aqueous Solution for Efficient Heat Transport"*. Invited Seminar, UCLA Thermo/Fluids Research Seminar Series, Los Angeles CA. May 13, 2011
4. *"Enhanced Inorganic Aqueous Solution for Phase Change Heat Transfer Applications"*. Poster Presentation at DARPA PI Meeting, March 15 2010, San Francisco CA.

1.0 INTRODUCTION

Electronics cooling is a large issue in the everyday lives of many people as computing power for electronics from super-computers down to cellular phones increases. On the large end of the scale, computing power for server farms for cloud computing, super computers, and even desktop computers are increasing rapidly. Small scale in this context refers to portable electronic devices; laptops, tablet PC's, and even smart phones. Both large and small scale electronics are limited in their processing power due to limits in their ability to be cooled.

Computer chips, large and small, convert power into switching transistors on and off and the rate at which they are capable of doing this is called the chip's clock speed. As this switching is not completely efficient, energy is dissipated in the form of heat from the chip as the switching takes place. As chips with higher and higher clock speeds come on the market, with more and more transistors, one can easily see how heat buildup becomes a significant issue in the longevity of a circuit. Junction temperature, the temperature between the chip and the circuit board upon which it is mounted, is often cited as a strong indicator of the reliability of an electronic device. Keeping these temperatures low is of paramount importance in uninterrupted functioning of any electronic device.

With the advent of file sharing and services like "Dropbox", cloud computing has become a major part of everyday life for many people. Cloud computing refers to the fact that one person's data, saved files or personal information, is stored both locally on a personal device and globally on an internet accessible server. This data structure requires immense digital space with which to store the data and is typically done so using large server farms. Both Google and the US government are either building and/or maintaining large data centers such as these which

consume massive amounts of energy and thus produce large amounts of heat in the process of maintaining these data centers. These data centers must be maintained at an acceptable temperature in order to continuously function. Each data center can contain hundreds of thousands of chips which are producing high heat fluxes (>100W/cm^2). Improving thermal efficiency is a critical method of extending the effective life of the data centers and also reducing energy consumption costs.

Furthermore, even home PC's are becoming extremely powerful. With the advent of powerful Graphical Processing Units (GPU's), many people can convert their home computer into a simple super computer with the sheer number of computing cores contained within. In order to maintain high clock speeds, where energy dissipation is high, effective means of heat spreading and rejection are required.

At a smaller portable scale, some of the same problems exist. As processors for laptops, tablets, and cellular phones increase in power, heat is becoming more and more of a concern. Recently, the advent of thin laptops and tablet PC's has created a generation of electronic devices which no longer have room for active cooling such as fans or liquid cooling. In these cases, the only means of thermal management is rudimentary heat spreading through the casing or regulating the clock speed of the processor so that unacceptable temperatures are not reached. This means that because of heat rejection related issues, an electronic device may not be able to function for more than a few seconds at a time at its advertised clock speed for fear of exceeding temperature limits.

This issue is especially severe in handheld devices where the clock speed has more than tripled in the last three years. Now that handheld device computing power is in the range of

laptops and PC's, more effective means of management of heat rejection are needed to maintain a high level of performance without throttling the processor of these high heat flux devices

For these types of applications many different methods have been used in order to achieve high local heat fluxes in small packages. Such methods include flow in micro-channels, jet impingement, and porous media. Micro-channel flow is able to achieve relatively high heat fluxes but suffers from the need for a large pressure drop in order to force liquid into the micro-channels. Furthermore, if boiling is initiated, there is the possibility of reverse flow of liquid due to pressure instabilities. Jet impingement is also effective but requires additional pressure drop in order to force liquid to interact with the component to be cooled.

Sintered material on the other hand, functions passively. It is able to transfer large amounts of energy by evaporation and in many cases is able to do so isothermally even when the effective thermal conductivity of the medium is not very high. This dissertation is focused on the application of porous material to passive cooling of high heat flux electronics devices. The goal of this work is to show how to modify porous media, specifically biporous media, for the purposes of predicting the performance of a wick under a given set of conditions and improving the performance in different devices. Given the range of performance one can achieve by varying the many geometric parameters of the sintered wick and the competing physical phenomena, a fast running fully validated model of two phase flow with heat transfer and phase change is needed if optimization is to achieved and full advantage of the potential capablility of the sintered wick is to be achieved.

1.1 Theoretical Considerations

The fundamental premise of this thesis is that a simulation model for predicting wick performance and evaluating experimental data can be used to suggest optimized wick geometries. In this section, background information for the thesis is presented. The background is divided into two parts; the first will detail experimental efforts that were designed to characterize various types and applications for porous material as well as some of their resulting empirical models. The merits and opportunities for improvement will be explained in relation to the work of this thesis.

The second part of this section focuses on modeling efforts in porous media. Their impact and approach are of particular interest as they form the motivation for the modeling effort detailed here. It is intended that the reader will understand the progression of modeling techniques that lead up to what is discussed in the present work.

1.2 Porous Material

When a heat flux is applied to a liquid saturated porous medium, the liquid will begin to evaporate into the surrounding media as the mass fraction of vapor in the environment is less than the mass fraction at the surface of the liquid. This evaporation typically takes place at a meniscus that forms between the solid, the liquid and the vapor.

The meniscus is comprised of three regions; the bulk region, the thin film evaporation region and the non-evaporating thin film region (sometimes referred to as the adsorbed film region) seen in Figure 1. In the bulk region, the liquid functions just as it would from a large pool of liquid; evaporation is driven by the mass fraction of vapor at the interface and the mass

fraction of vapor in the surrounding atmosphere. The liquid is heated by energy conducted into the bulk at the boundaries followed by convection throughout the pool of liquid. This phenomenon is well described and understood. As the liquid heats up, the mass fraction gradient will increase and as a result so will the evaporation rate.

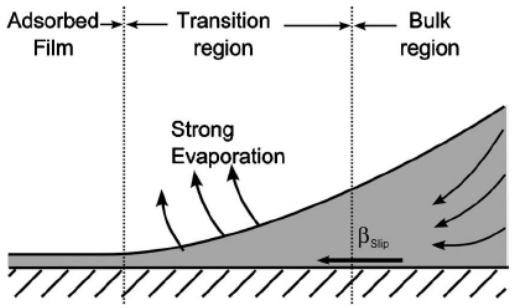

Figure 1: Schematic of meniscus [42]

The evaporating thin film region is somewhat different. Due to surface tension forces, the liquid surface is closer to the wall and as it becomes critically thin, the resistance to conduction of energy from the wall to the liquid surface becomes very small. Locally, this produces very high evaporation rates, relative to the bulk region. As the film becomes increasingly thin, attraction forces between the molecules in the liquid and the wall become significant and effectively increase the pressure of the liquid. This pressure change is referred to as the disjoining pressure, and when sufficiently large, prevents liquid from evaporating by reducing the pressure gradient between the phases.

Porous media are effective because they maximize the number of these menisci corresponding thin film evaporation area. Since the evaporation rate in the thin film is high,

performance can be increased by maximizing the number of pores where the evaporating thin film evaporation rate is significant. There are many different kinds of porous media ranging from metal fibrous coatings, open cell metal foams, screens, and sintered material. All try to maximize the surface area of pores in order to increase evaporation rate.

There have been a multitude of investigations into the performance of both heat transfer and flow in porous media. The range of interest runs from electronics cooling to civil engineering (2-phase flow in Vados layers). The works discussed in the present dissertation will be limited in scope to those that have particular bearing on the research goals of this thesis.

Chang [7] investigated the effect of geometry of non-conducting porous coatings on boiling performance. The monoporous wicks investigated in his work varied in particle size from 2- 70 mm and thicknesses from 30-250 mm with porosities approximately equal to 45%. This work compared pool boiling on smooth surfaces to those with a deposited porous layer.

The results of Chang's work were that for wicks that were thicker than the superheated liquid layer, wicks with larger particles (larger overall thicknesses) tended to have higher effective heat transfer coefficients than the smaller particles (smaller overall thickness) at lower heat fluxes (<2.5 W/cm^2). This was explained because at these lower power levels, the reduced vapor flow rate allowed the nucleation spaces to be farther apart in the larger particles, reducing the hydrodynamic resistance associated with the vapor escaping the wick, relative to the smaller particles. However, at higher heat fluxes, the trend was reversed as the smaller particles tended to have higher effective heat transfer coefficients. It was postulated by Chang that this reversal is due to the fact that at higher heat fluxes, there was less resistance to getting the liquid to the

surface in the thinner wicks, than the thicker ones. As it was easier to get liquid to the surface, less of the surface was coated in vapor.

As for critical heat flux (CHF), the porous coatings always increased the critical heat flux relative to the smooth surface. Chang noted that Kovalev [25] stated that a potential reason that porous coatings increased CHF was that the location of vapor jets exiting the porous media had to do with the geometry of the media rather than the Taylor instability wavelength. Their experiments noted that the vapor jets were closer together than the Taylor wavelength and as a result the vapor velocity was believed to be higher, which would increase the critical heat flux. These were all based on correlations developed by Zuber [56] and studied by Dhir [11] for boiling. The principles which govern a Taylor instability with boiling on a flat plate are most likely negated with porous media as thermal transport is more conduction dependant. Chang's data seemed to validate Kovalev's claim, but Chang did not investigate a conducting media, whereas Kovalev did, and so full validation is not possible.

Chang's work helps explain the relevance to the modeling presented in this thesis of using porous layers as a means to increase heat transfer. Furthermore, it was noted that in the wicks that Chang investigated, the large pore sizes of Chang's wicks tended to be about the mean diameter of a particle. Kovalev's insight, by way of Chang's experimentation, on the relationship between CHF and vapor jet proximity also helps reinforce the idea that pore geometry is one of the most important aspects of wick performance.

Bau [1] published a paper where he attempted to describe the conditions under which convection and boiling would take place in a porous media, and what effect that had on the temperature distribution. The porous material investigated was a monoporous sample, made

from Ottawa sand. The grain sizes ranged from 0.85 mm to 1.27 mm with an open cell porosity of 0.42. Using the Carmen Kozeny equation for permeability, the permeability was estimated at $1400*10^{-12}m^2$. The thermal conductivity of the water saturated bed was measured to be 2.15 W/m/K. Bau tested the porous media by heating from below and cooling from above. Fluidization of the sand was prevented by pressurizing the sand with a permeable plate so that it would be held static. A schematic of the experimental setup can be seen in Figure 2.

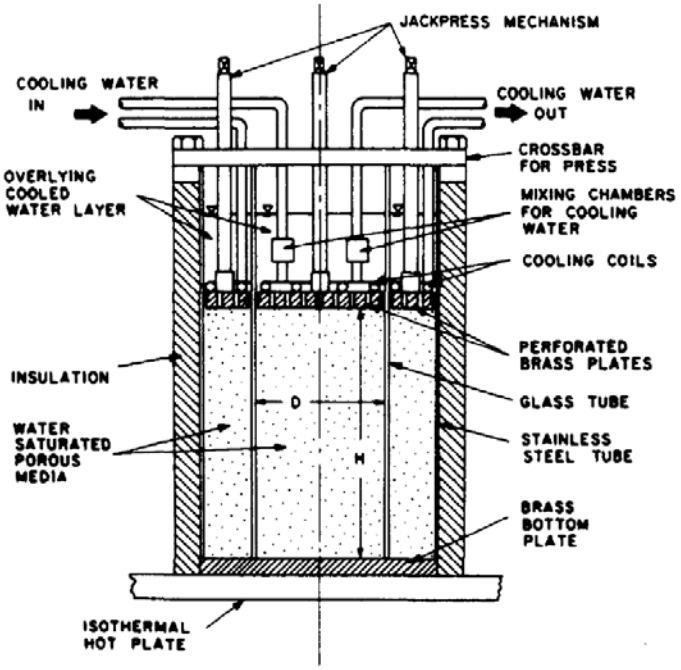

Figure 2: Experimental setup, Bau [1]

Experimentally it was determined that once ample heat flux was supplied in order to raise the wall temperature above the saturation temperature, nucleation would commence at the wall. This nucleation would build a 2-phase layer above the heater with a liquid layer on top.

The author's noted that in general, the determination of the Rayleigh number, relative to the critical Rayleigh number for onset of single phase convection, for the test conditions would lead to an understanding of whether convection took place in the porous media. When the Rayleigh number was below the critical value, cellular convection was not observed in the liquid layer and when it was above the critical value convection was noted in the liquid region. The Liquid and vapor were noted to be in counter-current flow in the 2-phase region. It was also noted that temperature fluctuations at the wall could be attributed to vapor forming at the wall, departing to percolate up through the wick, and liquid rushing back into the gap to cool it. The porous media mentioned in Bau's work had higher permeability and grain sizes than the wicks investigated in the present work but shows that convection in the liquid in the wick is unlikely under certain circumstances and shows that liquid and vapor flow are counter-current in the 2-phase regions.

Vasiliev outlined the use of micro heat pipes in various devices [42]. In his work he discussed how different types of wicks affect the performance of miniature and micro heat pipes. Particular emphasis was placed on the use of sintered copper as an effective evaporator wick. Vasiliev explained the progression of heat transfer modes of porous media; pure conduction, nucleation, variable conductance heat pipe behavior, and finally full porous boiling.

Vasiliev noted the phenomena of vapor nucleating at the base of the wick while the liquid at the upper portion of the wick was still subcooled, which would cause the vapor to condense and recirculate, rather than percolate up through the wick. The effects associated with this type of behavior are outlined in more detail by Smirnoff [47] and will be discussed later. Complex behaviors like these led him to suggest that more detailed modeling techniques were required for

sintered evaporators to achieve better designs. Specifically models should be developed that were less dependent upon empirical correlations. It was also mentioned in Vasiliev's paper that heat transfer enhancement was a strong function of evaporator surface area and that sintered porous media effectively increases surface area, relative to grooves.

The reason for this increase in performance has to do with the increase in the number of menisci. In a meniscus, there are three regions; the bulk fluid, the evaporating thin film, and the non-evaporating thin film. The bulk region circulates fluid in natural convection but does not contribute much to evaporation heat transfer as pore sizes are decreased. The effective heat transfer coefficient of the thin film evaporation region tends to be much higher than the bulk region, but its heat transfer is small at low super heats and large pore sizes. However, it was found by Wang [47] that more than 50% of the heat transfer takes places from the thin film region with pore sizes on the order of 2-3 μm and superheats of greater than 20K. Wang showed that at lower superheats and larger channel sizes, this effect was negated; thin film heat transfer contributed less than 20% of the total liquid film heat transfer. This explains why at lower heat fluxes, other methods of wicking tend to be better than sintered material as evaporators. Since the present work is mostly focused on higher heat fluxes, the superheats are sufficient to take advantage of this effect. It is clear that by maximizing the number of pores with a radius size on the order of the critical radius at which thin film evaporation is dominant, overall heat transfer rates will be increased. This is why the increase in surface area is so important to heat transfer and that increasing the surface area by maximizing the number of properly sized pores permits more heat transfer.

The increase in surface area, in particular, must be applied carefully. Annapragada [1] performed numerical analysis on the behavior of compressed metal foams to determine the impact on permeability and other heat transfer quantities. The foams used had considerably larger porosities than those used in the present study; Annapragada's foams all had porosities greater than 0.75. While these are quite porous, their internal structure is similar to the wicks discussed in the present work. He investigated both face centered cubic and body centered cubic arrangements. It was found that by compressing the foam so that it would deform plastically, they were able to increase the heat transfer by increasing Nusselt number and thermal conductivity in the transverse direction of fluid flow. Compression of foams in FCC and BCC layouts could very likely increase surface area per unit volume, if one assumes that the spheres are uniformly compressed. However, it was observed that compressing the foam also reduced the heat transfer and permeability in the parallel direction of flow. The relevance of this work is again, that increasing the surface area per unit volume can increase heat transfer, but that care must be taken in doing so, that flow resistances are not prohibitively increased.

Weibel [47] performed extensive tests on monoporous material in order to determine the particular performance characteristics associated with different geometries. The porous materials he used were particles ranging in size from 45 μm up to 355 μm and thicknesses ranging from 600 μm to 1200 μm. The wicks in this study were tested at various steady state heat fluxes in order to measure the effective superheats across the wick (measured from an interpolated wall temperature to a vapor temperature above the wick). The wicks were tested at saturation under atmospheric conditions by purging the air from the test chamber. The samples themselves were dipped vertically into the liquid reservoir.

The wicks tested in that study were shown to be very effective in terms of obtaining very low thermal resistances. The lowest resistances measured were approximately 0.2 ^{o}C/W for a monoporous wick of 302.5 μm particles (average sieve size of particle) and a thickness of 600 μm. The authors also detailed the important transition between surface evaporation and nucleation at the heater interface. The authors noted that nucleation at the heater interface did not indicate failure; in fact it signaled that the thermal resistance had decreased. This decrease in resistance was believed to correspond to the clearing of some spaces between the particles of liquid for efficient vapor shedding. The visualization studies carried out by Weibel [45] and Smirnov[38] seem to validate this; they show bubbles growing and departing from the surface of the wick even after nucleation has begun.

As stated, the wicks shown in Weibel's study were monoporous, rather than biporous. As this was an experimental study, no effort was made to predict the performance of the wick. Weibel [49] later performed experimental analysis of what he referred to as "patterned wicks", which were closer to the biporous wicks studied in the present work. Several different vapor chamber evaporator wicks were evaluated; monoporous material, monoporous material with structured carbon nano-tubes (CNT), as well as patterned wicks, with and without CNT's. A patterned wick is defined as a monoporous wick into which structured grooves are molded into the monoporous material. A grid pattern and a radial wedge pattern were used for patterned wick testing.

The major results of this study were that the addition of CNT's to monoporous material tended to cause boiling incipience to occur sooner than on bare copper material. It should be noted that the CNT's were coated with a nanometer thin layer of copper in order to make them

hydrophilic; CNT's are naturally very hydrophobic. The reduction in the incipience point was attributed to the fact that the presence of CNT's likely increased the wettability of the liquid in the pores of the sintered copper. The CNT coatings also had low permeability relative to the media on which they were deposited.

Also, patterning the wicks significantly reduced the thermal resistance of the wicks, relative to plain sintered material. This increase in performance is attributed to the fact that patterning the wick increases the effective vapor permeability of the wick. Weibel diagrammatically shows how patterning the wick affects the boiling regimes of the wick in conjunction with visual studies. These show that though there may be many nucleation sites along the surface of the heater, the vapor will preferentially travel into the pattern grooves and agglomerate into a larger vapor bubble before departing the wick. Coating the patterned wicks with CNT's was also investigated and was found to have a similar effect on the plain monoporous wicks. Boiling incipience occurred much sooner in the patterned wicks with CNT's in comparison to the bare patterned wicks. It was also noted that even though a reduction of thermal resistance was noticed at the onset of boiling incipience, it is very difficult to predict the onset of boiling incipience due to geometric and environmental factors.

Noting the complexity of porous media boiling, Weibel compared his experimental data to several modeling techniques and found that predicting the effective thermal conductivity of an active wick is quite difficult. The best results came from semi-empirical models but it is mentioned that additional geometries and working fluids are needed to be tested in order to validate the model. However, with the models that did compare well with his experimental data, it was noted that vapor permeability is a key factor in predicting boiling performance.

The results of Weibel's work are discussed later in this work, as a monoporous wick is modeled similar to what was used in his study, for validation purposes. Some authors have noted that nucleation will cause a vapor blanket to form at the heater interface which will cause the wick to fail but this type of failure was not observed in the experimental studies conducted in this thesis. This was likely due to the relatively large size of the monoporous particles coupled with the relatively thin layer of wick preventing this type of effect. The average size of the particles (~300 μm) was large enough that there was enough space between the particles for the vapor permeability to be high enough to escape the wick before forming a vapor blanket between the liquid supply and the heater interface. Also due to the thin nature of the wick, there would be less hydrodynamic resistance to pushing liquid from the spaces between the particles in order to shed vapor.

1.3 Biporous Media

Biporous wicks are a special kind of porous medium where there are two distinct pore size distributions. In other words, a typical monoporous material is comprised of pores that tend to be dominated by one characteristic pore size. In a biporous medium there exist "large" pores and "small" pores. The reason that biporous media are effective is that the small pores provide significant capillary pressure to bring the liquid to the heated surface while the large pores permit high vapor permeability. As mentioned in some of the previous monoporous material investigations, vapor permeability is key to performance enhancement.

This is not to say that the large pores do not take part in liquid transport. It is believed that the necking area between two clusters produces a "secondary" meniscus, which provides

high liquid permeability as well. This condition exists once vapor has begun to expel liquid from the large pores but before the heat flux is large enough to remove all liquid from the larger pores. A schematic of this situation is seen in Figure 3.

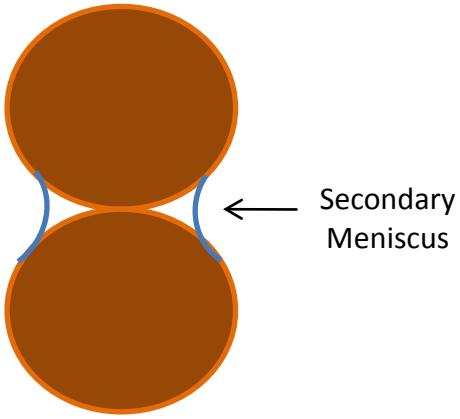

Figure 3: Secondary meniscus formation between clusters

These secondary menisci play an important role in the performance of the wick leading up to dryout. They will also be a factor in the enhancement of biporous wick performance as they allow better wetting of an augmented wick surface; this issue will be further discussed in Chapter 6, section 6.2.

The first mention of biporous wicks is by Vityaz [44], who oxidized sintered wicks in order to create a second distribution of pores. It was believed that a biporous wick would help stave off some common heat pipe limitations such as entrainment and capillary limits. Entrainment limits are a direct function of the area afforded to vapor flow, which is increased in a biporous wick and the capillary limit is associated with the available capillary pressure

available for liquid pumping, which is increased by the small pores in a biporous wick. Tests conducted on these wicks, and their positive results, were the catalyst for biporous wick investigation.

Rosenfeld and North [33] also looked at biporous materials and concluded that at higher heat fluxes, biporous wicks performed better than monoporous wicks. The wicks investigated in their work were sintered nickel material but theorized that the enhanced performance had to do with the extension of the liquid film over the various pores. They also pointed out that an isothermal heater interface property coupled with the high heat flux capabilities made biporous material a natural solution for optical components, where thermal loads tend to be high but varying.

Wang and Catton [47] attempted to model the performance of a heat pipe with biporous wicks, monoporous wicks, and a solid piece of copper. By basing the evaporator resistance on the resistance to conduction across the thin liquid film in the meniscus, they were able to determine that a biporous evaporator would perform with a lower thermal resistance than either solid copper or monoporous material at relatively high heat fluxes (>120W/cm^2). Furthermore, at these higher heat fluxes, the biporous material was capable of maintaining a uniform interface temperature.

In the work of Yeh [55], biporous wicks were constructed out of nickel powder and pore formers. Yeh's wicks were constructed by mixing a certain volume content of pore former into the nickel particles and then sintering the mixture together. The packing of the nickel particles created small pores and large pores were formed as the pore formers were discarded, after the construction process.

Yeh was trying to determine relevant parameters in the construction of biporous wicks, with regards to effective heat transfer coefficients. A statistical method was used that evaluated test results from many biporous wicks to try and determine statistically relevant parameters in these types of wicks. They also compared their results to monoporous wicks as reference. The main results they found were that smaller particles and larger pore former volume content yielded the best performing wicks. Also, there was a noticeable increase in performance as pore former content was increased. It was suggested by Yeh that the reason that performance was increased with larger pore former content was due to the fact that as pore former content increased, the size of the larger pores became greater. It was postulated that the larger pore size and pore former content contributed to increased connectivity between the large pores. This connectivity translates to less flow resistance for vapor exiting the wick and thus more efficient heat transport. This relates directly to the observations regarding cluster size and performance discussed later.

Other biporous wicks were investigated by Coso [10]. The wicks studied by Coso were biporous in that they had two distinct size distributions of pores but were constructed with silicon posts of varying pitch. Groups of posts were placed closer together in a grid format comprising the small pores and larger spaces were carved out between the close grouped pillars, forming large pores. This periodic structure allowed for relatively high overall permeability ($\varepsilon \sim 0.79$) and for precise control of the menisci size in the pores.

Coso's work showed that incipience of boiling increased the overall heat transfer coefficient of the wick versus simple evaporation from the upper surface and also extended the dryout heat flux. The highest increase in dryout heat flux occurred as the depth of the channels

became deeper and large pore widths held at 61 μm. This is likely due to the fact that deeper pores would have the capacity to retain more liquid at the heater interface.

Since these wicks were axially symmetric in the direction perpendicular to the heater interface, their vapor permeability should be relatively unaffected by the pore sizes, since liquid can only be transported parallel to the heater surface. This means that the large pores between "clusters" of small pores were primarily transporting liquid. This is in contrast to typical sintered biporous wicks in that the liquid flow path and cross sectional profiles are anisotropic, and the large pores serve primarily as a vehicle for raising the vapor permeability.

Coso was able to achieve higher heat dryout heat fluxes as the wick area to heater area ratio was increased. This is likely to do with the fact that the total heat input was reduced and therefore the mass flux was actually less relative to the capillary limit. Also, it was noted by the authors that in general, in order to increase performance, shrinking the small pores as a way to increase the interior of the surface area of the wick was most effective. While the structure of the biporous wick in Coso's work is somewhat different than the present work, one can see how the principles that govern performance are the same. Maintaining a high capillary pressure while limiting the decrease in the liquid permeability go hand in hand with a significant increase in interior surface area as a method to increase heat transfer.

The most extensive testing of the properties biporous materials, on which much of this work is based, was conducted by Semenic [35]. Semenic conducted exhaustive studies of the thermophysical properties of many different geometries of biporous material as well as analysis of the particle distributions. He was able to correlate many of the thermophysical properties of various biporous wicks to their geometric characteristics; typically either particle or cluster size.

Many of these correlations are evaluated later in the course of this work against estimates obtained from the pore size distribution, and are thus discussed later.

Semenic also performed many performance evaluations of different wicks using an experimental apparatus referred to as the boiling chamber. This chamber applied a heat flux to the base of the wick and evaporated liquid supplied to the wick at steady state values to develop heat transfer curves for different sized wicks. The properties of the wick were used by the model described by the present work and his performance evaluations were used as validation for said modeling efforts.

Semenic primarily focused on experimental work and tested wicks from a spectrum of interior geometries and thicknesses. He used wicks that were able to accommodate heat fluxes as high as 1.37 W/cm^2 and other thinner wicks with high effective thermal conductivities. At the end of his thesis, certain modifications to the structure of the wicks were suggested and are carried out in the present work and will be discussed later.

1.4 Numerical Modeling – Porous Material

There are a multitude of ways to model conjugate heat transfer in porous media. Many models use finite difference schemes, such as those proposed by Baliga and Patankar [2]. The method proposed in that work improved upon Patankar's SIMPLER algorithm. The algorithm was proposed as a way to compensate for the fact that typical Galerkin method approaches were inaccurate at larger Peclet numbers, due to higher flow rates. These situations applied to complex boundary shapes but were not applied to porous media.

There are similarly many different methods of modeling porous media. As phase change in porous media is an extremely complex process, direct modeling of all the solid/liquid/fluid interactions is not generally feasible, particularly for two-phase flow. This is because it is exceedingly difficult to know the exact structure of the wick, which makes dealing with the morphology difficult. Furthermore, accounting for the disjoining pressures between the three phases, as well as the temperature gradients present in each phase, makes it very difficult to ascertain the location of phase boundaries. In this section porous modeling techniques will be discussed. In general, the first techniques discussed will be ones applied to monoporous materials, but their principles can be applied to biporous media.

One of the fundamental challenges of modeling in porous media is establishing where different fluid phases are at any given time. The fundamental premise of the works discussed in this section is that under certain conditions for porous media, one can know where liquid and vapor are based on physical parameters of the medium. For wicks that have low capillary numbers, defined as,

$$Ca = \frac{\mu V}{\sigma} \qquad \textbf{(1)}$$

it can be assumed that the non-wetting fluid occupies the larger pores and the wetting fluid occupies the smaller pores in the matrix, referred to as channel flow (see Dullien [10]). While this is the assumed case for the biporous material studied in this work, there was some concern over how to handle the situation where some liquid water occupied the larger pores. This type of

flow, referred to as funicular flow, is observed less than channel flow, but might explain the high thermal resistance associated with low heat flux into a biporous material. In other words, there is resistance to pushing the wetting phase from the wick so that the non-wetting phase permeability can increase, and increases the evaporation area close to the heater, which reduces resistance.

Some simple models of porous evaporation emphasize the relatively high heat transfer rates provided by thin film evaporation, such as by Hanlon and Ma [15]. In that particular work, a monoporous wick is saturated with liquid and evaporation only takes place at the upper surface. The porous medium drastically increases the surface area available to this type of heat transfer. The evaporation from thin films is represented as the sum of the thin film evaporation of each meniscus over the upper surface of the wick. However, in Hanlon's model, failure is indicated when nucleation begins to take place in the wick. Hanlon and Ma argued that once nucleation begins, a vapor layer forms which prevents liquid from reaching the heater surface and heat transfer is across the low thermal conductivity vapor film causing a dramatic rise in temperature above the liquid saturation temperature. Such simple modeling techniques are appropriate for a monoporous wick with relatively small particles, but in a biporous wick heat transfer generally increases with nucleation and the onset of countercurrent flow because the vapor can get away from the heated surface without blocking the liquid inflow. As a result, performance is seen to increase as a result of vapor formation at the base of the wick.

Ranjan [25] developed a model for several different wicks found in common heat pipe devices. Ranjan conducted a parametric study to determine the impact of changing various parameters such as superheat and contact angle on the effective heat transfer coefficient. Their

work used the software packages Surface Evolver and Fluent in order to determine both the meniscus shape and relevant heat transfer parameters. That study was conducted with four different microstructures; 1) vertical microwires, 2) rectangular grooves, 3) screen mesh and 4) sintered material (monoporous).

Their work concluded that a sintered medium was the best performer in terms of heat transfer coefficient. They concluded that this was because heat transfer increased as the total thin film area increased, which corresponds to smaller characteristic lengths of the wicks; in this case the diameter of the particles. This means that in general, an increase in surface area per unit volume at the micro-level will increase the thin film evaporation zones and increase the overall heat transfer. This relates to the biporous wicks in this work because it would suggest that smaller particles would be more effective for heat transfer because an increase in the surface area at the micro-level aids heat transfer.

Ranjan [28] also attempted to couple micro-scale pore models with large scale macro-models of heat pipes. The goal of that work was to evaluate at what point the micro-scale effects associated with thin film evaporation from small pores began to have a large impact on the overall performance of a heat pipe. A 3-D model was developed utilizing a macro-scale model originally developed by Vadakkan [42], and the micro-scale model of Ranjan. The idealized wick investigated was a mesh screen and the evaporation heat transfer coefficient was developed from kinetic theory. The author's noted that it would be difficult to determine the exact value of the accommodation coefficient and so two values were chosen that were thought to bracket the actual value, for comparison. The macroscale pressure distribution was used in order to initially estimate the curvatures in each meniscus and was corrected by the micro-scale model.

The model showed that a macro-scale model would under predict superheats in the wicks under certain conditions. As a result, the thermal resistance associated with evaporation was seen to increase with a coupled model when the wick thickness became very small (<100 μm), the thermal conductivity of the wick structure was high (> 100W/m/K) or the accommodation coefficient was small (<0.1). The modeling effort in the present work does not include a coupled model, like the one described in Ranjan and Vadakkan's work because the vapor space is the upper boundary rather than included in the control volume of interest.

While an effective modeling technique is presented by Ranjan, it is limited to low superheats and very regular geometry. The superheats seen in Ranjan's work were very small, on the order of several degrees Kelvin while in the present work they are typically well over 20 Kelvin. There is no percolation of liquid up through the porous media being modeled by Ranjan since there is no nucleation. Also, in the present work it is unnecessary to use the Brinkmann-Forcheimer equation used in Vadakkan's model since the Reynold's number is much lower and the wick is continuous. Also, the mesh wick that was investigated had a very regular layout, making it easy to know the geometry of the wick at any point. It is clear that in order to apply modeling techniques to higher heat fluxes and more complicated geometries, a different modeling technique is needed.

Rao [28] developed a model of porous media that uses a simplified method to incorporate the geometry into the model and to predict performance. His modeling was used to investigate monoporous material at relatively low heat fluxes. The primary goals of his work were to determine the percentage contribution of latent heat to total heat transfer, relative to convection. He also compared different geometric arrangements in order to determine the proper orientation

of the material he was investigating. The results of his modeling were positive. He started from the Darcy equation in order to determine the pressure distribution inside the porous media. His model focused mainly on vapor flow ignoring counter current flow. He used a geometric parameter that was the number of active pores per unit area (N/A) in order to incorporate the geometry. Rao also determined that the latent heat comprises almost all the heat transfer in a highly porous media.

An important parameter in Rao's modeling, the number of active pores per unit area, was approximated by estimating its value based on the characteristic particle size of the media he was using. Since typical pore sizes are not reported in much of the available literature, Rao estimated them using various permutations of a bed of spheres model. As such, he uses estimates for the pore size that range anywhere from 20% up to 70% of the mean particle diameter in order to estimate the pore size. He is able to validate his data with reasonable accuracy but was only able to draw conclusions about monoporous material with spherical particles. It is clear that in order to improve the accuracy of Rao's work, a more accurate way of generating an estimate of the active pore density is required.

An extension of Rao's biporous modeling is the work of Kaya [16]. In his work, he assumed that when nucleation was initiated, a vapor region would form similar to what was mentioned earlier. However, this was not assumed to be a failure mode. Instead, it was assumed that this was simply an approximation of the physical case where the vapor region was actually part of a larger two phase region. Again, for the present case, it was desirable to be able to account for both liquid and vapor occupying the same region in varying fractions.

Further modeling work on biporous wicks is that done by Lin [22]. The goal of Lin's work was to model the wick used in a loop heat pipe and incorporate knowledge of the capillarity and the pore size distribution of the wick to increase the accuracy of previous models. The equations, for the most part are quite similar to what is used in the present work except for expressions for the liquid and vapor permeabilities. In Lin's work, since they were investigating a loop heat pipe compensation chamber, their wick was described as having a radial configuration as it formed an annular lining to the cylindrical compensation chamber. They split the wick into 3 distinct regions; liquid, 2 phase, and vapor. These regions were assumed to have distinct boundaries and the effect of these boundaries was determined by comparison with experimental data. The pore size distribution was used as a method to determine where these phase boundaries were.

The wick described in their work had a higher overall porosity than the present work but generally smaller pore sizes. How they determined their pore size distribution was not discussed. There was also a focus on how to best approximate the effective thermal conductivity of their wicks. Several different correlations were used and compared against one and another. They validated their modeling effort against experimental work and found good agreement.

However, there are several differences between their work and what is done presently. First of all, Lin's work breaks the wick into 3-regions which the current work does not. Using Lin's method, the assumption must be made that there are very well defined boundaries between phase and phase mixture regions. As the origin of the pore size distribution is not stated, it is difficult to comment on its accuracy, but the liquid saturation is based more on the selection of the boundaries between the regions than the pore size distribution. The model developed for this

thesis does not make the liquid saturation distinctions on the basis of regions since more appropriate methods are available.

Vadnjal [37] developed a simple model for estimating the dryout heat fluxes of biporous material. His model assumed that a biporous wick was effectively an arrangement of similar unit cells which were comprised of stacks of porous clusters, effectively forming fins. He solved for the heat transfer and temperature distribution as if a stack of clusters were a fin by assuming radial symmetry and using this unit cell as the elementary volume for a volume averaged estimation. His results compared well with experimental data collected by Semenic [35], but he was only able to estimate the dryout heat flux, because it was assumed that at dryout, the large pores between clusters were only filled with vapor, and liquid occupied the small pores inside the clusters. This condition leaves open the need to effectively estimate the heat transfer in regimes outside of the singular point of large pore dry-out.

Smirnov [37] wrote a comprehensive review of boiling modeling in many different types of porous media modeling. In many ways Smirnov was trying to show that there are a multitude of potential physical arrangements of liquid and vapor in a porous media. The reason for his review was to look at different modeling techniques and assess them relative to their utility for various applications.

The porous media flow regimes he referred to could be divided into two groups; the first group occurred when the heater surface remained wetted and the second group referred to regimes where the heater surface was no longer wetted and vapor filled some or all of the interstitial spaces of the wick. A diagram of the regimes in group one can be seen in Figure 4.

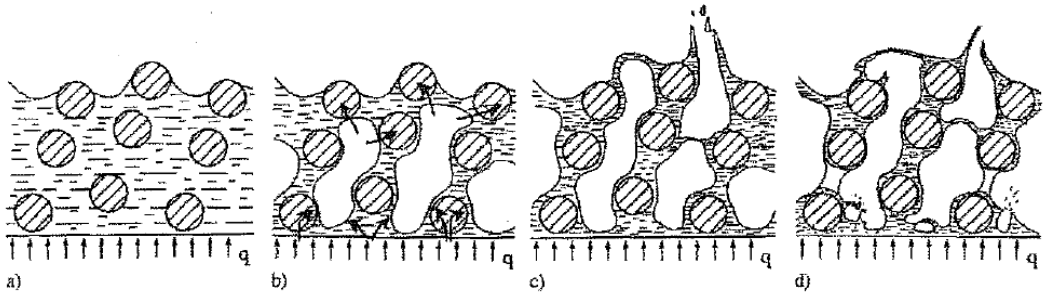

Figure 4: Regimes of evaporation, group 1, Smirnov [37]

The primary regimes of interest within the present work are in group 1. Referring to Figure 4, in part a, there is only evaporation from the upper surface and as heat flux increases, the radius of curvature for the menisci on the upper surface will continue to increase. Part b is where the local superheat at the wall is high enough for evaporation but the majority of the solid wick and liquid are subcooled, resulting in a "micro-heat pipe" region, where vapor is circulated in vapor bubbles within the wick. The regime in part c represents the point at which the average temperature throughout the wick has at least reached saturation, so that vapor can escape from the upper surface. The final regime, part d, shows the point at which that the superheat has reached a high enough value in the hot region that boiling occurs in the fluid itself, which is the start of a vapor blanket forming. This vapor blanket, referred to because there is film boiling at the heater interface, effectively cutting off the heater interface from liquid, will cause a massive increase in the surface temperature in the vicinity of the blanket. At sufficiently high heat fluxes, the vapor can completely cover the heater surface and prevent liquid from reaching it anywhere. For the purposes of the present work, that point will be interpreted as a failure of the wick since

the temperature difference across the wick will drastically increase relative to the boiling regimes in group 1.

In Figure 4, the wick depicted is taken to be monoporous, but it is still clearly evident that the physical processes involved in boiling liquid in porous media are quite complex. Smirnov reviewed several different porous modeling techniques and is critical of all of them, including Kovalev, on which the present work is based. However, Smirnov's grievances are primarily with the issue that the Kovalev model cannot accurately predict transitions between group one and group two regimes, and to a lesser extent the transitions between different regimes within group 1. However, since the present work is primarily focused on the behavior of part c of group 1 of Smirnov's regimes, this problem is believed to be circumvented. He also raised concerns that in many visual studies of boiling, liquid films are clearly observed on the surfaces of the wicks with distinct nucleation centers. In this case, he is referencing to experimental studies of boiling with screen wicks which have a very well defined porous structure, relative to biporous media and are capable of trapping vapor below the screen.

While the Kovalev technique does not explicity treat the situation of a liquid film in an evaporating pore, it should be noted that in less regular media, such as biporous media, it is necessary to make certain approximations to the geometry, especially in the case where the pore sizes and shapes are highly irregular. To that extent, many of the tortuous paths through the wick are approximated by groupings of pores and since some of those are assumed to have liquid and some with vapor, it is an acceptable approximation of liquid film existing in on the periphery of large pores containing vapor in biporous material. Smirnov is correct to point out that the pores are not easily assumed to be binary; that is some with liquid and some with vapor.

However it should be noted that the approximations upon which the Kovalev technique are based, to a certain extent, account for that behavior. Furthermore, Smirnov himself goes on to conclude that significant future work is needed in order to provide worthwhile analysis of biporous and multiporous media. It should be noted that Smirnov made another useful observation specifically related to sintered coatings. First, Smirnov makes the distinction between "thin" and "thick" wicks of sintered coatings. Thin wicks are defined as wicks which are less than approximately five pore sizes thick and wicks greater than ten pore sizes thick are considered thick. The implications of this distinction are discussed later in establishing a heat transfer coefficient between vapor regions and liquid regions for different wicks.

In a Kovalev type model, certain assumptions are used to circumnavigate the more complex aspects of flow and evaporation in porous media. The central assumption made by Kovalev is that within the wick, there is a pore size R* where larger pores are vapor filled and smaller pores are liquid filled. In general, it is assumed that there is thermal equilibrium between all phases, to make the calculations reasonable. It is generally assumed that there is a pressure gradient seen by the liquid which causes liquid to flow into the wick and a separate pressure gradient which allows vapor to be forced out of the wick, in the opposite direction to liquid flow.

In this way, the relative permeabilities of liquid and vapor can be calculated locally based on the current level of liquid saturation, vapor or liquid filled pores. Doing so connects the pore size distribution to the liquid saturation by defining it as the fraction of pore sizes filled with liquid over the total number of pores in the media. A more extensive explanation of the method by which the model is constructed and implemented is discussed at length later in Chapter 2.

What makes the Kovalev modeling technique so powerful for biporous materials is that when a reasonable estimate of the pore size distribution can be made, the solutions can be obtained relatively rapidly compared to full numerical solutions. The Kovalev method is basically a crude volume averaging scheme, where the pores inside each elementary volume are approximated by a series of parallel cylindrical pores. While the pores in a typical biporous wick are very tortuous, the assumption can be made that the vapor will be in the large pores based on Dullien's work. Thus, so long as the elementary control volumes are not too large, an estimate of the wick interior geometry can be made. Knowing the local saturation values and being able to estimate liquid and vapor permeabilties with alacrity can help provide considerable insight into the underlying processes taking place inside the biporous wick during evaporation.

With regards to the efficacy of the Kovalev technique, Uhle [39] utilized to model heat transfer in magnetite deposits. Her work focused on the heat transfer inside of a nuclear reactor core where hot liquid laden with chemicals created a porous wick on the surface of the fuel rods. Phase change within the porous layer led to deposits that slowly grew. While Uhle was investigating what amounts to a monoporous wick, she was able to achieve good agreement between experimental and modeling results. Furthermore, she made measurements of the permeability and pore size distribution using mercury porosimetry in order to compare these values. Based on her efforts, it can be seen that the Kovalev technique, though simplistic can readily be applied to complex porous media in order to provide reasonable insight into the performance of a particular medium

1.5 Summary

It is clear that there has been a great deal of study of the modes and methods of heat transfer in porous media. Specifically, the present work is concerned with both simulation and experimental techniques to optimize the heat transfer performance of biporous media. It can be shown from the works discussed here that the key parameters that augment biporous material are high vapor permeability, high capillary pressure, and interior surface area. Experimental efforts conducted will be presented in Chapter 6 were new ways in which these parameters have been augmented will be shown.

The modeling efforts that have been outlined show just how complex the task of giving an adequate treatment to the physics of porous media evaporation can be. However, by utilizing the techniques proposed by Kovalev, and making certain modifications, a modeling effort will be presented that produces reasonably accurate estimates of both heat transfer performance and dry-out heat fluxes for biporous wicks. This dissertation will show both by experimental and modeling, effective means by which one can enhance and optimize biporous evaporator wicks.

This dissertation is divided into two parts. The first part develops and validates a model which can be used to predict the performance of a biporous wick. This model aids in the understanding of the physical processes governing the performance of the wick. Part one will encompass three chapters; the Kovalev modeling technique, thermophysical properties, and the validation of the model. In Chapter 2, the governing equations will be derived using the Kovalev technique along with the numerical method used to solve the equations. Chapter 3 will show how the thermophysical properties in the governing equations are evaluated; either empirically or

by the pore size distribution. Chapter 4 will validate the model by comparing predictions with experimental data.

Part 2 of the dissertation uses the model to develop the best way to optimize the performance of a biporous wick. This is done by estimating the point at which dry-out of the wick will occur and suggesting methods to delay dry out of the wick, seen in Chapter 5. Dryout is first established by observing the liquid saturation and the maximum capillary pressure of the wick. By relating the liquid saturation, the pore size distribution, and the maximum capillary pressure, a methodology for delaying dry out is developed. Chapter 6 shows the results of various experimental studies carried out by the author to validate the suggestions made in Chapter 5. Several different geometries and working fluid variations were investigated in order to delay dry-out. Their results will be discussed and analyzed so that a recommendation can be made allowing one to obtain most effective wick modifications.

Based on the work accomplished, future work will then be suggested to continue exploration of optimization of biporous performance. At the conclusion of this dissertation, the author's determination of the nature of performance enhancement as a result of biporous material is detailed as well as a recommendation on an optimized biporous wick. The goal of these efforts, is to show the method by which the design of biporous wicks can be optimized through predictive modeling.

2.0 APPLICATION OF KOVALEV MODELING TECHNIQUE

Smirnov [37] stated at the conclusion of his review of various methods of porous media modeling techniques that significant future effort would be needed in order to accurately predict the behavior of biporous and multiporous media. While he had concerns about the use of the statistical method employed by Kovalev for porous material, careful application could overcome these concerns. Due to the complexity of biporous material, especially the type investigated in this work, it is necessary to employ a modeling technique which is flexible enough that it can be easily implemented but detailed enough that it incorporates some of the important geometric features of the wick.

The extensive research conducted by Semenic [35] led to a desire to model the performance of wicks with their geometric features incorporated into the determination of the thermophysical properties of the media. By doing so, accurate predictions of wick performance could be obtained and allow one to optimize a wick geometry to meet demanding performance requirements.

In this section, the Kovalev model will be explained and derived then related to the type of biporous material and experiments conducted in this work. A derivation of the relevant equations and a discussion of the numerical method used to solve those equations will be shown. The ultimate goal is to develop a method that will lead to better understanding of the behavior of a biporous wick so that better design tools can be developed.

2.1 Explanation and Justifcation

In a Kovalev type model, certain assumptions are used to circumnavigate the more complex aspects of flow and evaporation in a porous medium. The central assumption made by Kovalev is that within the wick, there is a pore size R^*, where larger pores are vapor filled and smaller pores are liquid filled. The efficacy of this assumption is based on Dullien's [13] assertion about flow through porous media when the capillary number is low ($Ca < 10^{-3}$) and it can be assumed that liquid and vapor flow in separate channels. In this regime, the wetting fluid will preferentially occupy the small pores and the non-wetting fluid will occupy the larger pores. In the case of evaporation from a biporous wick, the wetting fluid is water and the non-wetting fluid is water vapor. R^* can vary in any direction through the wick due to the pressure and temperature gradients within the wick. In general, it is assumed that there is thermal equilibrium between all the phases to make the calculations reasonable. In reality there would be a slight increase in temperature of the liquid in the small pores due to the liquid being at a higher pressure, but in a small enough control volume, this difference is negligible. It is also generally assumed that there is a pressure gradient seen by the liquid which causes liquid to flow into the wick and a separate pressure gradient which allows vapor to flow out of the wick in a direction opposite of the liquid (countercurrent flow).

This particular type of modeling was used extensively by Uhle [39] in the development of a boron concentration problem in a nuclear reactor. In order to derive the equations necessary to obtain a solution, Uhle used the equations originally presented by Kovalev. Uhle modified the equation to include a viscous term as suggested by Brinkman [5]. This extra term is usually used in order to better model flow in porous media between different types of media. In this case, Uhle dealt with flow from the free stream into a magnetite deposit and then back into a bulk

convective flow. In the present work, this term is not included since the porous region is continuous and the open space above the wick was not included. Likewise, a Forcheimer term was not included as the Reynolds numbers were small enough to neglect additional inertial effects.

Uhle's model was used as a road map for the efforts described here. The Kovalev method can be thought of as a crude form of volume averaging; representative elementary volumes are in this case cylindrical disks with a distribution of pores ranging in size from small to large. The mean values of the coefficients of the Kovalev equations are calculated in each control volume and are assumed to be constant in the local control volume. The difficulty here is choosing a control volume which is small enough that an averaging assumption is appropriate while large enough that its calculation times can be brief relative to a full numerical solution. A schematic of a control volume, with an R*=R4, can be seen in Figure 5.

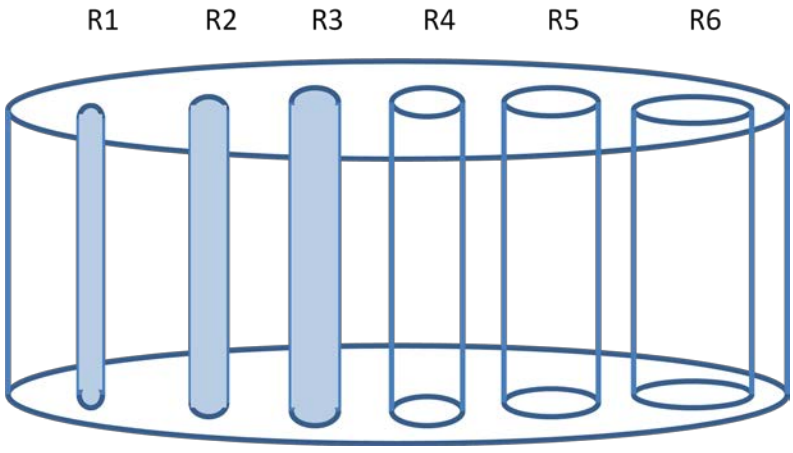

Figure 5: Schematic of Kovalev Control Volume

In Figure 5, the pore sizes smaller than R4 (R1-3) are filled with liquid and the pore sizes larger than R4 (R5-R6) are filled with vapor. In pore R4, there is a meniscus forming the boundary between the wetting and non-wetting phases. It is assumed that the meniscus in R4 is hemispherical and the driving capillary force providing liquid to the wick in this control volume. While this is a gross assumption, if a small enough control volume is chosen, the error introduced by the assumption can be mitigated since the pore sizes do not have an equal probability of existing.

The statistical portion of the Kovalev model comes by way of the pore size distribution. The distribution displays the likelihood that a pore of a particular size exists. A biporous wick is expressly defined as having two pore sizes which are dominant above all others. This will have a strong effect on the liquid saturation and determination of thermophysical properties. This simple assumption regarding which pores are filled with liquid and vapor provides a powerful tool that can be used to analyze wick behavior.

This simplification is used in all Kovalev based models, such as those by Chernysheva [9]. In Chernysheva's case, a model is presented where a pore size distribution and R^* is used to interpret the location of liquid and vapor in the wick. However, it differs slightly in that the model uses the size and orientation of a supposed two-phase region in order to describe phase change. When nucleation begins, a computational two phase region is formed inside this region and a heat sink term appears in the energy equation to account for evaporation. The determination of R^* was made by comparing the minimum pore radius required for continued nucleation and maintaining the capillary pressure necessary to pump liquid to the heater interface.

As with any modeling effort in which averaged values are utilized, there is some error associated with the truncation of potentially important information during the averaging process. In the present work, it was assumed that the efficacy of any assumption could be evaluated using available experimental data for validation enabling the averaging error to be mitigated.

Further, a statistical method such as Kovalev's will struggle to capture transitions between different boiling/flow regimes, also noted by Smirnoff [37]. As a result, a secondary condition is needed to treat the transition from pure conduction to two phase boiling, and again from two phase boiling to full dryout. One could determine the incipience of bubble formation by any number of empirical correlations for boiling on a flat plate to determine when boiling begins, but this would not address the "heat pipe" effect described by Smirnov. Also, it was suggested by Semenic [35] that the point at which the large pores dry out (i.e. no liquid between the clusters, only inside of them) could be discerned by finding the point at which the effective heat transfer coefficient is a maximum, and that its decline signaled that the wick was beginning to dry out.

While it can be readily shown that the Kovalev method of modeling is effective for many different types of porous material, it must be made clear why it was chosen for the biporous structure. Since ample data were provided by Semenic [35] on the distribution of particle sizes, it was believed that a good estimate of the pore size distribution could be derived. The statistically based method developed by Kovalev provided an easy way to connect the geometry of the wick to its thermophysical properties and performance. Using experimental data for validation and building upon the success of others who had used this method, the Kovalev

modeling method was determined to be the best pathway to deeper understanding of the nature of biporous material.

2.2 Derivation and Solution Technique

In order to determine wick behavior, the performance of the wick is divided into three regions; saturated liquid, two phase, and vapor. In the saturated liquid phase, energy is only conducted through the solid material. This is assumed because the thermal conductivity of the wick is much larger than the thermal conductivity of the liquid. Liquid flows vertically to the upper interface, but the Reynolds numbers associated with this flow are too low for convective heat transfer to be important (i.e. $Re<<1$).

Once the temperature difference between the heated surface and the fluid is sufficiently large, vapor bubbles will growat the interface between the substrate and the wick. Once nucleation begins, energy is transferred through evaporation in parallel with conduction through the wick. This point represents a significant drop in the overall thermal resistance of the wick as the formation of vapor and percolation though the wick is a considerably more effective heat transfer method. As the heat flux is increased, more evaporation takes place, expanding the evaporation area. As more vapor is produced, the pressure drop due to vapor flow through the evaporation region to the ambient becomes larger.

At a certain point, the pressure drop will exceed the maximum available capillary pressure, and liquid will no longer be able to reach the heater surface. The heat flux at this point is defined as the “maximum heat flux” after which performance will decline due to liquid receding into the clusters. When the liquid is fully depleted from the clusters, the biporous

region is assumed to only have vapor/solid interfaces and a catastrophic dryout results. Once there is no more liquid, the vapor will become superheated and the heater temperature will increase rapidly as a function of heat flux. Consequently, the wick will not function again until it is re-wet by reducing the heat flux. These regimes can be seen schematically in Figure 6.

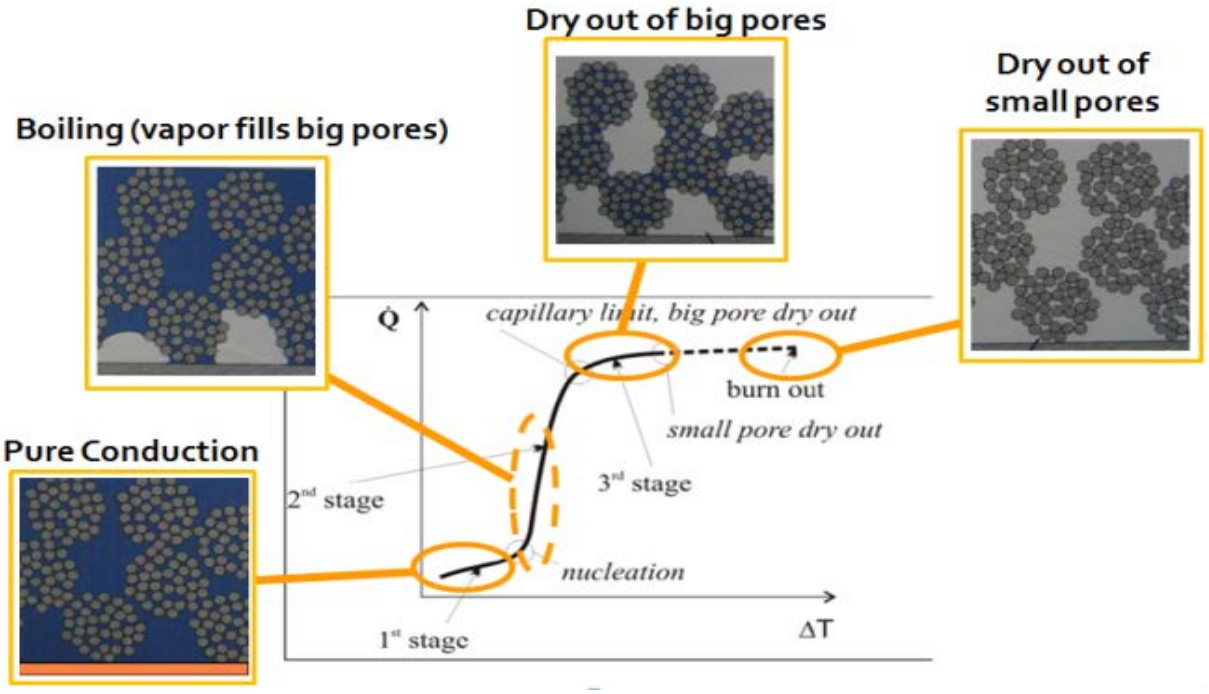

Figure 6: Schematic of Biporous Media Boiling Regimes [9]

This work is primarily focused on the so-called two phase boiling region. While it is possible to operate the model in the pure conduction region and the dry-out regions, as mentioned previously, determining the transition between the regions is very difficult. This model will primarily be used to predict the performance of the biporous wick in the boiling

region and to investigate the wick's behavior as it transitions to dryout. The following derivation and computational results correspond only to these processes.

2.2.1 Momentum Equation

The equation of motion used in this work is for Darcy flow. The flow is assumed to be at steady state and incompressible. Equations (3) and (4) are the Darcy flow momentum equations for the liquid and vapor , respectively. As a check to assess the validity of the Darcy equations, a quick calculation can be made to determine the Reynolds number. Generally, if the Reynolds number is less than 1, Darcy flow is valid, though it can vary as high as 10 and still be valid. Using the definition of Reynolds number from Smirnov [37], the Reynolds number will be defined as,

$$\mathrm{Re} = \frac{G}{\mu_v}\left(\frac{\beta_o}{\alpha_o}\right) \qquad \textbf{(2)}$$

where G is a mass flux and μ_v is the viscosity of the vapor phase. (β_o/α_o) is a characteristic length formed by taking the ratio of the measured permeability and the average diameter of the pore (κ_v/d_v), which from Semenic's [36] data was measured to be approximately $1.313\text{x}10^{-6}$m. Smirnov commented that this characteristic length was more readily determined from experimental data rather than nominal estimates of pore structure. For a conservative estimate, a high heat flux of 400 W/cm^2 is chosen which corresponds to a mass flux of 1.77 kg/m^2/s assuming the enthalpy of vaporization is $2.257\text{x}10^6$ J/kg. Assuming a vapor viscosity of $1.8\text{x}10^{-5}$

Pa-s, this results in a Reynolds number of 0.129, indicating that Darcy flow is valid even at higher heat fluxes. The Darcy flow momentum equations for liquid and vapor are,

$$\frac{\partial P_l}{\partial z} = -\frac{\mu_l}{\kappa_l} v_l \qquad \textbf{(3)}$$

$$\frac{\partial P_v}{\partial z} = -\frac{\mu_v}{\kappa_v} v_v \qquad \textbf{(4)}$$

where, k_l and k_v are the relative phase permeabilities for liquid and vapor respectively.

The Darcy Flow equations are combined with the Young-Laplace equation,

$$\nabla P = \frac{2\sigma}{R^*} \qquad \textbf{(5)}$$

to obtain an expression for the capillary pressure. The Kovalev model is based on the principle that an imaginary cutoff radius , R*, exists where pore sizes larger than R* are filled with vapor and pore sizes smaller than R* are filled with liquid. Since this imaginary radius represents a pore where the meniscus between the liquid and vapor is located, the r in the Young Laplace equation is replaced with R*. The Young-Laplace equation is then differentiated with respect to z and combined with the pressure gradient terms. The result is

$$\frac{\partial \Delta P_c}{\partial z} = \frac{\partial P_v(z)}{\partial z} - \frac{\partial P_l(z)}{\partial z} = \frac{-2\sigma\cos(\theta)}{R^{*2}}\frac{\partial R^*}{\partial z} \quad \textbf{(6)}$$

When substituted into Eqs (3) and (4), there results,

$$\frac{\partial P_v(z)}{\partial z} - \frac{\partial P_l(z)}{\partial z} = -\frac{\mu_v}{\kappa_v}v_v + \frac{\mu_l}{\kappa_l}v_l = \frac{-2\sigma\cos(\theta)}{R^{*2}}\frac{\partial R^*}{\partial z} \quad \textbf{(7)}$$

The velocities of the liquid and vapor phases are assumed to be proportional to the vapor mass flux, G(z) and the flow is assumed to be steady. Also note that in this case, it is assumed the liquid and vapor are in counter flow within the wick and that the liquid is supplied from the top of the wick. Since this is a 1-D model, lateral liquid flow within the wick is not considered resulting in a model that is only valid over the heater region of the wick. The resulting equations are

$$v_l(z) = \frac{-G(z)}{\rho_l \phi(R^*)} \quad \textbf{(8)}$$

$$v_v(z) = \frac{G(z)}{\rho_v(1-\phi(R^*))} \quad \textbf{(9)}$$

ϕ represents the liquid saturation and is related to the cumulative distribution function (CDF). The liquid saturation is the integral of the probability mass function, f(r), from the minimum pore size in the distribution to the cutoff pore size, R*. The range of the integral represents the pores filled with liquid.

$$\phi = \int_{R_{\min}}^{R^*} f(r)dr \qquad \textbf{(10)}$$

Combining equations (7), (8), and (9) results in a first order partial differential equation for the cutoff pore radius R*,

$$\frac{\partial R^*}{\partial z} - \frac{R^{*2}\, G(z)}{2\sigma \cos(\theta_d)} A(R^*) = 0 \qquad \textbf{(11)}$$

where,

$$A(R^*) = \left(\frac{\mu_v}{\kappa_v} \frac{1}{\rho_v (1-\phi(R))} - \frac{\mu_l}{\kappa_l} \frac{1}{\rho_l \phi(R)} \right) \qquad \textbf{(12)}$$

2.2.2 Energy Equation

For the energy equation, convection in the liquid was ignored as the flow velocities led to convective heat transfer coefficients that were negligible compared to the evaporation heat transfer. The Reynolds numbers for a majority of the input powers investigated were of order 1 or less leading to the assumption that convection was not a significant factor.

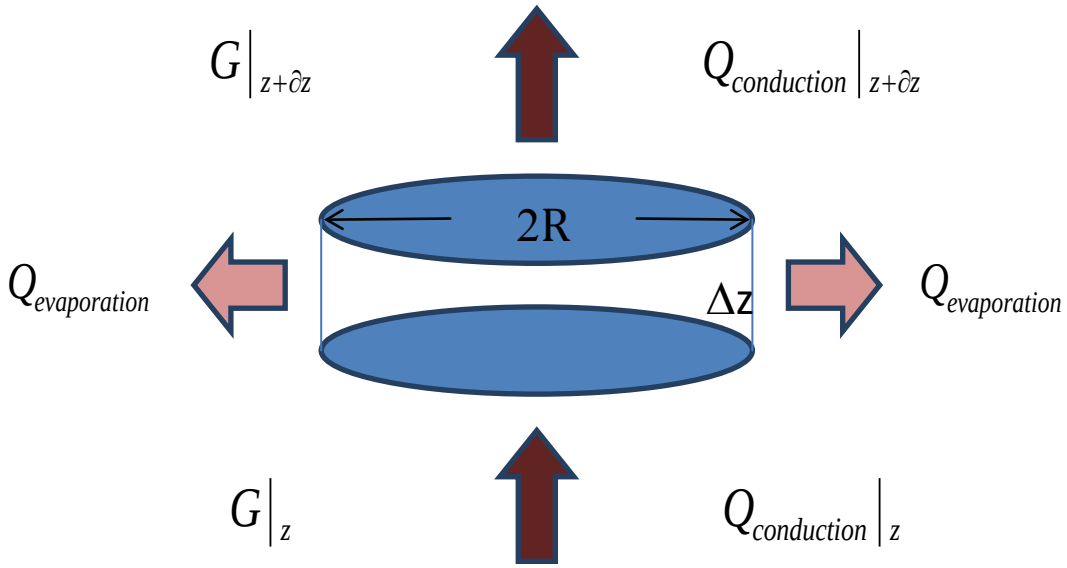

Figure 7: Schematic of Control Volume

The energy equation derivation was based on an arbitrary control volume in the wick, see Figure 7. Energy is conducted through the wick, the vapor mass flux passes through the open pores and the liquid is evaporated through the open pores. The energy conservation in the control volume is,

$$q_c + q_h = 0 \qquad \textbf{(13)}$$

$$\left(q_c\left(z+dz\right) - q_c\left(z\right)\right) + q_h = 0 \qquad \textbf{(14)}$$

where h denotes evaporation. Using Fourier's law of conduction, the heat conducted through the solid skeleton is

$$q_c = -k_{eff}(1-\varepsilon)\frac{\partial T_d}{\partial z} = -k_{eff}(1-\varepsilon)\frac{\partial \theta}{\partial z} \qquad \textbf{(15)}$$

The energy transport in the horizontal direction resulting from phase change between the region where R< R_{cr} is,

$$q_h = \Delta z\left[\varepsilon\int_{R^*}^{R_{\max}} f(r)dr\right]\alpha_n(T_d - T_{sat}(P_v)) = \Delta z\left[\varepsilon(1-\phi)\right]\alpha_n\theta \qquad \textbf{(16)}$$

where α_n is a volumetric heat transfer coefficient accounting for evaporation within the wick. The change in z direction input power in the region where R< R_{cr} is given by.

$$\left(q_c\left(z+dz\right) - q_c\left(z\right)\right) + \Delta z\varepsilon(1-\phi)\alpha_n\theta = 0 \qquad \textbf{(17)}$$

where α_n is a volumetric heat transfer coefficient accounting for evaporation. Taking the limit as Δz approaches zero in (17) results.

$$\frac{\partial q_c}{\partial z} + \alpha_n\varepsilon(1-\phi)\theta = 0 \qquad \textbf{(18)}$$

Substituting for q_c, given by Eq. (15) into Eq. (18) results in

$$\frac{\partial}{\partial z}\left(-k_{eff}\left(1-\varepsilon\right)\frac{\partial \theta}{\partial z}\right) + \alpha_n\varepsilon(1-\phi)\theta = 0\,, \qquad \textbf{(19)}$$

and with k_{eff}, assumed to be constant,

$$\frac{\partial^2\theta}{\partial z^2} - \frac{\alpha_n(R^*)\varepsilon(1-\phi)\theta}{k_{eff}(1-\varepsilon)} = 0\,. \qquad \textbf{(20)}$$

Equation (20) is conservation of energy and includes the volumetric heat transfer coefficient. Note that the volumetric heat transfer coefficient, $\alpha_n(R^*)$, must be a function of R* because it is at R* where phase change takes place.

2.2.3 Vapor Flux Equation

An equation governing vapor flow is needed to complete the set of equations. It is assumed that the flux of vapor in a given control volume is equal to the energy convected away from the region where r < R* by the external vapor flow. The equation is obtained from a mass balance in the same way that the energy equation, Eq.(20), was constructed. The change in vapor flux is given by

$$\left(G\left(z+dz\right)-G\left(z\right)\right)+\frac{q_h}{h_{fg}}=0. \qquad \textbf{(21)}$$

The relationship between heat transfer and vapor production is given by

$$\begin{aligned} q_h &= \Delta z\varepsilon\left(1-\phi\right)\alpha_n(T_d - T_{sat}(P_v)) \\ &= \Delta z\varepsilon\left(1-\phi\right)\alpha_n\theta \end{aligned} \qquad \textbf{(22)}$$

Combining Eqs (21) and (22) yields the relation for vapor flux,

$$\frac{\partial G}{\partial z}+\frac{\alpha_n\varepsilon\left(1-\phi\right)(R)\theta}{h_{fg}}=0 \qquad \textbf{(23)}$$

2.2.4 Summary of Equations

The set of equations will be solved using an Euler method. This requires that the equations be written as a system of first order partial differential equations. The energy equation is reduced to a set of two first order equations, by replacing

$$\frac{\partial^2\theta}{\partial z^2}=\frac{\alpha_n(R)\theta}{k_{eff}} \qquad \textbf{(24)}$$

with

$$\frac{\partial \theta}{dz} = W \qquad \textbf{(25)}$$

$$\frac{\partial W}{\partial z} = \frac{\partial^2 \theta}{\partial z^2} = \frac{\alpha_n(R)\theta}{k_{eff}} \qquad \textbf{(26)}$$

The remaining system of first order partial differential equations are shown below.

$$\frac{\partial R}{\partial z} = \frac{R^2 G(z)}{2\sigma \cos(\theta_d)} A(R) \qquad \textbf{(11)}$$

$$\frac{\partial \theta}{dz} = W \qquad \textbf{(25)}$$

$$\frac{\partial W}{\partial z} = \frac{\partial^2 \theta}{\partial z^2} = \frac{\alpha_n(R)\varepsilon(1-\phi)\theta}{k_{eff}(1-\varepsilon)} \qquad \textbf{(26)}$$

$$\frac{\partial G}{\partial z} = -\frac{\alpha_n \varepsilon (1-\phi)\theta}{h_{fg}} \qquad \textbf{(23)}$$

$$\frac{\partial P_v}{\partial z} = -\frac{\mu_v}{\kappa_v} \frac{G(z)}{\rho_v(1-\phi(R))} \qquad \textbf{(9)}$$

$$\frac{\partial P_l}{\partial z} = \frac{\mu_l}{\kappa_l} \frac{G(z)}{\rho_v(\phi(R))} \qquad \textbf{(8)}$$

A shooting method and iteration are used to determine the unknown boundary conditions and its application is explained later.

2.2.5 Boundary Conditions

The equations that will be used to solve for the unknown variables in the domain, including temperature and pressure, have been developed. In order to determine these unknown variables, boundary conditions must be set. There are 6 first order equations in the domain to be solved and so six boundary conditions are required. The boundaries of the computational domain are the heater wall and the top of the wick, which is exposed to the vapor space, shown in Figure 8.

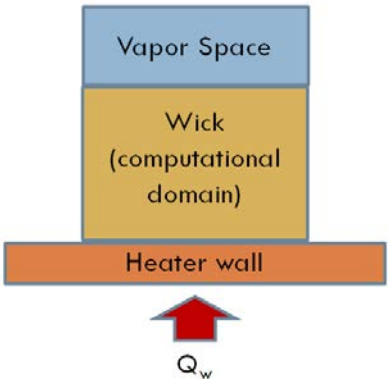

Figure 8: Schematic of Computational Domain

The equations and a summary of the boundary conditions can be found in Table 1. The boundary conditions are broken into two groups; those at the heated wall and those at the top of the wick (where it is exposed to open vapor space).

Table 1: Table of Equations and Boundary Conditions

Heater Wall Boundary Conditions	Domain Equations		Vapor Space Boundary Conditions
$R\big\|_w = ??$	$\frac{\partial R}{\partial z} - \frac{R^2 G(z)}{2\sigma\cos(\theta_d)} A(R) = 0$	Cutoff Pore Size	$R\big\|_\delta = R_{\max}$
$\theta\big\|_w = ??$	$\frac{\partial \theta}{dz} = W$	Dummy Variable	$\theta\big\|_\delta = 0$
$q\big\|_w = -k\frac{d\theta}{dz}\big\|_w = known$	$\frac{\partial W}{\partial z} = \frac{\partial^2 \theta}{\partial z^2} = \frac{\alpha_n(R)\varepsilon(1-\phi)\theta}{k_{eff}(1-\varepsilon)}$	Temperature	$q\big\|_\delta = -k\frac{d\theta}{dz}\big\|_\delta = 0$
$G\big\|_w = 0$	$\frac{\partial G}{\partial z} + \frac{\alpha_n\varepsilon(1-\phi)\theta}{h_{fg}} = 0$	Vapor Flux	$G\big\|_\delta = \frac{q_w}{h_{fg}}$
$P_v\big\|_w = ??$	$\frac{\partial P_v}{\partial z} + \frac{\mu_v}{\kappa_v}\frac{G(z)}{\rho_v(1-\phi(R))} = 0$	Vapor Pressure	$P_v\big\|_\delta = P_{sat}$
$P_l\big\|_w = ??$	$\frac{\partial P_l}{\partial z} - \frac{\mu_l}{\kappa_l}\frac{G(z)}{\rho_v(\phi(R))} = 0$	Liquid Pressure	$P_l\big\|_\delta = P_{sat}$

While there are six boundary conditions known at the top of the wick, they do not produce solutions for various heat fluxes, and so they cannot be used to produce unique solutions to the variables of interest as a function of heat flux. This means that in order to determine the values of temperature, pressure, and liquid saturation as a function of heat flux, a shooting method must be utilized with the combination of known and unknown boundary conditions at the wall in order to adequately predict wick performance. The boundary conditions will be discussed in more detail followed by an explanation of how the shooting method was implemented.

<u>At the wall:</u>

$$R\big|_w = unknown \qquad \textbf{(27)}$$

where $R < R_{max.}$ R_{max} is the maximum allowable cutoff pore size, indicating a condition where there is only liquid. This could be the case on a boundary and throughout the wick before nucleation has begun as it is fully saturated. The temperature

$$\theta\big|_w = unknown \qquad \textbf{(28)}$$

where θ must be greater than 0 at the wall for any energy to flow into the system. The mass flow,

$$G\big|_w = 0 \qquad \textbf{(29)}$$

must be the case because no vapor can penetrate through the wall. With no flow at the wall, the velocity must be zero at the wall. The heat transfer at the wall is prescribed by the user at the outset of the modeling run and so is assumed to be known.

$$q\big|_w = -k\frac{d\theta}{dz}\big|_w = known \qquad \textbf{(30)}$$

The wall heat flux represents the independent variable of the modeling problem as it allows for the determination of wick performance. The liquid and vapor pressures are assumed to be unknown at the wall.

$$P_v\big|_\delta = unknown \qquad \textbf{(31)}$$

$$P_l\big|_\delta = unknown \qquad \textbf{(32)}$$

At the top of the wick (interface with vapor space):

The condition at the top of the wick for the 1-D model must represent all liquid entering the wick,

$$R\big|_\delta = R_{\max} \qquad \textbf{(33)}$$

The temperature boundary condition at the top of the wick is

$$\theta\big|_\delta = 0 \qquad \textbf{(34)}$$

because it is assumed that all of the vapor above the wick is at saturation and at equilibrium.

At the top of the wick, the vapor flux must be enough to carry away all of the energy added at the lower boundary leading to

$$G\big|_{\delta} = \frac{q_w}{h_{fg}} \qquad \textbf{(35)}$$

where at the top of the wick, the vapor mass flux is equal to what can be produced using all the the energy being conducted in at the bottom. Thus

$$q\big|_{\delta} = -k\frac{d\theta}{dz}\Big|_{\delta} = 0 \qquad \textbf{(36)}$$

Again, q_{δ} is known at the top as it is assumed all energy is used up by evaporation within the wick. Both the liquid and vapor pressures are assumed to be at saturation at the top of the wick.

$$P_v\big|_{\delta} = P_{sat} \qquad \textbf{(37)}$$

$$P_l\big|_{\delta} = P_{sat} \qquad \textbf{(38)}$$

2.2.6 Euler Method

The resulting equations are a system of first order ordinary differential equations best solved using an Euler method. A single first order equation or series of first order equations are used to solve for the variables over the computational domain. In this case there are 5 equations for the five different variables of interest. In order to solve for the variables within the domain, an appropriate spatial step is selected and the new values are calculated using a first order approximation of a Taylor series. This is represented by

$$f(z+\Delta z) = f(z) + \Delta z\left(\partial f(z) \big/ \partial z\right)\lambda \qquad \textbf{(39)}$$

where λ is a relaxation parameter added to improve stability. The relaxation parameter reduces the changes between spatial steps and helps to smooth out the solution process. The spatial step Δz must be sufficiently small that there is not an issue with stability. The boundary conditions are entered as the initial value of f(z) and the solution is marched across the domain until it reaches the upper surface. At this point, the resulting boundary values are compared with the boundary conditions and a determination is made as to whether to iterate the solution again. The method for selecting the next boundary value, should one be required, is discussed in the next section.

2.2.7 Solution Method Closure

Due to the presence of unknown boundary conditions at each end of the boundary, a shooting method was employed in conjunction with the Euler method in order to solve the domain. In a shooting method, the unknown values at the initial boundary are guessed and then the domain is solved. Assuming the domain is solved from bottom of the wick to the top, the error between the known boundary conditions at the top and those that were calculated based on the guessed left hand boundary conditions are tabulated. In order to close the shooting method, a Taylor series

expansion is used with a gradient method to reduce the errors in the calculated values at the top of the wick, and these values are used to make another guess at the next wall (bottom) value. An example of this type of calculation is

$$ER^1 = R_{\max} - R^1(H) \qquad \textbf{(40)}$$

$$ET^1 = \theta^1(H) \qquad \textbf{(41)}$$

where ER and ET are the errors associated with the cutoff pore radius and the temperature difference. For the purposes of developing a Jacobian, a dummy variable Y is introduced to represent R and θ.

$$Y_1 = R \qquad \textbf{(42)}$$

$$Y_2 = \theta \qquad \textbf{(43)}$$

The Jacobian of the two error calculations is then computed.

$$\frac{\partial ER}{\partial Y_1} = -1 \qquad \textbf{(44)}$$

$$\frac{\partial ER}{\partial Y_2} = 0 \qquad \textbf{(45)}$$

$$\frac{\partial ET}{\partial Y_1} = 0 \qquad \textbf{(46)}$$

$$\frac{\partial ET}{\partial Y_2} = 1 \qquad \textbf{(47)}$$

A Taylor Series Expansion of the error equations, evaluated at the top of the wick is developed as follows:

$$ER = (R_{\max} - R(H)) + \frac{\partial ER}{\partial Y_1}\Delta Y_1 + \frac{\partial ER}{\partial Y_2}\Delta Y_2 \qquad \textbf{(48)}$$

$$ET = (\theta(H)) + \frac{\partial ET}{\partial Y_1}\Delta Y_1 + \frac{\partial ET}{\partial Y_2}\Delta Y_2 \qquad \textbf{(49)}$$

Next, the set of equations is converted to matrix form.

$$\begin{bmatrix} ER^i \\ ET^i \end{bmatrix} = \begin{bmatrix} R_{\max} - R^{i-1} \\ \theta^{i-1} \end{bmatrix} + \begin{bmatrix} -1 & 0 \\ 0 & 1 \end{bmatrix} \begin{bmatrix} \Delta Y_1^{i-1} \\ \Delta Y_2^{i-1} \end{bmatrix} \qquad \textbf{(50)}$$

ER and ET are set equal to 0 in order to solve for the delta Ys,

$$-inv\left(\begin{bmatrix} -1 & 0 \\ 0 & 1 \end{bmatrix}\right) \begin{bmatrix} R_{\max} - R^{i-1} \\ \theta^{i-1} \end{bmatrix} = \begin{bmatrix} \Delta Y_1^{i-1} \\ \Delta Y_2^{i-1} \end{bmatrix} \qquad \textbf{(51)}$$

The ΔYs are then used to construct a guess of the unknown boundary conditions at the wall for the next computation

$$Y_1^i = Y_1^{i-1} + \lambda * \Delta Y_1^{i-1} \qquad \textbf{(52)}$$

$$Y_2^i = Y_2^{i-1} + \lambda * \Delta Y_2^{i-1} \qquad \textbf{(53)}$$

λ is a relaxation parameter, used to smooth out the oscillations in the guesses and speed convergence. The above equations, boundary conditions and solution method are run until convergence is reached. Convergence is assumed to have occurred when the delta Y vector has a magnitude less than 10^{-3}.

2.3 Summary

In this chapter, the equations used in the Kovalev modeling method were derived along with the boundary conditions and solution technique. The development of a model has been detailed from its initial framework based on the work of Uhle, through the derivation of the governing equations. The Kovalev technique is a simple tool which can provide new insight into the behavior of biporous wicks. The governing equations were solved using a shooting method which used an Euler technique in order to solve for the domain. The shooting method was iterated until the boundary values converged, and a steady state solution resulted.

This model provides the basis for a method that will yield predictions of the performance of a biporous wick and the relationship between performance and geometry of the wick. It is this

relationship that will allow the model to be used as a tool to predict the performance of biporous wicks and be used for their optimization. In the following chapters, the development of the thermophysical properties used by the Kovalev model will be explained and the model will be validated against experimental data. With a validated model, the performance from nucleation to dry-out of the wick can be predicted and made use of as design tool for optimization of wicks. .

4.0 THERMOPHYSICAL PROPERTIES

In the previous section, the Kovalev technique for modeling of porous material was explained. The equations necessary in order to solve for the temperature, pressure, and liquid saturation fields were derived and a solution method for these equations was proposed. While that section provided an overview of how the model was developed, the coefficients in the equations need further elaboration if they are to be used in the governing equations. The values for density, viscosity and enthalpy of vaporization are those of water at a temperature determined by the model as it allows variable fluid physical properties to be accounted for.

Again, the overarching goal of this thesis is to produce a tool that can be used to design and optimize biporous wicks. This section will focus on the development of the coefficients introduced in the previous chapter that are needed to support the model and relate the performance of a biporous wick to its pore size distribution. This section will be divided into two main parts; the development of the pore size distribution and the determination of direct properties of the wick determined from the geometry. The properties determined in this section will bring closure to the Kovalev equations so that they can be validated against experimental data. Once validated, these equations provide the basis for the optimization of biporous media.

3.1 Pore Size Distribution

One of the goals of the modeling effort was to tie as many properties of the porous media under investigation to the geometry of the wick expressed in terms of the pore size distribution as

possible. The pore size distribution incorporates the most important features relevant to the two-phase flow in the system and if they can be related to the construction of the wick, better designs can be produced. This approach has the added benefits of both increasing the accuracy of the results and making the method less dependent on empirical data. This is what makes the variation of the Kovalev modeling method utilized here different from other similar modeling efforts.

The pore size distribution used in this work was constructed from data collected by Seminic [35]. As part of his thesis research, he extensively analyzed the particle and cluster size distributions of the material that were used to construct a wick using a particle analyzer and an optical microscope. This was done in order to have an accurate estimate of the characteristic sizes of the particles and clusters based on the sieve size used to separate them. The particle sizes shown in the legend are the average sieve sizes used to separate particles. The results of the particle analyzer analysis are shown in Figure 9 and Figure 10.

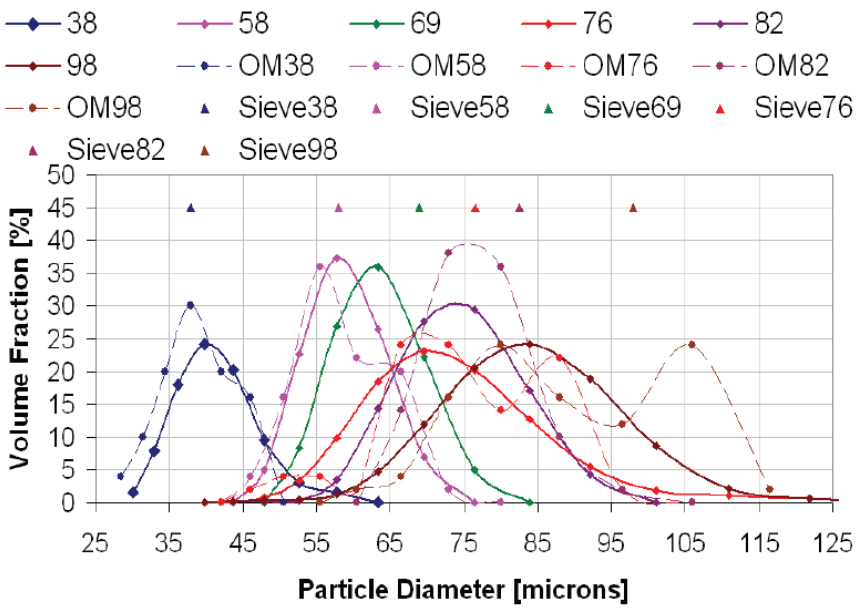

Figure 9: Particle diameter distribution [35]

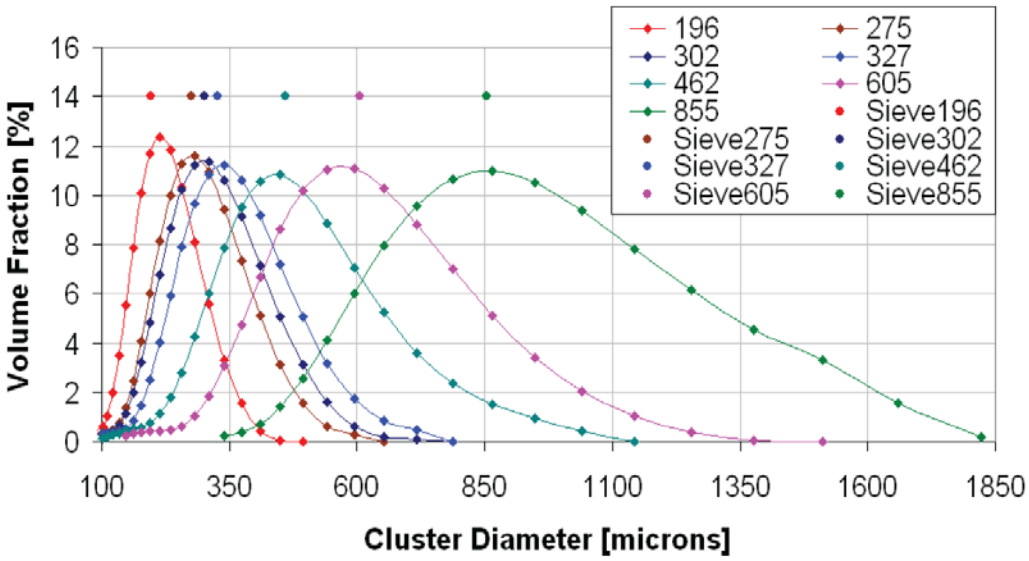

Figure 10: Cluster diameter distribution [35]

Figure 9 and Figure 10 are the Probability Mass Functions (PMF) of the particle and cluster sizes respectively. These display the probability that any particle or cluster diameter is likely to exist in a particular volume fraction. Semenic [35] compared his particle analyzer results for the different particle sizes to those obtained with an optical microscope, designated by "OM" in the legend. The characteristic diameter of a particular sieve size of particles is the peak in the curve. Due to the nature of the PMF, the wider that the curve spreads, the greater variance there is in object size that was sieved. Note, that in several cases, the average sieve size and the peak diameter are not the same. One could infer that this variance and the difference between the sieve and average diameters implies a less regular shape of the particles in question if the spaces in the sieve are assumed to be regular. The particle sizes tend to vary much less than the clusters based on this principle, and the variance in the cluster sizes is a strong function of cluster diameter. With these distributions, the task is now to construct a pore size distribution from the knowledge of the particle and cluster geometry.

There are two things to remember when using the Kovalev method to describe the biporous wicks used in this work. First, by its very nature, this model only looks at small control volumes that are typically less than a micron tall, and not the entire wick. As such, the pore size distribution is taken to be local, not global for the wick. Secondly, the Kovalev method approximates the pores in a highly irregular wick as a series of regular, parallel interconnected pores. Because of the irregular shape of the clusters, there can be many cases where the tortuosity of the space between the clusters can create many more active pores than would be anticipated were the clusters perfectly spherical.

One of the principal challenges in determining the pore size distribution was to determine the relationship between particle/cluster size and pore size. At first, it was hypothesized that a pore would be represented as a displacement in the solid that was the same size as the object in question, either a particle or a cluster. However, this led to a porosity that was not consistent with the experimental results of Semenic (Biporous porosity ~ 0.64). Semenic's results indicated that the biporous porosity was mostly constant with respect to both particle and cluster size. This tighter packing led to the idea that the clusters in the wick could potentially be represented as a packed bed of spheres.

This packing argument was based on knowledge of the typical characteristics of a packed bed of spheres. However, considering that the loosest possible packing of spheres in a close packed arrangement yields a porosity of approximately 0.4764, which is about 36% smaller than the porosity of a biporous wick ($\varepsilon = 0.642$), the large pores will be larger than those seen in packed bed of spheres. This is for a bed of spheres with diameters on the order of the cluster sizes. The reason the biporous material has a higher porosity is because the spheres themselves are porous, further increasing the amount of open space. The clusters themselves are made up of monoporous material of a porosity on the order of $\varepsilon = 0.277$. Care was taken in the production of these wicks in order to maintain a contact area of approximately 20% of the diameter as this was found to be the most effective by Semenic [35].

The pore sizes should be larger than what is seen in the biporous structure because the overall porosity is higher than what would be expected for a packed bed of spheres. The estimate of the pore sizes should, however, be limited on the upper end because the porosity is not as high as what is seen in compressed metal foams by Anapragada [1], leading to estimates

of the pore sizes that are of the same order as the particles and cluster sizes excessive. The pore sizes must lie somewhere in between these estimates.

Typically, the pore radius for a packed bed of uniform spheres (assuming a Face Centered Cubic arrangement) is assumed to be 21% of the particle diameter [13] but can vary to greater than 40% depending on the assumptions of a particular researcher. These estimates vary but are all based on the assumption that the constituent objects in the porous material are perfectly spherical. This is not the case in biporous material, especially at the cluster level. Figure 11 shows the standard deviation of the particle and cluster sizes calculated using Semenic's particle analyzer data.

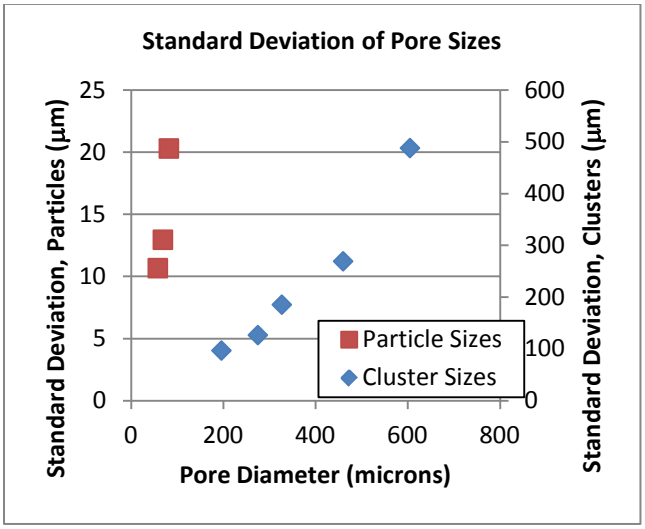

Figure 11: Standard Deviation of Particle and Cluster Sizes

The standard deviation of both the particle and cluster diameters increases as a function of nominal sieve size. As was apparent in the PMFs shown earlier, the cluster diameter is a much stronger function of size and can thus be assumed to vary more in shape. This is

interpreted to mean that the smaller the size of the object, the more regular its shape is, or the more appropriate an assumption of it being spherical becomes. This has particular bearing on both the estimation of the pore sizes from particle analyzer data and for the estimation of the surface area to volume ratio as a function of cluster sizes.

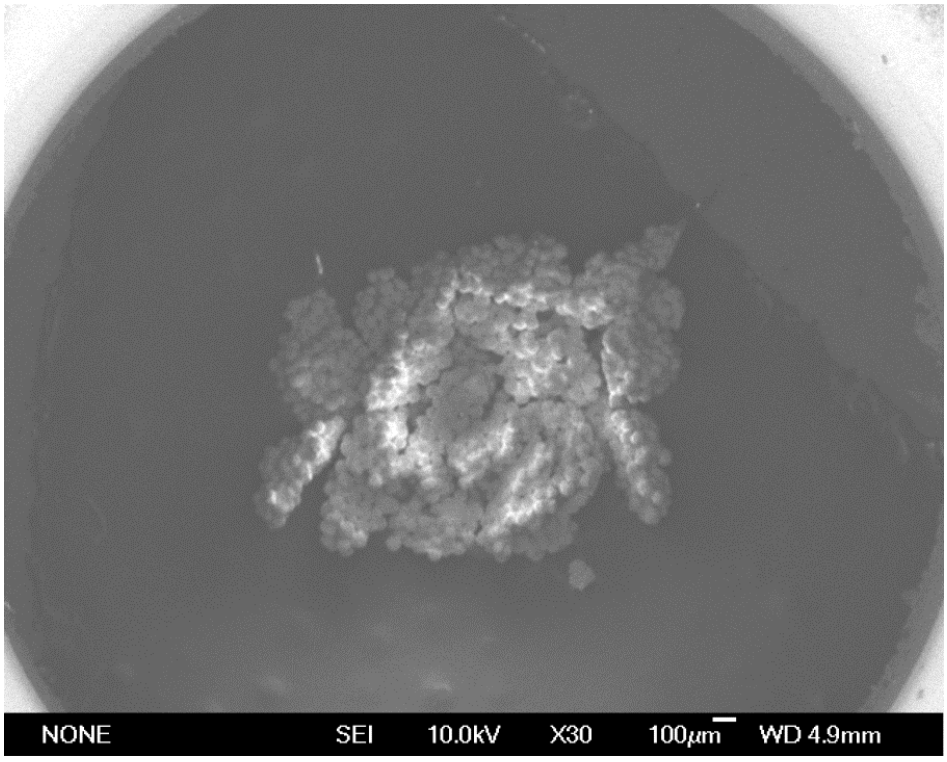

Figure 12: SEM of clusters

After inspecting SEM's of various wicks (see Figure 12), the pore radii are assumed to be 40% of the particle/cluster diameter. This is approximately half way between the largest possible estimate of the pore sizes (the same size as the particles or clusters) and the smallest pore size, estimate based on the packed bed of spheres.

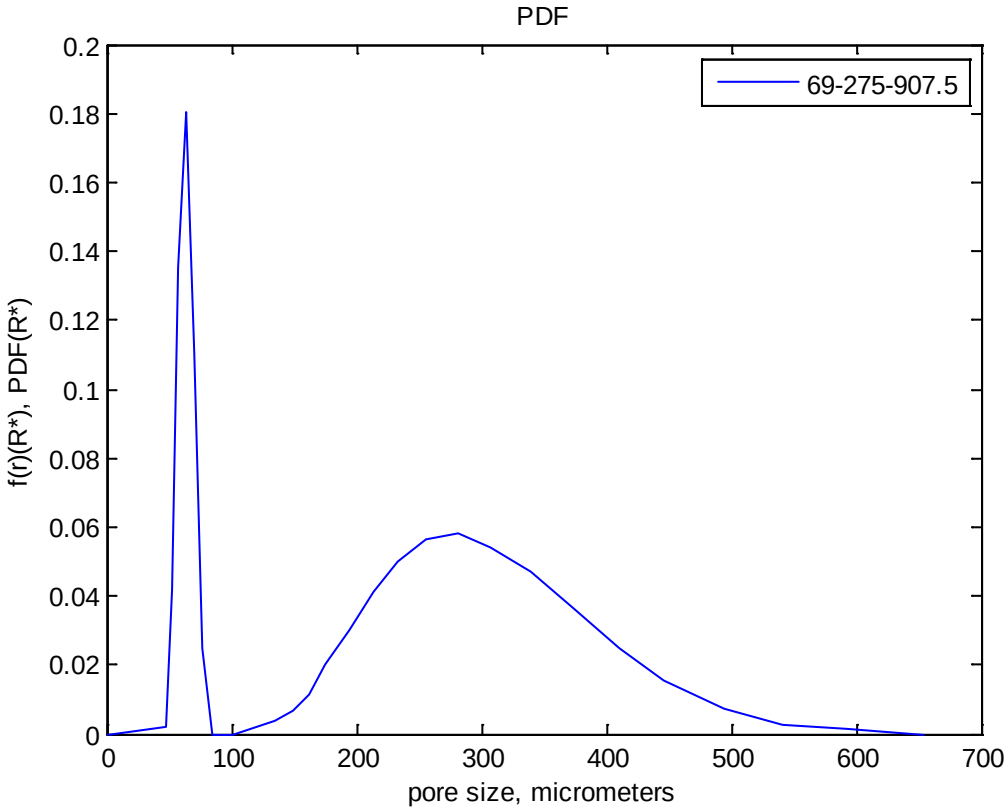

Figure 13: PDF of pore size distribution, 69_275_907.5

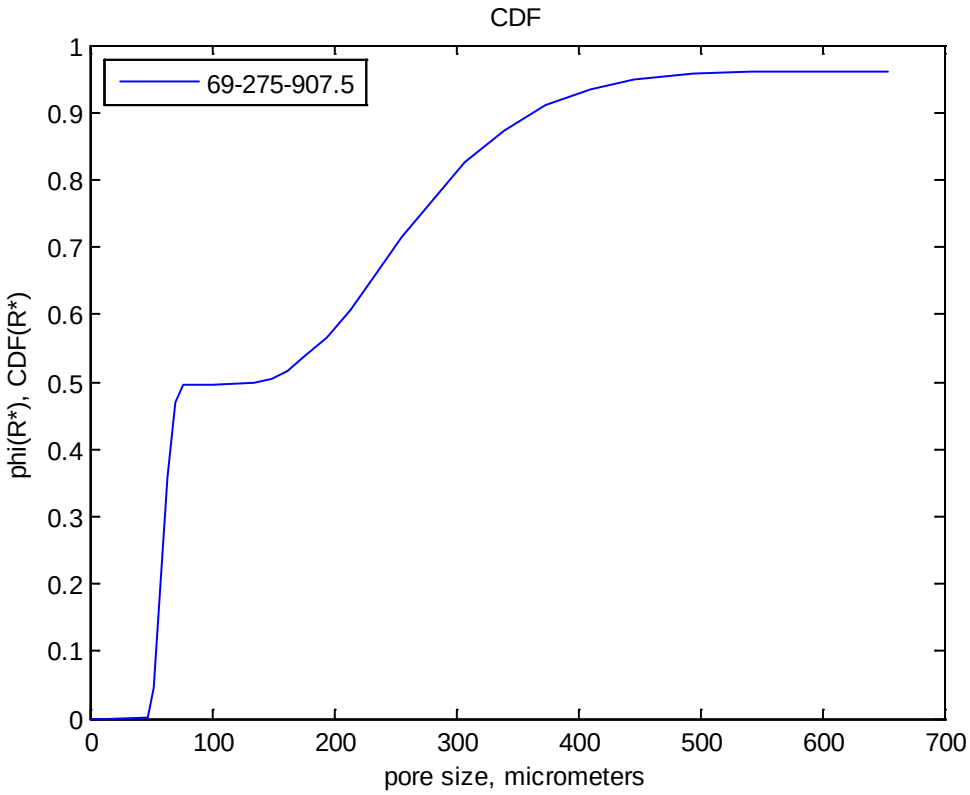

Figure 14: CDF of the pore size distribution, 69_275_907.5

The resulting Pore size distribution (PMF) and cumulative distribution function (CDF) are shown in Figure 13 and Figure 14. The CDF (f(x)) is the probability that a random variable with a given probability distribution will be found at a value less than or equal to a particular value of the pore radius, x. Mathematically it can be represented by Eq. (53).

$$CDF = \int_0^x PMF(x)dx \qquad \textbf{(53)}$$

The CDF is the integral of the PMF from 0 to the value of interest, x. This will be used to estimate the liquid saturation using the R* cutoff radius proposed by Kovalev. Within the context of a pore size distribution, when looking at the CDF at a particular R*, the probability that all the pores up to R* are filled with liquid can be found. Note that the nomenclature of Uhle [39] has been adopted to describe the PDF and CDF as f(r) and ϕ(r), respectively.

Note the characteristic double peak in the PMF and the plateau in the CDF, are indicative of a bivariate distribution. It is important to note that the peak for the particles is much steeper than for the clusters, indicating less variation in their shape. This work is focused primarily on the period after nucleation has begun, when vapor is generated within the wick and is able to escape. The transition from pure conduction to nucleation and percolation within the wick is complex and outside the scope of this work. These transitions would occur on the far right hand side of the PDF.

3.2 Liquid Saturation

The next component of the model to be discussed is the relationship between the pore size distribution and the liquid saturation where liquid saturation is defined as the local fraction of the porosity occupied by the liquid phase.

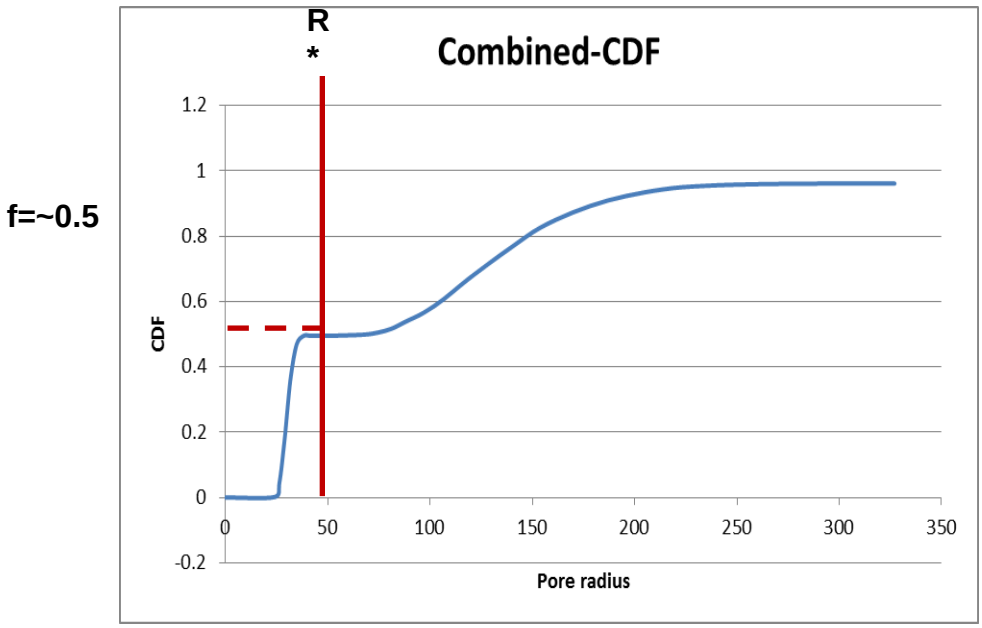

Figure 15: Generalized CDF of wick

Once evaporation has begun in the wick, some of the liquid will be cleared from the large pores and the liquid saturation will have a value less than 1 (1 = 100% liquid saturation). The liquid saturation, as R* decreases from its maximum value, will decrease until the plateau occurring at a CDF value of approximately 0.5. This can be seen schematically in Figure 15. The sharp drop off at CDF values less than 0.5 is the point at which the small pores begin to dry out and the small pores are the only remaining wetted pores.

For instance, if the cutoff pore radius was 50 μm, then this would correspond to a liquid saturation level of approximately 0.55, or 55%. This is the method by which the code determines the liquid saturation, by comparing the pore size distribution to the CDF in order to estimate the percentage of pores filled with liquid.

3.3 Permeability

The permeability is based on the pore size distribution and liquid saturation and is calculated numerically following the method originally used by Uhle [39]. Equations (52), (53), and, (54), from her work, show how these values are calculated. First, the overall permeability, K_o, is calculated from

$$K_0 = C \int_{r_{min}}^{r_{max}} r^2 f(r) dr \qquad \textbf{(54)}$$

where r_{min} is the smallest pore radius in the distribution, r_{max} is the largest, and C is a correction factor. The liquid and vapor permeabilities follow once $\phi(R^*)$ is known,

$$\kappa_l \phi(R^*) = C \int_{r_{min}}^{R^*} r^2 f(r) dr \qquad \textbf{(55)}$$

$$\kappa_v (1 - \phi(R^*)) = C \int_{R^*}^{r_{max}} r^2 f(r) dr \qquad \textbf{(56)}$$

The relative permeabilities are weighted by the liquid saturation.

In order to determine the relative liquid and vapor relative permeabilities, the domain is split into the pore sizes filled with liquid and the pore sizes filled with vapor. This division, by definition, occurs at the cutoff pore size, R*. They are then scaled by their respective saturations. Note that since liquid water and vapor are the only constituents, the sum of their

saturations must be equal to one, and thus one can be calculated from the other. The results of this analysis for a 69_275_907.5 wick are shown in Figure 16 and Figure 17.

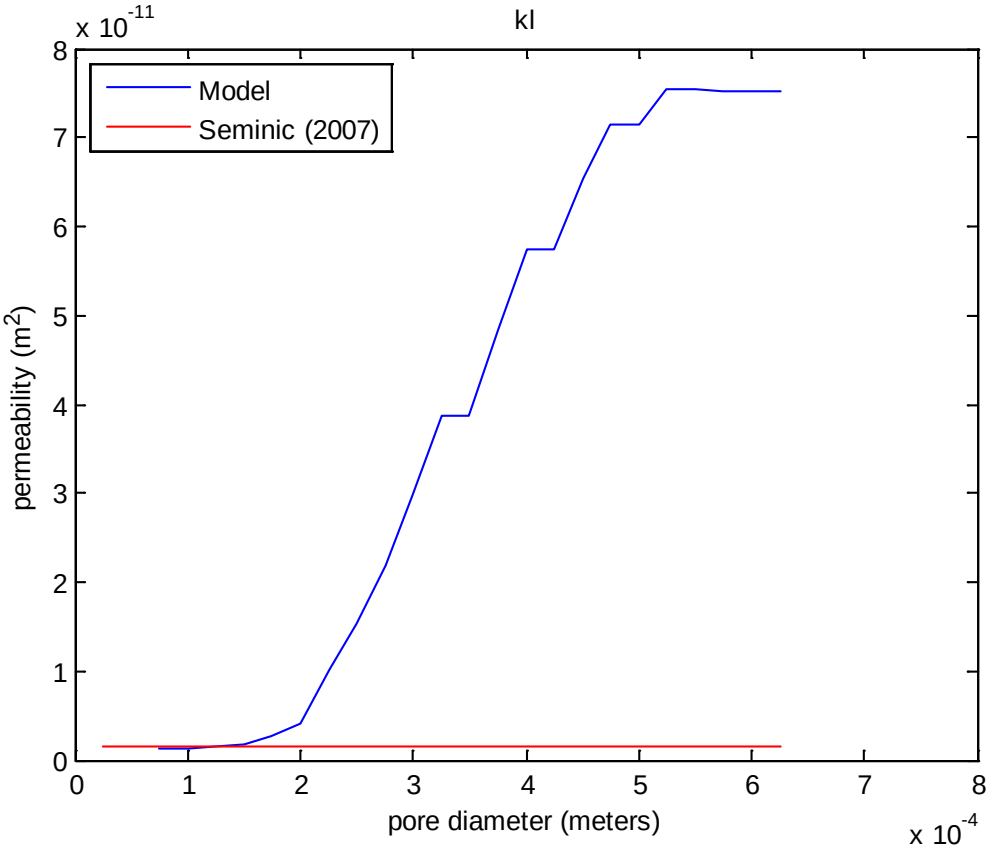

Figure 16: Liquid relative permeability, 69-275-907.5

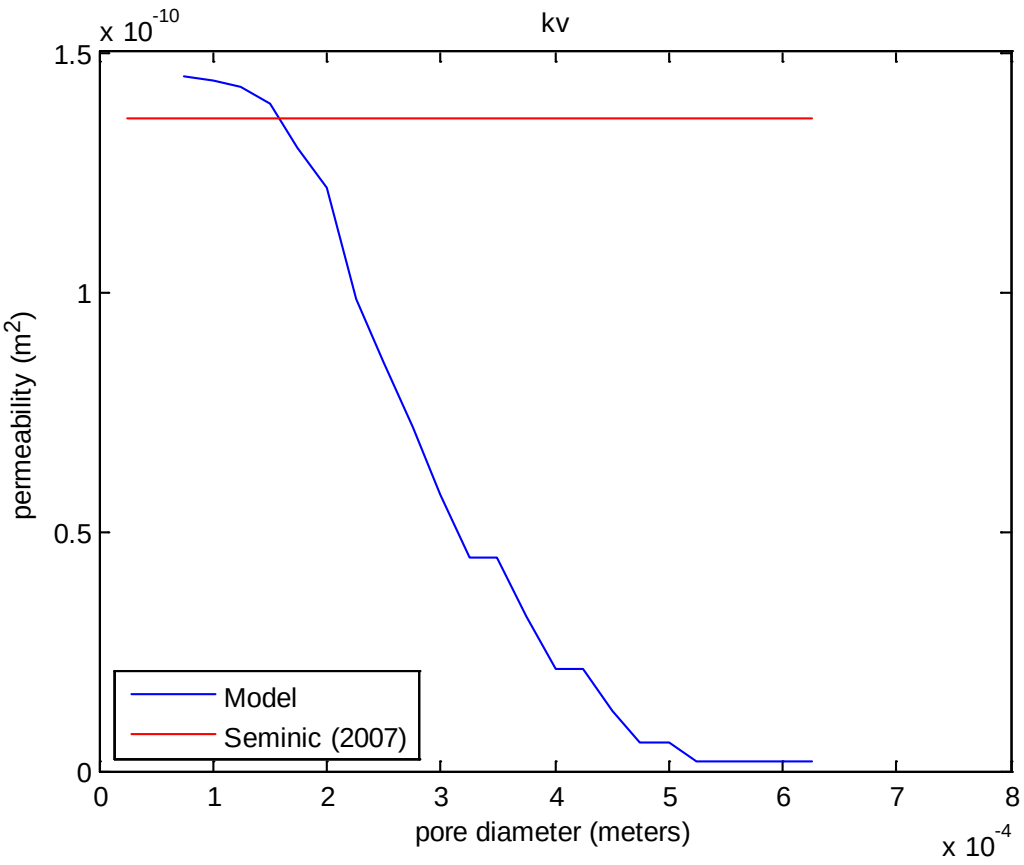

Figure 17: Vapor relative permeability, 69-275-907.5

The red lines on the graph indicate the empirical correlations of permeability obtained by Semenic as a reference. It is worth noting that the values he calculated represented a minimum and a maximum for the liquid and vapor permeabilties, respectively. In the case of the liquid, he measured the liquid permeability of a single cluster, as it would have been prohibitively difficult to obtain it experimentally across the range of irregular large pore sizes. This means that the liquid permeability could have been higher in cases where liquid existed in the large pores. The vapor permeability was measured using monoporous material with particles on the order of the cluster sizes, to approximate flow around the wick. As liquid saturation increases, the available

space for vapor would necessarily decrease, decreasing vapor permeability as a result. These trends are reflected in Figure 16 and Figure 17.

In order to obtain the above results, a fitting parameter, C, was used, as was the case in Uhle's [39] work. The number used for C was the same for both the liquid and vapor permeabilities. Part of the reason for these corrections is due to the fact that the experimental measurements of permeability were made under single phase conditions.

While there is a wide variation in the potential permeabilities, in practice, there was very little variation between values produced by the model and those measured by Semenic. This is because typical cutoff pore sizes were less than 200 μm in diameter for typical liquid saturation values obtained by the model. In this way, single phase estimations of the limiting permeabilities do not necessarily yield inaccurate results as the permeabilities are fairly constant.

3.4 Heat Transfer Coefficient

The volumetric heat transfer coefficient will now be discussed. Similar to Uhle's work, a single coefficient is used to account for the heat transfer within the wick due to evaporation. In this work, the heat transfer coefficient used was a volumetric value that accounts for the latent energy used to convert the liquid inside the wick to vapor. This coefficient includes effects of both the geometry and the fluids. These effects include the tortuosity, interior geometry and flow conditions inside of a wick as well as the saturation state of the liquid. Following the work of Vadnjal [41] it is assumed that at the interface between liquid and vapor, the liquid is at saturation. This is because from a thermal resistance standpoint, the resistance due to conduction

through the wick to the evaporating surface is far greater than the resistance (convection) of the vapor.

In order to determine the heat transfer coefficient, an area based heat transfer coefficient was used as a starting point and then rescaled to a volumetric coefficient by dividing by the local specific surface area (the surface area per unit volume). The area based heat transfer coefficient used in this work was initially derived from the equation for the kinetic limit of heat transfer developed by Carey [7]. In this case, the thermal resistance of the liquid film is dominant and the interface is close enough to saturation to assume that the kinetic theory expression given by Eq.(55) is sufficient.

$$h_e = \frac{2\Psi}{2-\Psi}\left(\frac{h_{fg}{}^2}{T_v v_{fg}}\right)\frac{1}{\sqrt{R_g T_v 2\pi}}\left(1-\frac{p_v v_{fg}}{2h_{fg}}\right) \quad \textbf{(57)}$$

For the wicks examined in this study, the value of h_e was found to be about $2.0\text{x}10^4$ W/(m^2*K), which is consistent with the work of Vadnjal [41] and others. In examining the experimental results of various biporous wicks, it is clear that some geometries transfer heat more efficiently than others. This is likely due to variations in the surface area per unit volume, probably the most defining feature of different sized wicks.

As a side note, a smaller cluster size was chosen, 275 microns, for the first calculation of specific surface area as it had one of the smallest standard deviations of pore radii. It is believed that this smaller spread in pore radii indicates that the particles are more spherical in nature and

thus more regular, and a better approximation as a bed of spheres. Obviously, in the case of a biporous wick, this would still be a conservative estimate due to the fact that the surfaces of the clusters will not be smooth as they are composed of many small particles and pores.

While use of the bed of spheres approximation is adequate for smaller cluster sizes, it becomes less accurate as the cluster size increases. This is due to the fact that the irregularity of cluster and particle shape increases as diameter increases. This is evidenced by the linear increase in standard deviation of cluster sizes seen in Figure 11. This means that the standard deviation is indirectly a measure of how spherical the clusters are and that as they become less spherical, their surface area per unit volume increases. This direct relationship of surface area per unit volume to cluster diameter accounts for the increase in heat transfer seen at larger cluster sizes relative to smaller, more spherical clusters.

3.5 Thermal Conductivity

A correlation for the thermal conductivity of the wicks was taken from Seminic [35]. The thermal conductivity of the (biporous) wicks was correlated with the cluster size of the wick,

$$k_{eff} = 2987 * D(\mu m)^{-0.9} \qquad \textbf{(57)}$$

Note that the thermal conductivity is not a function of particle geometry. This is because contact between clusters is the limiting resistance to thermal conduction relative to the connection to the clusters as there is a physical bottleneck. The cluster to cluster contact is a series of particles in contact, but if one takes into account how many of these interfaces lie in a

single cluster, and that there are far less in the “neck” where two clusters come together, it is easy to see how the reduction in area limits conduction. This equation typically yielded an effective thermal conductivity on the order of 18 W/(m^{o}K).

3.6 Capillary Pressure

The capillary pressure was calculated using a statistical technique similar to what was done to calculate the liquid saturation of the wick. The meniscus in each possible pore was assumed to be hemispherical and the Young Laplace equation was used to calculate the maximum potential capillary pressure of the pore

$$\Delta P = \frac{2\sigma}{R^*} \qquad \textbf{(58)}$$

The maximum probable capillary pressure provided by the pore was then scaled by the probability that the pore existed; i.e. the pore size distribution. This resulted in what is referred to as the “total capillary pressure curve”. The integral of this curve represents the total possible capillary pressure able to be supplied by the wick. An example of this graph is seen in Figure 18.

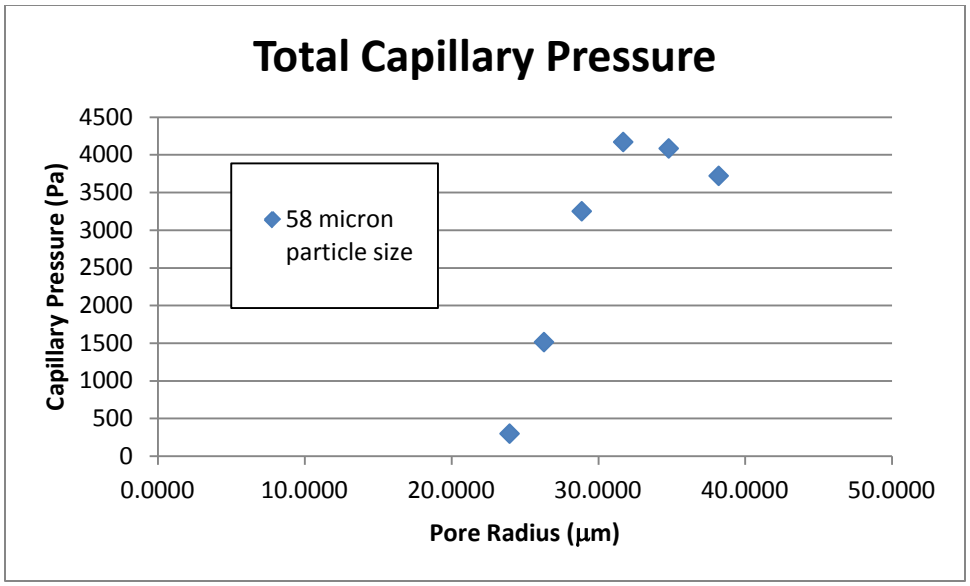

Figure 18: Total Capillary Pressure, Monoporous

Note that there is a well defined peak in the curve that is a function of the pore size distribution. In order to investigate this method, data collected from experiments by Semenic were used for validation. Semenic tabulated the total capillary pressure of several different sizes of monoporous powders for use in his characterization studies. The experimental capillary pressures were determined by increasing the pressure on the menisci in the wick until a fluid column below the wick "broke", indicating the maximum capillary pressure had been reached. The results of validating the numerical estimates of the capillary pressure with Semenic's data are seen in Table 2.

Table 2: Estimations of total capillary pressure of monoporous wicks

Particle Size (average Sieve size)	Model Value of Total Capillary Pressure (kPa)	Seminic (2007) Correlation value of Total Capillary Pressure (kPa)	Error (%)
58	17.04	16.32	4.464
69	16.44	15.43	6.557
82	14.90	13.54	10.03

As seen in the table above, the maximum error in the calculated value of the total capillary pressure is 10.03 %, which is good agreement with experimental data. The pore distributions used were taken from particle analyzer measurements made by Seminic [2007]. Note that the error does increase with larger particle sizes; this is believed to be the result of increasing standard deviation of the particle sizes as size is increased. The fact that the error between the statistical estimate of the capillary pressure and experimental data is less than 11% for all cases seems to indicate that the model is valid in this range of particle sizes. More data would have to be collected to investigate the maximum capillary pressure at larger particle sizes but this represents the range of particle sizes considered in this work.

3.7 Summary

The thermophysical properties used in the model developed in this work are developed and discussed. Some properties used were derived from tables, some from empirical results, and

some from the pore size distribution. It is the properties derived from the pore size distribution which are of the most interest for designing a wick. Expressions for the coefficients used in the Kovalev equations have been developed and it remains to show that results produced by the model can be validated by comparison with experimental data. Once the model is validated, the methods outlined in this chapter to determine the coefficients that can be used to investigate the effect of modifying the geometry to obtain specific performance results from the wick. This can be extended to correlating the dominant geometric effects with the parameters that most positively influence the performance of the wick. The thermophysical properties in this chapter and the model discussed in the previous chapter is the basis for tailoring biporous wicks to specific performance envelopes.

4.0 MODEL VALIDATION AND VERIFICATION

In the previous chapters, the governing equations for a biporous media model were developed based on the work of Kovalev. The thermophysical properties and coefficients were derived from both experimental data and numerically from the pore size distribution. The remaining obstacle to using the Kovalev technique as a practical tool for wick optimization is validation of the model. Validation was accomplished by comparing predictive results of heat transfer using the Kovalev model with experimental data. In this section, the model will be used to predict the behavior of an evaporator composed of porous material. The equations are first validated on a simpler scale by modeling a monoporous wick. After the validation of the monoporous wick, the model will then be validated against a more complex biporous wick.

The validation consists of comparison of the relative superheats of the wicks as a function of heat flux. The mean absolute error (MAE) between the measured and calculated values will be determined and used as a basis for assessing the accuracy of the model. There will also be a discussion about why the results of this model are more effective than simple models which produce similar results.

Once the efficacy of the Kovalev modeling technique is established, the possibility for its use in gaining a deeper understanding of how a biporous wick works is available. This knowledge will provide a method to more accurately predict the dryout of a biporous wick using its pore size distribution. Knowing the relationship between the dryout point and the pore distribution will permit the development of advanced biporous wicks which can further delay the onset of dryout.

4.1 Results and Discussion

4.1.1 Monoporous Wick

In order to verify the assumptions mentioned in the previous chapter, the first wick that was validated was a monoporous wick. This was done because the monoporous wick structure is considerably more regular than a biporous wick and thus it was easier to assess the validity of inferences about the structure of the biporous wick. For instance, a monoporous wick is more likely to be approximated as a bed of spheres and so parameters such as the surface area per unit volume is more easily determined. The monoporous wick is a well known porous media configuration that is more readily understood than biporous material and so is a natural bridge for model validation.

The monoporous wick chosen for comparison was one which was originally tested by Weibel [52]. Weibel's work was chosen due to the relative symmetry between his experimental setup and those of the biporous wicks used for validation. He was testing a range of particle size and wick thicknesses but the primary wick that was used for comparison was one consisting of monoporous particles of 275 μm diameter and 600 μm thickness. The reason this wick was chosen was because the particle sizes in Wiebel's study were on the same order as the cluster size in one of the wicks tested by Semenic [35] that was used for validation of the biporous wicks.

One goal of this approach was to verify that the surface area per unit volume is a valid method of scaling the heat transfer coefficient. In order to test this assumption, an estimate of the pore size distribution for the wick used by Wiebel was generated so that the Kovalev model could be used. The surface area per unit volume was calculated for Wiebel's wick based on the porosity and packing estimate. The packing was estimated by comparing the porosity that

Wiebel measured with known open porosities for different packed bed of spheres arrangements. The scaled heat transfer coefficient and pore size distribution were then input into the Kovalev model. This resulted in a temperature difference versus input power curve which was compared to Wiebel's data in order to determine accuracy. The results of this comparison are displayed in Figure 19.

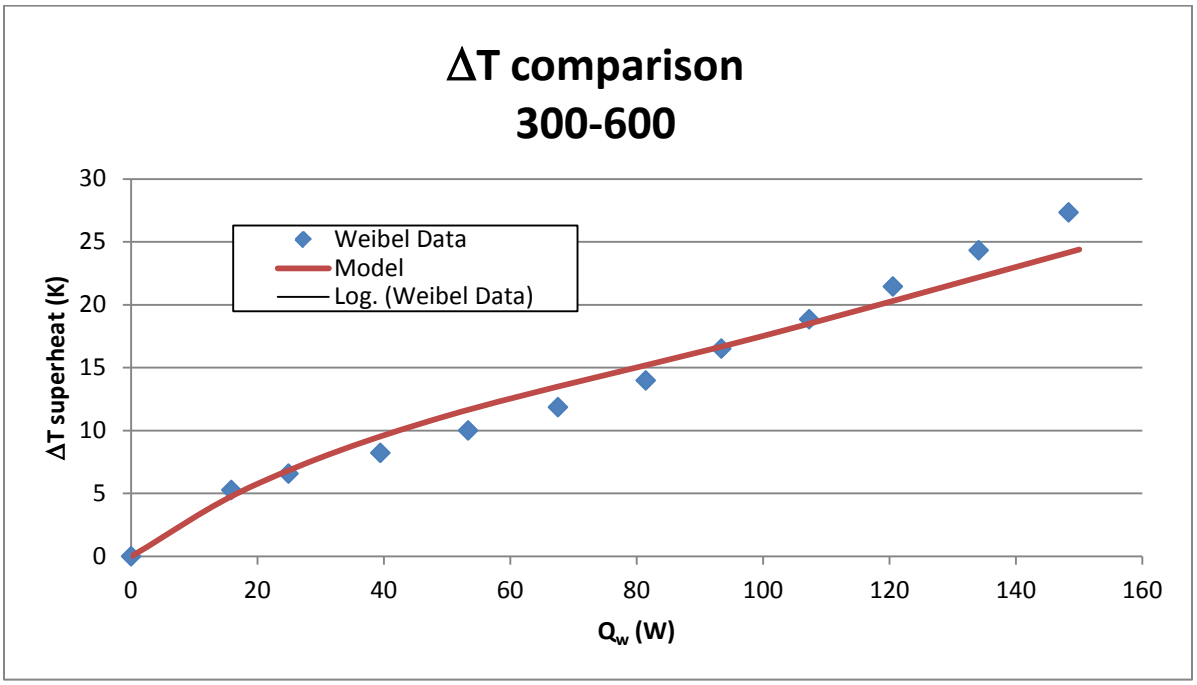

Figure 19: Thermal Performance, Monoporous

For the purposes of this particular investigation, the distribution of 275 μm cluster sizes was used in place of the particles used in Weibel's study as this was the closest approximation to the particle sizes in his work. It is believed that the actual sizes of the particles in Wiebel's wick would have a smaller standard deviation than biporous clusters. However, the distribution of the particles in his work was unavailable.

For the thermal performance, the mean absolute error was 1.42 deg. K. The mean absolute error was calculated using Eq. (57).

$$MAE = \frac{1}{n}\sum_{i=1}^{n}\left| f_i - y_i \right| \qquad \textbf{(59)}$$

where f_i is the i^{th} measured value from experimental data and $_i$ is the corresponding i^{th} value calculated by the model. The relatively low value of the mean absolute error seems to indicate good agreement with experimental data and validation of the model. The results of the relative liquid saturation of the wick are shown in Figure 20.

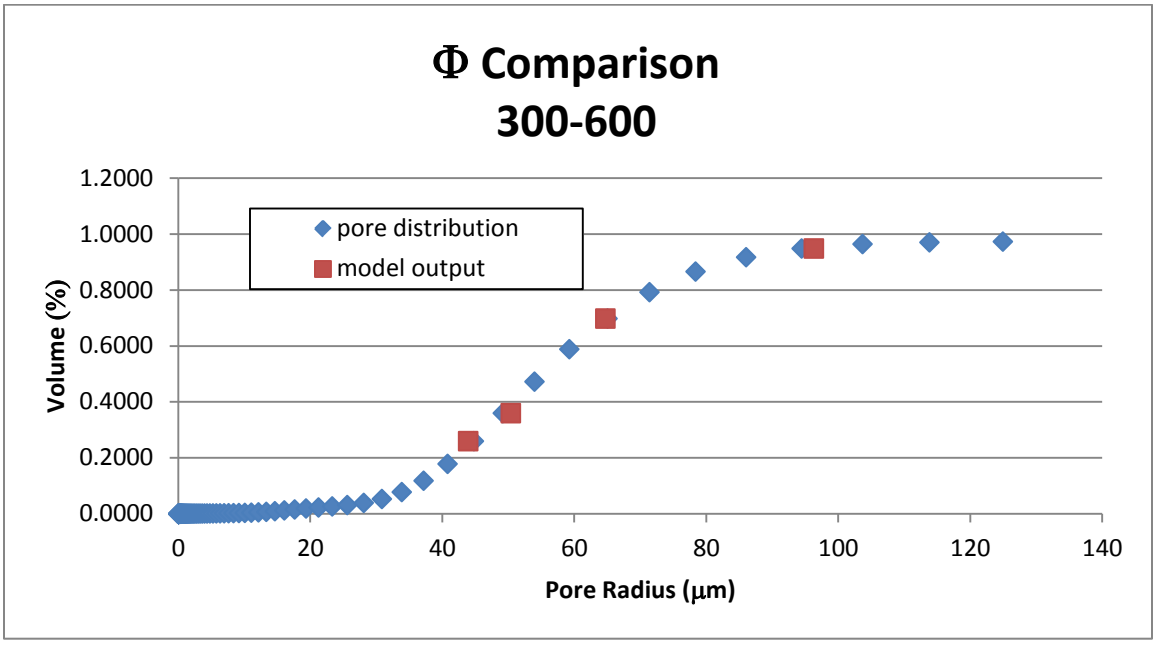

Figure 20: Liquid Saturation, Biporous

The above figure shows not only the relative saturation of the wick but how close the model's prediction of the cutoff pore radius actually is to the pore size distribution of the wick. In this case the results are again very close. This would indicate that the model is an accurate predictor of the cutoff pore radius and that the pore size distribution is reasonably accurate.

In both cases, the results from the modeling showed close agreement with the measured experimental data and pore size distribution respectively. The evaporation heat transfer coefficient was scaled directly as being the kinetic limit multiplied by the surface area per unit volume as discussed in the previous section. Given that the heat transfer data was matched well, it stands to reason that for spherical particles in an evaporator wick, it is valid to assume that the volumetric evaporation heat transfer coefficient is a direct function of surface area per unit volume. Furthermore, because the heat transfer calculation is coupled to the pore size distribution, and by extension the liquid saturation (ϕ), it is reasonable to conclude that it is possible to couple heat transfer and fluid flow to the cutoff pore radius.

With the assertions about the heat transfer coefficient and the overall efficacy of the Kovalev model resolved for monoporous material, the goal will now shift to the application to biporous material. Biporous material adds a new layer of complexity to the model and can now be addressed with confidence because key assumptions have been validated.

4.1.2 Biporous Wicks

As mentioned earlier, a biporous wick is a porous material with two distinct size distributions of pores. The wicks investigated throughout this thesis are composed of sintered copper. To make a biporous wick, a monoporous material is first manufactured. This

monoporous material is then pulverized into small clusters of monoporous material which are sieved in order to render groupings of clusters with similar diameters. It was noted previously that the overall regularity of the cluster sizes was a strong function of average sieve size, with the larger diameter clusters tending to be more irregular. Clusters of a desired diameter are then re-sintered together in order to form a biporous wick. The spaces between the clusters comprise the large pores and the pores between the particles that make up the clusters are the small pores. The construction of a pore size distribution from particle analyzer data was addressed in the previous chapter.

In this section, the pore size distributions for biporous media will be used in order to predict the performance of biporous wicks. The model is used to predict the heat transfer performance of several biporous wicks tested by Semenic [35]. By accurately predicting the heat transfer performance with the model, it is possible to look at how the pore size distribution effects the liquid saturation within the wick and this data will also be analyzed. The method by which the mean error between the curves was determined will also be discussed. The reasoning behind why particular wicks were chosen over others will also be discussed along with the distinction between thin and thick wicks, as described by Smirnov [38].

The results for the five different wicks used for validation are shown below. All the wicks are referred to by a three number designation; the first number is the particle size of all copper particles in the wick, the second number is the average sieve diameter of the cluster size, and the third number is the overall thickness of the wick. All dimensions are considered to be in micrometers.

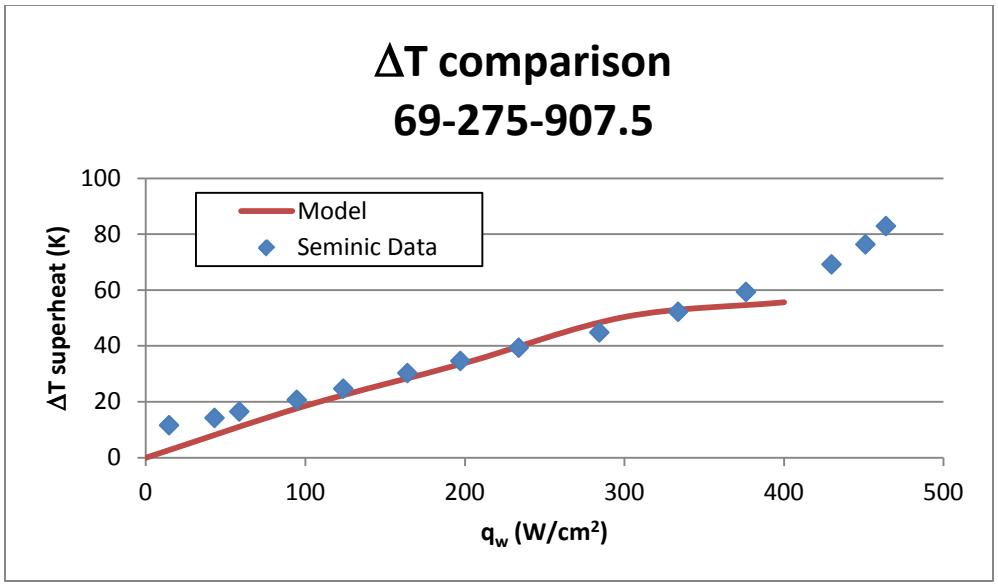

Figure 21: ΔT comparison 69-275-907.5

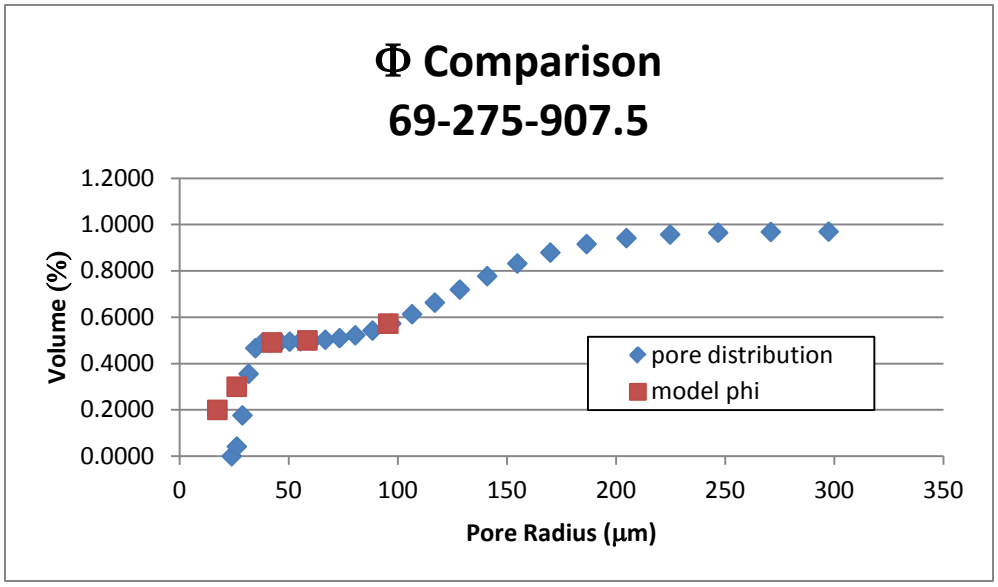

Figure 22: Liquid saturation comparison 69-275-907.5

In the case of the 69-27-907.5 wick, the thermal data matched fairly close but on the last point, the calculated DT appears to be slightly below the trend of the experimental data collected by Seminic. This also corresponds with a relatively low liquid saturation value, seen in Figure

22. This divergence is most likely due to dryout phenomenon and the mechanism behind this behavior is discussed in more detail in the next section.

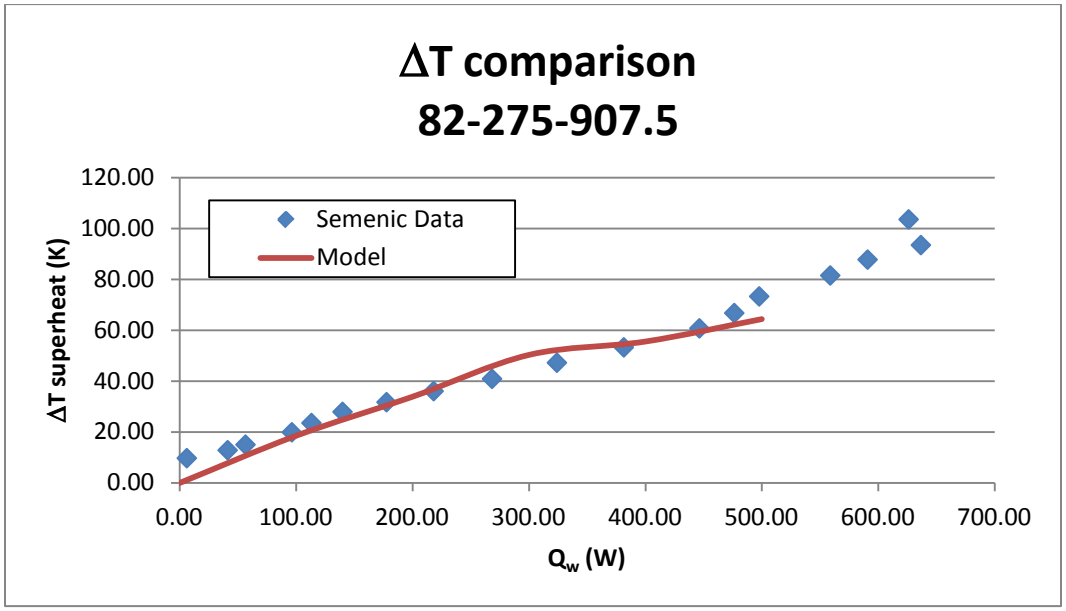

Figure 23: ΔT comparison 82-275-907.5

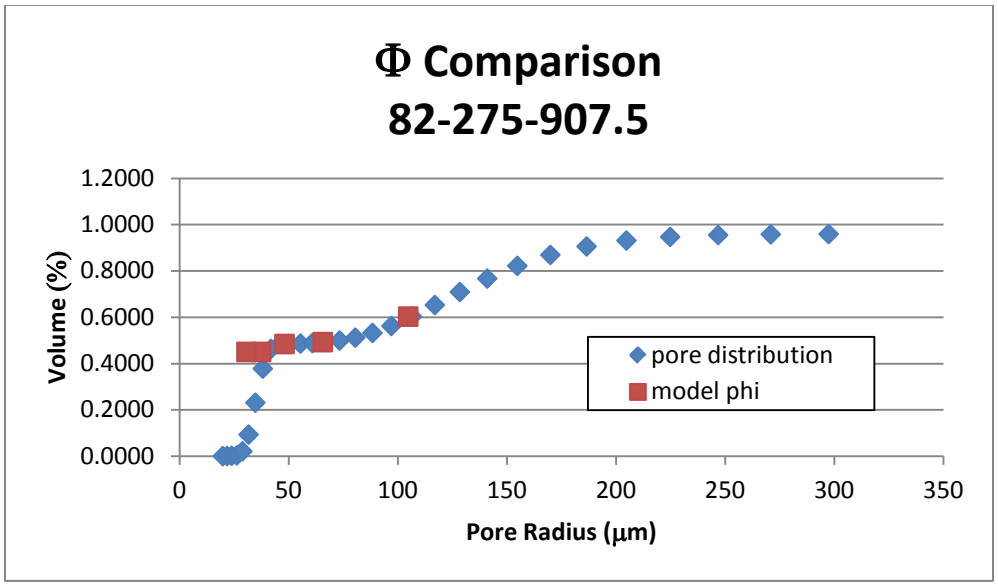

Figure 24: Liquid saturation comparison 82-275-907.5

In the 82-275-907.5 wick, there is some scatter in the heat transfer data but note the slight divergence of the liquid saturation from the pore size PMF, as the volume percentage goes below 50%. This is not the same type of dryout situation noted in the previous wick, though the wick is clearly close to it.

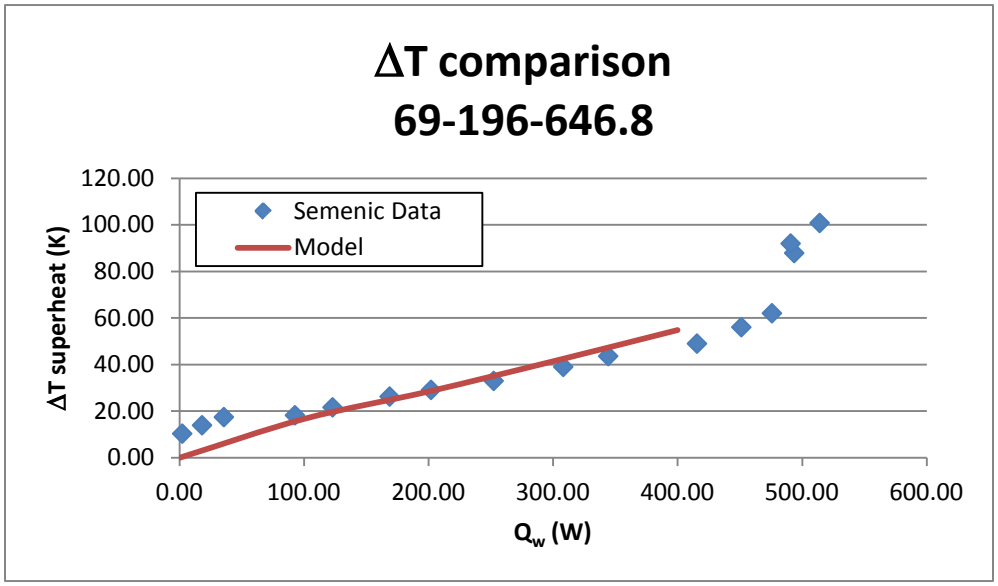

Figure 25: ΔT comparison 69-196-646.8

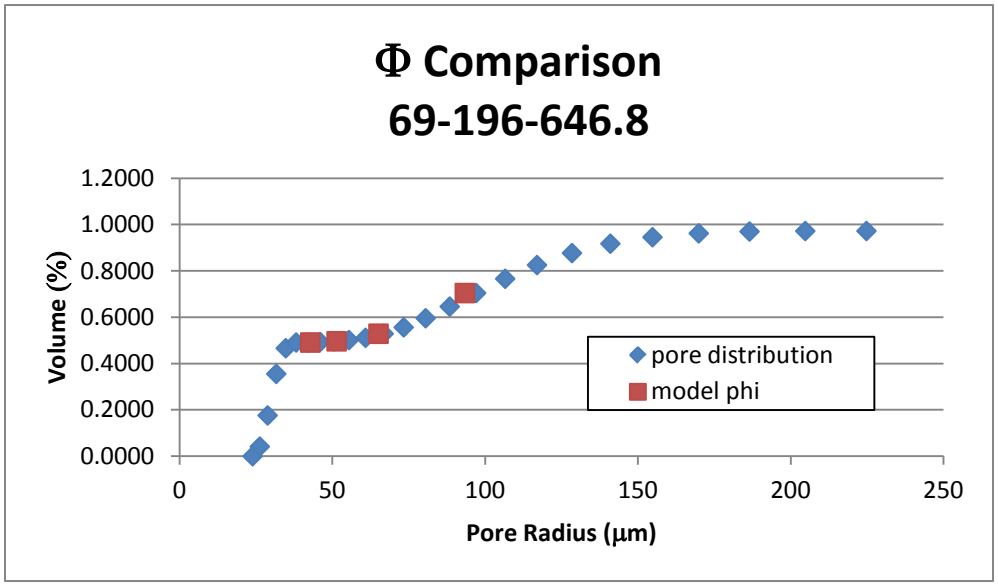

Figure 26: Liquid saturation comparison 69-196-646.8

The 69-196-646.8 wick experimental data most clearly show the trend towards dryout. Here it is noted that the liquid saturation data has not traversed the "cliff" on the left hand side of the PMF, nor have the predictions of ΔT diverged very much from the experimental data, indicating that dryout had not yet occurred.

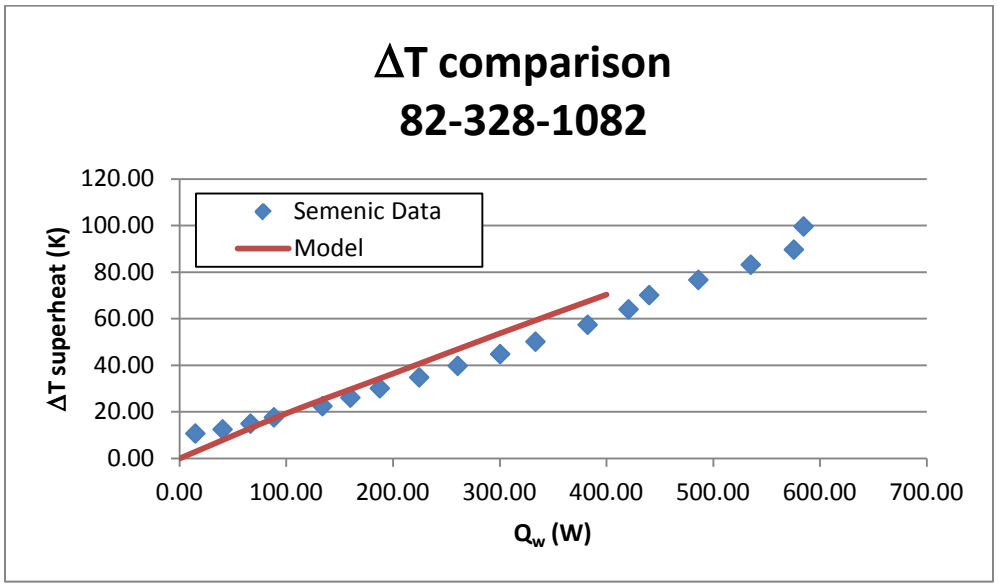

Figure 27: ΔT comparison 82-328-1082

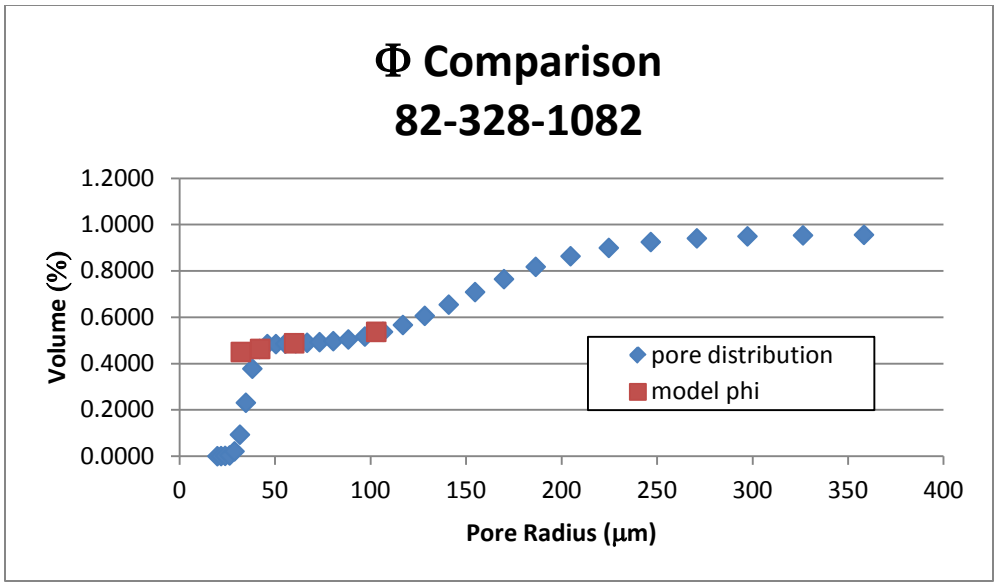

Figure 28: Liquid saturation comparison 82-328-1082

The results of the 82-328-1082 wick are very similar to the 82-275-907.5 wick in that it can be seen how the liquid saturation curve diverges somewhat from the pore size PMF. This could be a feature of the 82 micron pore distribution specifically as it was not observed in wicks of other particle sizes.

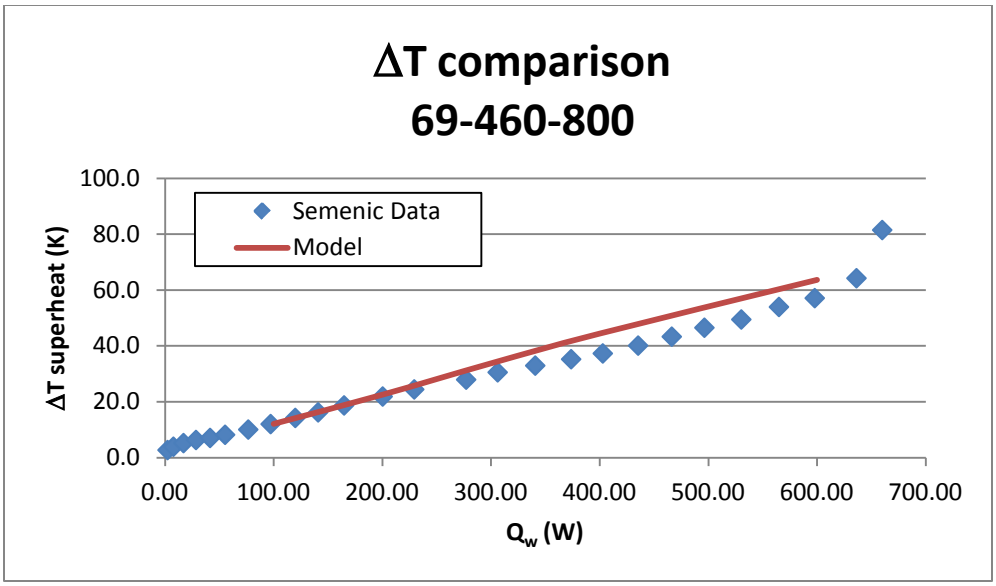

Figure 29: ΔT comparison 69-460-800

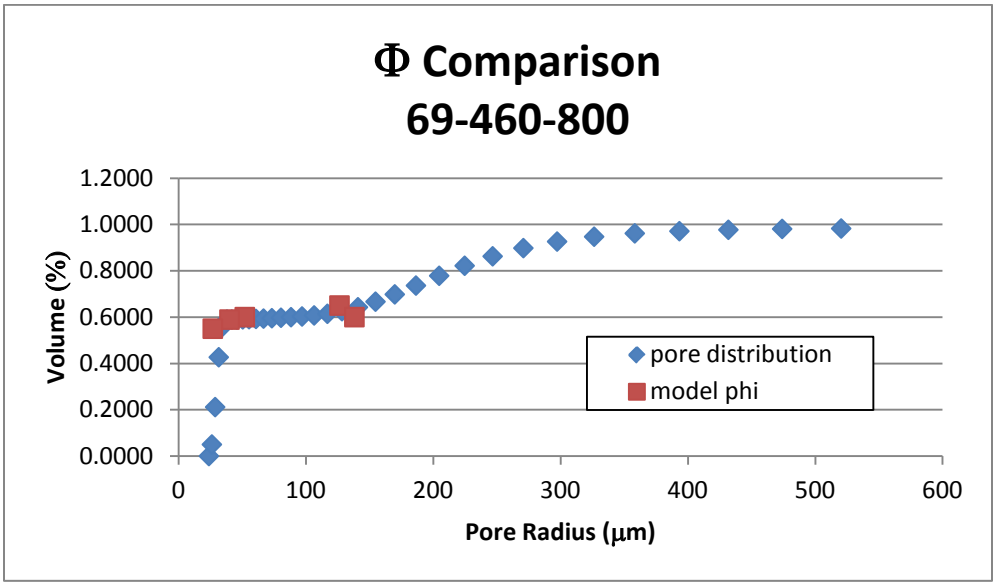

Figure 30: Liquid saturation comparison 69-460-800

The results for the 69-460-800 show that the model predicts very linear behavior throughout the region of interest but over predicted the temperature differences in the region of input powers from 300W to 600W. There was also a unique clustering over the data on the pore

size PMF. The cutoff pore radius changed suddenly between 300W and 400W without much change in the liquid saturation, which remained above 50%. Furthermore, the liquid saturation indicates that it is about to drop precipitously with any further reduction in cutoff pore size meaning it is close to dryout. This is observed in the experimental data where the measured temperature drops make a sharp increase beyond 600W.

The results above are for 5 different biporous wicks showing both their thermal performance and the liquid saturation as a function of cutoff pore radius. The modeling was conducted for particle sizes between 69-82 μm and for clusters varying from 196-460 μm. A table of the mean absolute and relative errors can be seen in Table 3.

Table 3: Mean Absolute Errors for Model Validation

Wick	MAE (K)	MRE (%)
69-275-907.5	5.90	13.30
82-275-907.5	6.16	13.54
69-196-646	5.28	10.15
82-328-1018	6.67	15.25
69-460-800	3.52	12.05

For all the wicks, the maximum mean average error was 6.67 ^{o}C, for the 82-328-1018 wick and the minimum error was 3.52 ^{o}C with the 69-460-800 with 10.15% and 15.25% mean relative errors, respectively. The mean relative error is calculated using Eq. (58), where *f* is the measured experimental data and *y* is the calculated value.

$$MRE = \frac{1}{n}\sum_{i=1}^{n}\frac{\left|f_i - y_i\right|}{y_i} \qquad \textbf{(60)}$$

The error was determined by fitting a least squares regression curve to the experimental and model data. These curves were then compared to each other in order to produce an estimate of the mean absolute and relative errors for the data. For the temperature ranges of the measurements, type K thermocouples were used which have an uncertainty of +/- 1.1 ^{o}C. Even though the mean absolute error exceeds the uncertainty of the thermocouple, the fact that the measurement was generally under 16% relative error for all of the wicks indicates that a good prediction was made.

It is worth noting, that the model started to underpredict the experimental data as heat flux was increased into the region where it was believed that the wick was drying out. Dryout is marked by a sharp rise in the ΔT's with little change in input power. The model deviates from the performance in this region because a separate criterion is needed to determine dryout, which will be discussed later. Once the dryout criterion is met, the model is no longer adequate for predicting the performance of the wick because the wick is in a different region of performance.

With respect to thermal performance, the predicted data matches very well with experimental results. For the most part, in the regions of interest, the performance is somewhat linear, but this is to be expected as the liquid saturation will not vary by much once the spaces between the wick begins to clear out. This phenomenon was also noted by Lin [22]. All of the modeling runs for the biporous material were started at an input power of 100 W because the transition between pure conduction and evaporation within the wick was not a primary focus of this work. The modeling runs went up to between 400-500 W of input power and then concluded because it was believed that this is where the main dryout of the wick began to take place. This

was partially indicated by the divergence of the numerical curve from the experimental one. Further analysis of the physics that govern dryout will be discussed in Chapter 5.

The code seemed to also accurately predict cutoff pore radii, as they were consistent with the pore size distribution. There tended to be increased scatter after the cutoff pore size decreased below the peak of the small pores. There is likely to be some instability here due to the fact that this region would correspond to the point where the liquid meniscus would begin to retract into the clusters and performance would degrade until complete dryout. One could expect this instability in both the numerical and experimental cases. In the numerical case, there is a drastic slope change in the pore size PMF and the sudden change in saturation values would have an adverse effect on convergence. Relaxation coefficients were used in the code in order to help smooth out the transition around the "cliff" formed by the transition from large pore dry out to small pore dryout. The relaxation coefficient tended to be the smallest (meaning that the relative change from one numerical step was the smallest) at this "cliff".

Likewise in the experimental case, there would be instability as the large pores dried out. The biporous wick, by its very nature, is very complex and the large pores are highly irregular and tortuous. Dryout of these pores would not be uniform, especially in large pores where very little vapor could flow through relative to other large pores. Since all large pores (and small pores for that matter) are not created equal, the dry out process would be very heterogeneous with respect to spatial location within the wick. As such, dry out is a very convoluted process that is not easy to quantify and, as a result, is generally only discussed in qualitative terms, such as a sudden temperature rise.

The results of the comparison between the model and experimental data show that the Kovalev type modeling is reasonably effective at predicting the performance of thin monoporous

and biporous wicks. Several biporous wicks were investigated as well as a monoporous wick experiment that was conducted at Purdue. It was desired to obtain results over as wide a range of particle and cluster sizes as possible and so any data from Seminic's studies that could be used, was. The investigation conducted by Weibel was included as a reference to help convince the reader that this modeling methodology was valid since it could be used to predict different types of wicks, not just biporous. As stated in the background, many assumptions are made in modeling biporous material to make the modeling tool versatile and care is taken so that the assumptions do not introduce more error.

Several of the models discussed in the background section, that used similar methods to predict the thermal performance of porous material also showed validation results that are on the same order of this work. The differences between those works and this one are detailed in the background but it is believed that since this work utilizes the pore size distribution on a local level and doesn't make the distinction various phase boundaries, it captures more of the heat transfer phenomenon in biporous wicks than previous modeling efforts. Being able to directly correlate the liquid saturation to a pore size distribution profile permits the use of this modeling tool to directly relate performance to a desired pore distribution. This can be used to optimize wicks and/or tailor wicks for particular applications such as a maximum heat flux, or factor of safety before critical dryout.

4.2 "Thin" vs. "Thick" wicks

The distinction "thin" is made based on the suggestion of Smirnoff [37] and is discussed here to explain why the model used here is only suitable for use in "thin" wicks. The application to wicks of other geometries is the focus of future work. This is based on his assumption that a thick wick has a thickness considerably higher than 10 times the pore size. All of the wicks

investigated in this work are thinner than this when bases on cluster size and are thus considered to be thin by this definition. This is important because the behavior of wicks can vary greatly as their dimensions change. Smirnoff suggested that certain transition phenomena can take place within wicks at lower heat flux. For instance, at low heat fluxes, when there is sufficient power to nucleate, bubbles will form but as they exit the thermal boundary layer near the wall, condensation will begin to take place within the vapor bubble and the channel will function much the same as a heat pipe. That is to say that vapor will be produced at the base of the bubble and condense at the top, in continuous circulation until the heat flux is increased to where the vapor will escape.

The reason this is being brought to the reader's attention, in reference to the thin wicks investigated in this work, is to explain why a relatively high heat flux was chosen to begin the modeling runs of each wick and the reason by which this model is not used for thicker wicks. Seminic's wick that did not dry out at heat fluxes up to 1.37 kW/cm^2 was 2mm thick, making it considerably larger than the wicks investigated here. If one looks at plots for the effective heat transfer coefficient of a thin wick, there is a single peak, which is believed to be the point where liquid begins to retreat into the clusters. However, a thick wick has two peaks, of which it is postulated the first peak corresponds to the maximum of the "heat pipe" effect, and the second is similar to the thin wick peak where liquid retreats into the clusters.

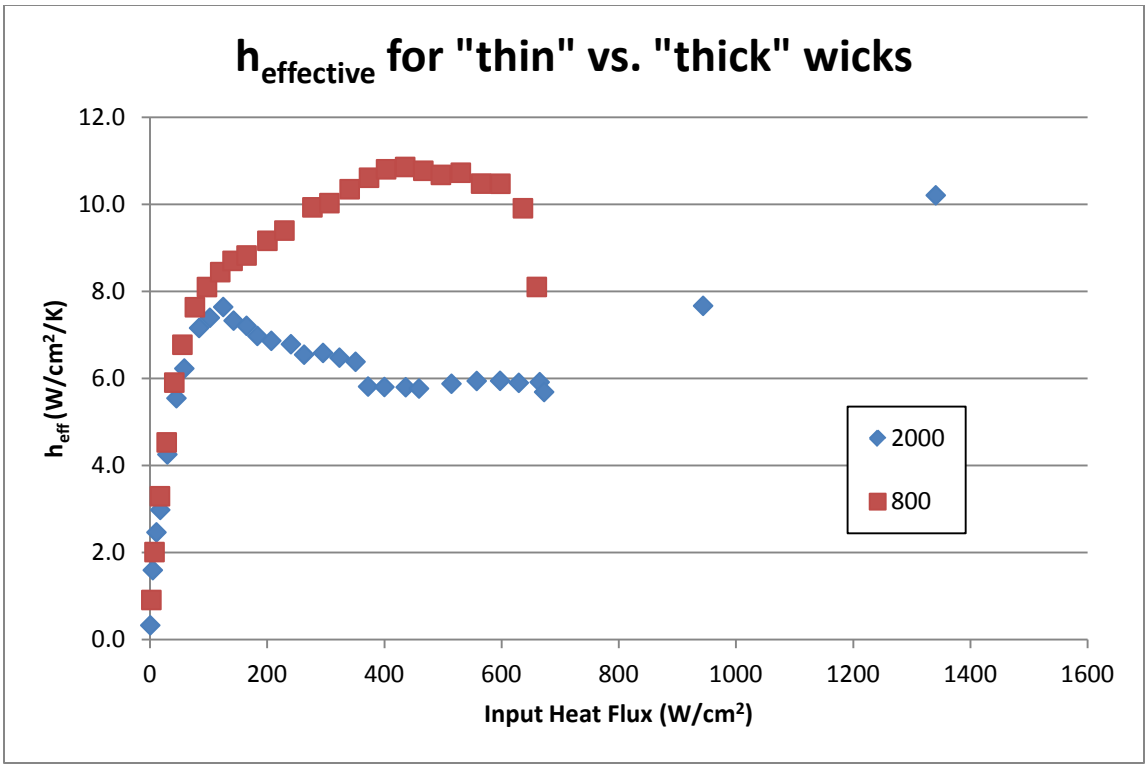

Figure 31: Heat Transfer Coefficients for Thin vs. Thick wicks [35]

The modeling results presented in this section were validated against experimental data from multiple sources for a range of geometric parameters. Since there is good agreement with experimental data across this spectrum of wicks, it is believed that this modeling technique is an adequate predictive tool for the boiling transition region of bidisperse wicks. Using this methodology, the model will now be used as an analytical tool to try and understand the physical processes taking place in the wick such as maximum heat transfer coefficient and dryout phenomena.

4.3 Summary

In this chapter, the validation of the Kovalev modeling method for thin monoporous and biporous wicks was presented. The model takes as an input the amount of power entering the

wick from the heater and produces a temperature difference from the heater interface to the vapor space as a result. The results of the validation showed that the model predicted the performance of the biporous and monoporous wicks to within a maximum mean relative error of 6 ^{o}C and maximum mean relative error of 16%. These maximum errors were collected on a range of particle sizes from 69-82 μm and cluster sizes from 196-460 μm. Over the range of wick geometries studied by Semenic [35], an experimental error of 16.5% was determined. Since the average error of the model from experimental data was on the order of the experimental error, the model was considered to have been validated.

The range of wick geometries that were investigated provides a space in which to investigate the physical processes that govern dry out in the wick. The model was tested up to input powers that were believed would cause dry out in the wick. In the following the chapter, the results of the model will be analyzed in order to determine the quantitative parameters which precipitate dry out in biporous wicks. This information can help form a definitive statement on how to design wicks which can delay the onset of catastrophic dry out and optimize performance.

5.0 DRYOUT

The previous chapters of this dissertation were primarily concerned with the development and validation of a model which could accurately predict the performance of biporous wicks. This was done by using knowledge of the pore size distribution to estimate the thermophysical properties of the wick and the results were validated against previously collected experimental data. Having completed this task, the remaining portion of this dissertation details the effort to apply the model as a tool to optimize biporous material. This will be done by using the model to predict the dryout point of a biporous wick based on its pore size distribution. By determining what parameters of the pore size distribution the dry out of the wick is most sensitive to, optimized pore size distributions and wick geometries can be suggested.

In this section, the statistical method used to estimate biporous wick dry out will be detailed. The method compares the required pressure drop between the liquid and vapor phases determined by the model with the maximum effective capillary pressure from the pore size distribution. The maximum effective capillary pressure was discussed in Chapter 3 and is an estimation of the total capillary pressure based on the pore size distribution. Once the method for determining dryout is explained, it will be validated with experimental data. The results of validation will be used as a basis for suggesting better wick geometries for postponing dry out.

5.1 Dryout Phenomenon

Before the method used to determine dryout is discussed, it is important to distinguish what the term dry out refers to in the present work. In Semenic's work, he believed that the wick began drying out at the point where the large pores, the spaces between clusters, began to dry out. He

theorized that, at this point, the liquid would begin to retract into the clusters and the efficiency of the heat transfer would decline. Without liquid on the periphery of the clusters, there would be far less surface area taken up by evaporation and the frictional losses seen by the vapor would increase since the vapor would now need to exit through the small pores and into the large pores before leaving the wick. Note, the wick would still be wetted and would continue to function. However, the performance would begin to decline as liquid retracted into the clusters.

A catastrophic dryout would occur when liquid was no longer able to be supplied between the clusters and the heat transfer would be dominated by conduction, not evaporation. Due to the porous nature of the material, the thermal conductivity would be quite low meaning the surface temperature would also rapidly increase. It is catastrophic because the temperature drop across the wick associated with conduction would be nearly an order of magnitude larger than any case where evaporation dominates.

Seminic hypothesized that a wick begins drying out when the overall heat transfer coefficient of the wick begins to decline. The overall heat transfer coefficient is defined as the input heat flux divided by the temperature difference between the wall/wick interface and the vapor temperature above the wick. This effect was observed as a trend in his experimental data; the heat transfer coefficient would rise to a peak value before declining and then eventually the wick would catastrophically dry out. In order to compare with his data, the model's prediction of dry out will be validated against this point.

This makes logical sense as the largest heat transfer coefficient would be observed where the maximum number of small pores are wetted and exposed to the large pores. This arrangement of the wick exploits the biporous wicks greatest strengths in that the maximum

capillary pressure is available as the liquid vapor interfaces are all within the small pores and with no liquid in the large pores, maximum vapor permeability is attained.

At heat fluxes lower than the one associated with the maximum effective heat transfer coefficient, a portion of the large pores is filled with liquid, which decreases the overall area available for thin film evaporation. At heat fluxes larger than the critical value, liquid contained within the cluster is evaporated away, causing the menisci to recede into the cluster. This reduces the overall heat transfer because the frictional losses increase as vapor must be pumped out through the small pores into the large pores.

The present work generally adopts Semenic's terminology with respect to dry out. Dry out will be assumed to be when the large pores of the biporous wick are dry and the small pores have receded significantly into the clusters, initiating a decline in the effective heat transfer coefficient of the wick. This differs slightly with Semenic's explanation as the modeling effort seemed to indicate that dryout occurred slightly after the small pores began to dry out rather than at the conclusion of the large pores emptying.

5.2 Method of estimating dry out

The technique used to model biporous material and determine the capillary pressure will be briefly discussed. A more detailed explanation of how it was implemented can be found in earlier chapters. In a Kovalev type model [19], certain assumptions are used to circumnavigate the more complex aspects of flow and evaporation in porous media. In a porous wick, Kovalev assumes the wick to be a collection of parallel pores which vary in size from small to large. The

central claim of the Kovalev technique is that within the wick, there is a pore size R* above which the pores are vapor filled and below which, are liquid filled. This is illustrated in Figure 32, assuming that R4 is the cutoff pore radius, R*.

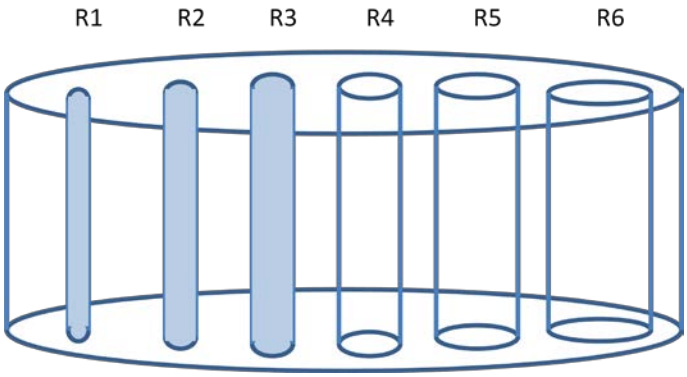

Figure 32: Kovalev Schematic

In general, it is assumed that there is thermal equilibrium between all phases, to make the calculations reasonable. It is generally assumed that there is a pressure gradient seen by the liquid which causes liquid to flow into the wick and a separate pressure gradient which allows vapor to be forced out of the wick, in the opposite direction to liquid.

With regards to the efficacy of the Kovalev technique, Uhle [39] utilized the technique in order to model heat transfer in magnetite deposits. Her work focused on the heat transfer inside of a nuclear reactor, where steam, laden with chemicals, deposited a porous wick on the surface of the fuel rod. This porous material augmented the heat transfer of the walls but was continuously depositing. While Uhle was investigating, what amounts to a monoporous wick,

she was able to achieve good agreement between experimental and modeling results. Furthermore, she made measurements of the permeability and pore size distribution using mercury porosimetry in order to compare these values. Based on her efforts, it can be seen that the Kovalev technique, though simplistic, can readily be applied to complex porous media in order to provide reasonable insight into the performance of a particular medium. The present work is an effort to combine many of these methods in order to better understand dryout in biporous material.

As mentioned previously, there exists some maximum capillary pressure at which the small pores can remain filled with liquid and the large pores filled with vapor. This maximum effective capillary pressure is referred to as the MECP. The MECP is derived from the cumulative distribution function (CDF) of the particle size distribution. Again, the pore size distribution was constructed by superimposing particle analyzer data obtained from Semenic, seen in Figure 33 and Figure 34, and estimating the pore sizes from the particle/cluster sizes.

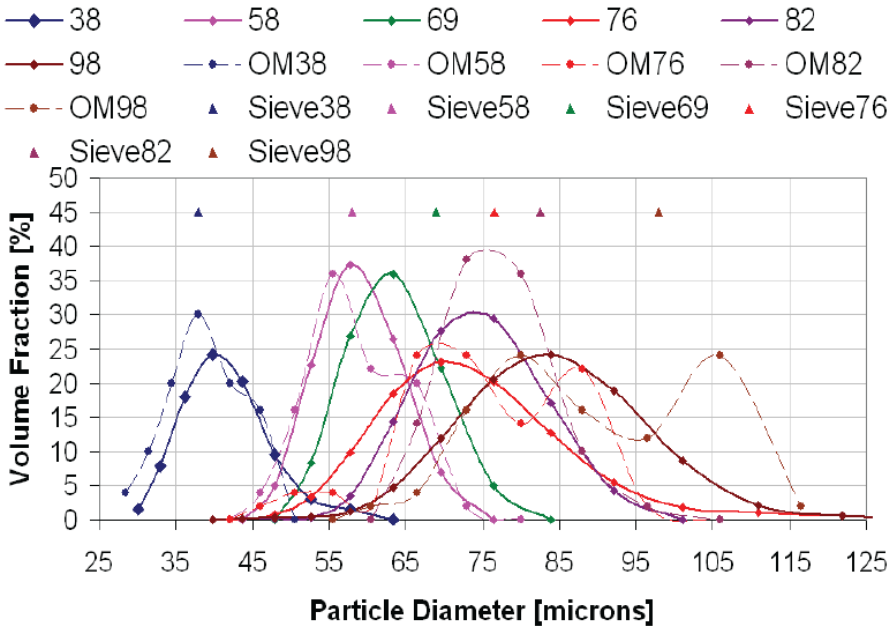

Figure 33: Particle diameter distribution [35]

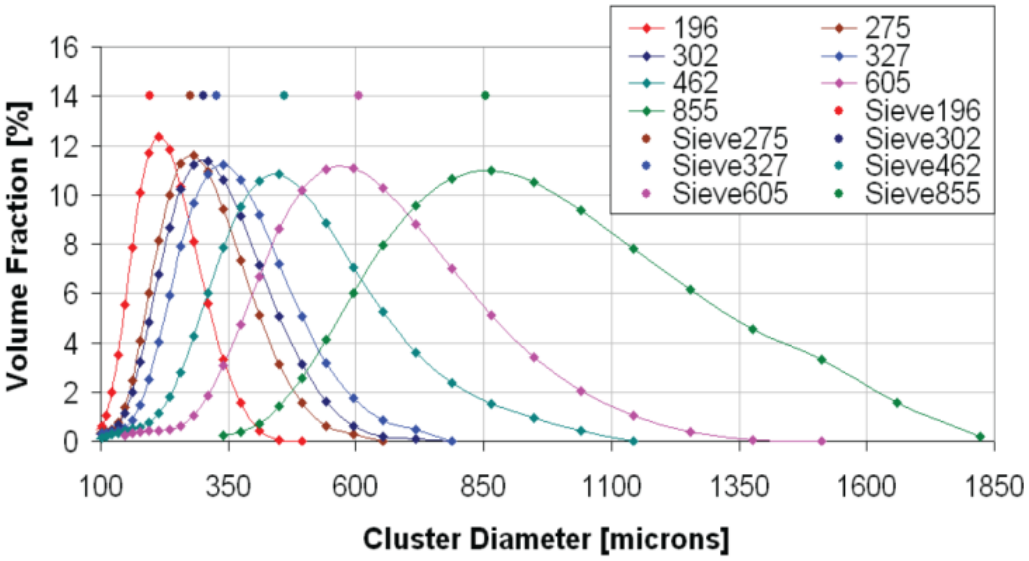

Figure 34: Cluster diameter distribution [35]

The particle analyzer results show the volume percentage various particle and cluster sizes. One important observation of these graphs is that the spread of the distribution tends to have a direct relationship with size. Thus it can be shown that the standard deviation of the particle sizes increases as a function of size. For further reference to the derivation of the pore size distribution, please see Chapter 3. A typical pore size cumulative distribution function is seen in Figure 35.

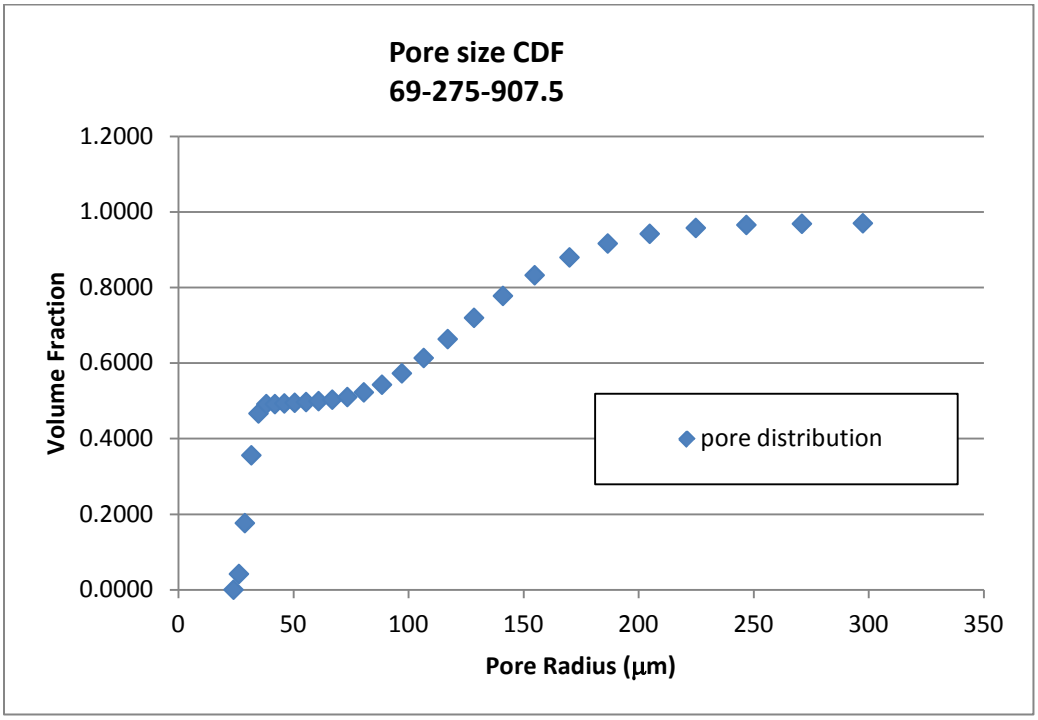

Figure 35: Pore Size CDF; 69-275-907.5 wick

The pore size CDF is the probability that the pore size will be found at a value less than or equal to x. For example, when looking at a pore size of 50μm, there is a roughly 50% chance

that a pore will be less than or equal to 50 μm. The CDF is used to determine the liquid saturation in the wick based on the cutoff pore radius.

In order to translate this into a capillary pressure, it is assumed that there is a potential capillary pressure associated with each individual pore, if it had a liquid vapor interface. This determined by assuming a hemispherical meniscus and using the Young Laplace Eq. (59).

$$\nabla P = \frac{2\sigma}{R^*} \qquad \textbf{(61)}$$

Referring back to Figure 32, if R4 is the cutoff pore radius, then assumptions of the Kovalev model lead one to conclude that a liquid vapor interface exists in pore R4 and there is an associated capillary pressure related to the pore radius. If the CDF value is known at a pore size R4, then the probability that the capillary pressure is less than or equal to the value for R4 and is is also known. If the maximum potential capillary pressure provided by each individual pore, assuming it has a vapor interface in it, is scaled by the probability that a pore size is less than or equal to its size, then the MECP curve is obtained. An example MECP curve is seen in Figure 36.

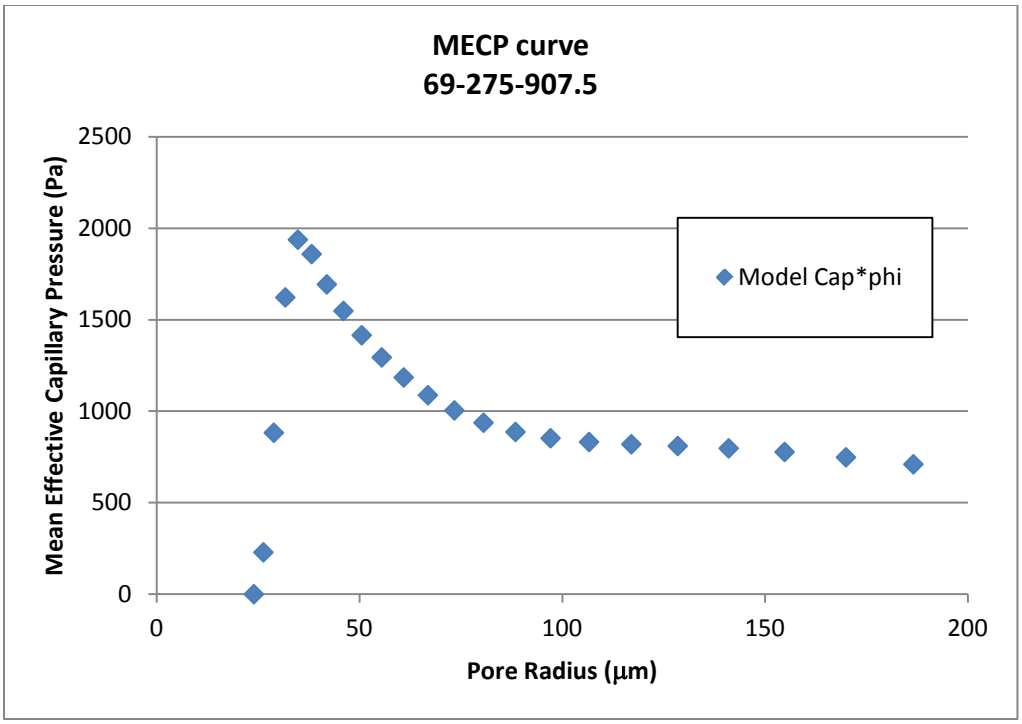

Figure 36: Mean Effective Capillary pressure derived from pore size CDF

Note that the curve in Figure 36 indicates that as pore radius decreases from approximately 200μm (the maximum pore size for the listed wick), the capillary pressure increases until the cutoff pore radius reaches approximately 45 μm. After this point, the curve abruptly drops off. There is a natural peak the capillary pressures because the maximum capillary pressure is achieved when the small pores all effectively contain a vapor liquid interface. This peak value of pressure is referred to as the MECP.

Furthermore, as more of the small pores become depleted, the availability of capillary pressure will also decrease. This peak point is the MECP and will be the point which is of most interest with regards to estimating the dryout of biporous wicks using the previous modeling code.

In order to compare the results, two correlations are needed; the capillary pressure as a function of cutoff pore radius and the input power as a function of cutoff pore radius. The required capillary pressure derived from the modeling code as a function of cutoff pore radius is superimposed over the MECP curve, as shown in Figure 37. This allows the determination of the cutoff pore radius at which the required capillary pressure exceeds the MECP value. This cutoff pore radius is then used to determine what the input power would be the MECP is exceeded and drying out the large pores has occurred. The results of this analysis for five wicks are discussed in the following section.

5.3 Results and Discussion

Figure 37 illustrates both the predicted estimate of the required capillary pressure generated by the model and the MECP curve for a 69_275_907.5 wick, which is derived from the pore size distribution. Note that in Figure 37 the “predicted curve begins underneath the model curve and only exceeds the maximum value sometime at about the same point it crosses the curve.

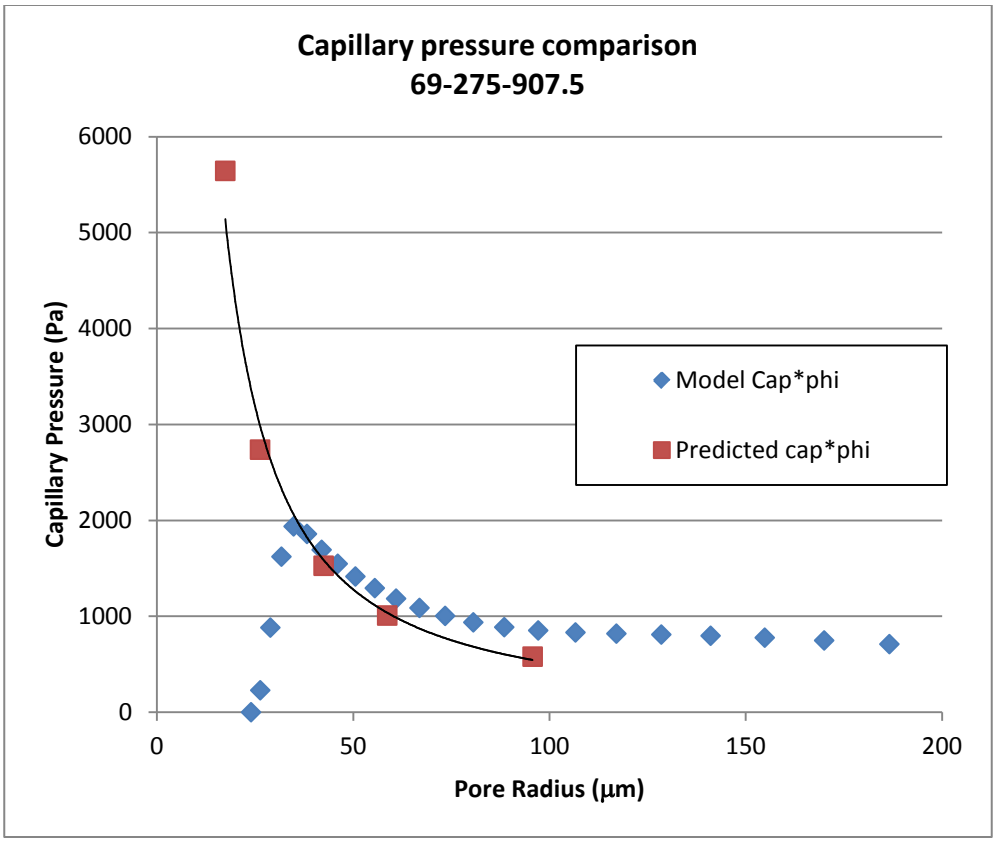

Figure 37: Dryout Prediction, 69-275-907.5 wick

It is important to note that the capillary pressure predicted by the code continuously increases whereas the MECP curve peaks and falls away. The behavior of the MECP curve has already been discussed. However, the reason for the continual increase in the predicted capillary pressure is due to the fact that the model has no way to know when dryout occurs on its own. It must be determined externally so that the code will know to exit this particular heat transfer regime. The code simply outputs what the pressure drop would have to be in order to maintain liquid at the surface. This analysis was carried out for an additional 4 wicks and the results tabulated in Table 4.

Note that in Figure 38, Figure 40, and Figure 41, the predicted curve begins underneath the model curve and only exceeds the maximum value sometime at about the same point it crosses the curve. Only in the wick seen in Figure 39 did the two curves cross well ahead of the actual dry out point.

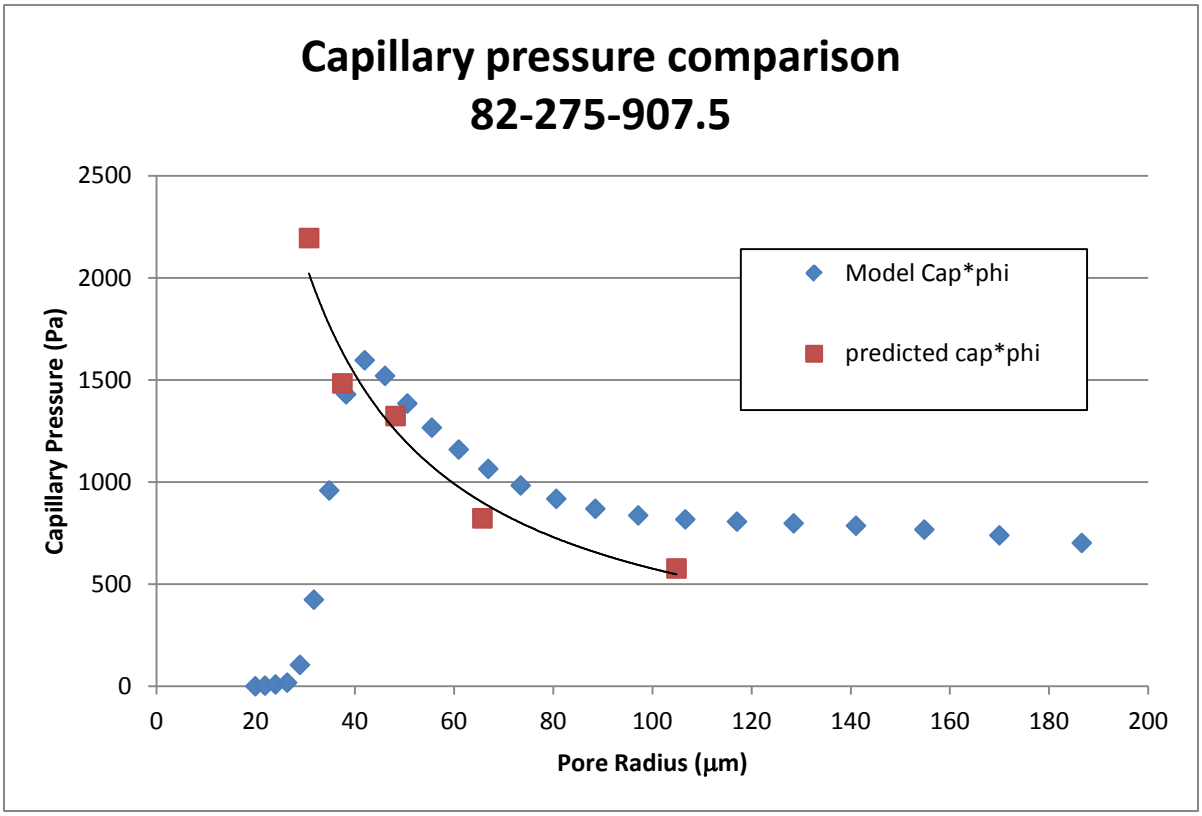

Figure 38 Dryout Prediction, 82-275-907.5 wick

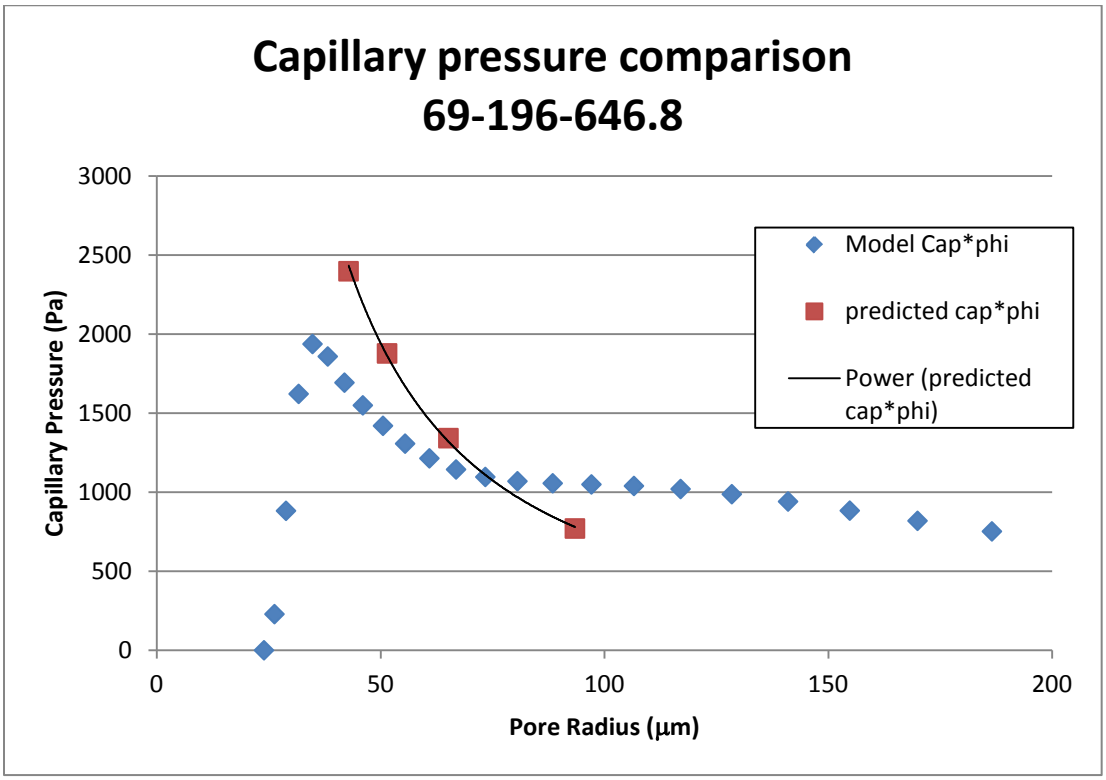

Figure 39 Dryout Prediction, 69-196-646.8 wick

Figure 39 shows the results for the 69-196-646.8 wick, which clearly shows that the predicted curve exceeds the model capillary pressure values well in advance of excceding the maximum value. As this wick had one of the highest errors between the predicted and observed experimental values, it is possible that the pore size distribution used was not sufficiently accurate.

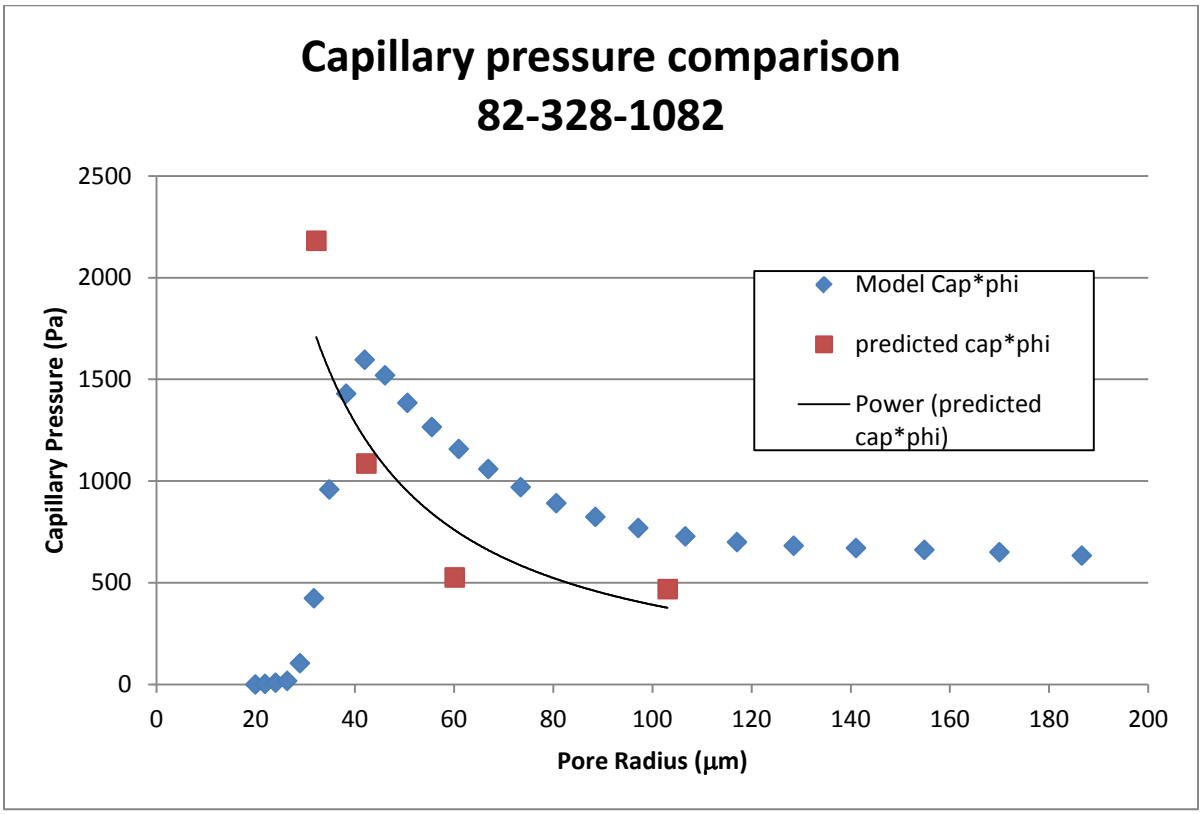

Figure 40 Dryout Prediction, 82-328-1082 wick

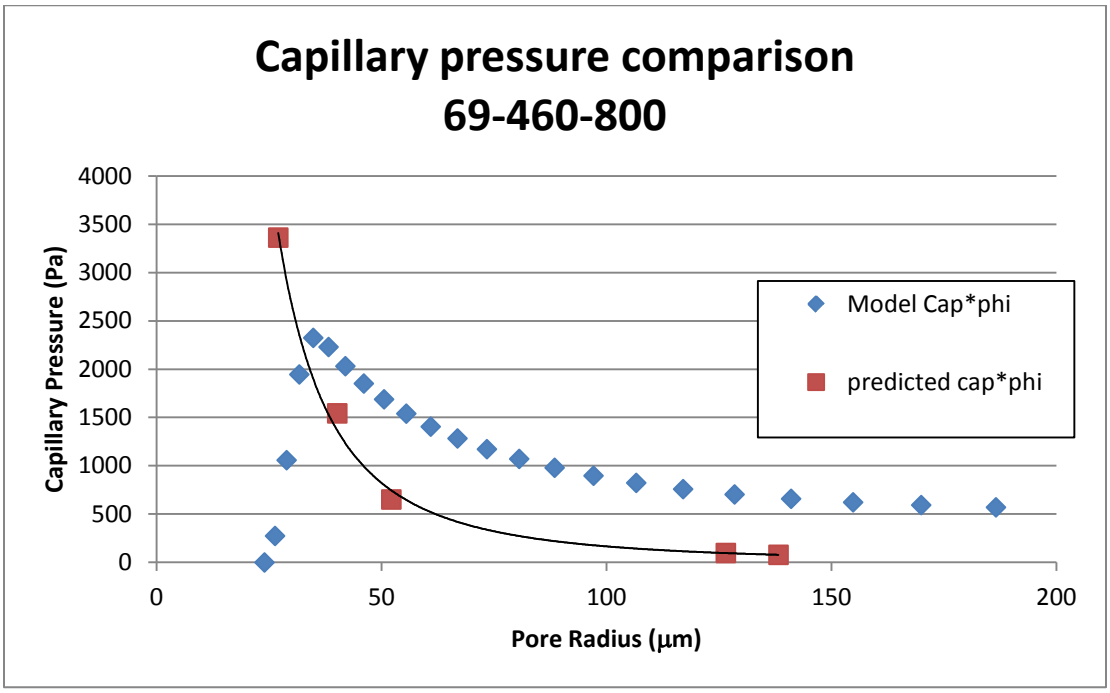

Figure 41 Dryout Prediction, 69-460-800 wick

Table 4: Tabulated dry out data

Wick	predicted	Semenic	error
69-275-907.5	295.59	333.70	11.42
82-275-907.5	388.61	446.56	12.98
69-196-646	311.36	415.65	25.09
82-328-1018	385.70	300.53	28.34
69-460-800	488.66	435.53	12.20
	average error		18.01
	median error		12.98

The full results of this analysis are displayed in Table 4. Three of the wicks had errors on the order of approximately 12% while the remaining two were on the order of 25%, leading to an

average error of 18%. Considering that complex phenomena taking place and the averaging assumptions used to close the model, this was considered to be an acceptable error for the prediction of dry out. For comparison, the average experimental uncertainty associated with Semenic's experimental determination of the performance of biporous wicks was approximately 16.5%. Consider that, even if 18% error is expected on average, this still provides a reasonable method to predict dry out in biporous wicks if the primary goal is to simply delay dry out.

For a biporous material, there is obviously a more complex situation to consider. The methodology, however, is similar to what was used to determine the maximum capillary pressure in monoporous material. It is worth noting that the predominant contribution to the maximum capillary pressure value is from the monoporous material, but some pressure is provided by the large pores at higher liquid saturations. This is expected, as the traditional interpretation of the onset of dry out was when the large pores were depleted of liquid. When the required capillary pressure from the code exceeds the maximum capillary pressure provided by the wick, then it is believed that the onset of dry out has begun in the wick.

In looking at the results, the wicks with the highest experimental and predicted dry out heat flux were the 69_460_800 and 82_275_907.5. The next section discusses what the reason for this is and how to exploit this observation and to optimize a biporous wick.

5.4 Optimization of biporous wicks

The question now becomes, how does one use the information presented by the prediction of dry out to design better wicks? In looking at the schematic pore size distribution, as seen in Figure 42, the dry out tends to occur when the cutoff pore size is small enough that, the liquid saturation

falls of the cliff at around 50% liquid saturation. Generally speaking, as heat flux is increased from 0 W up to dry out, the R* value moves from right to left on the graph in Figure 42. If it was desired to delay dryout, how could one alter the pore size distribution to do this?

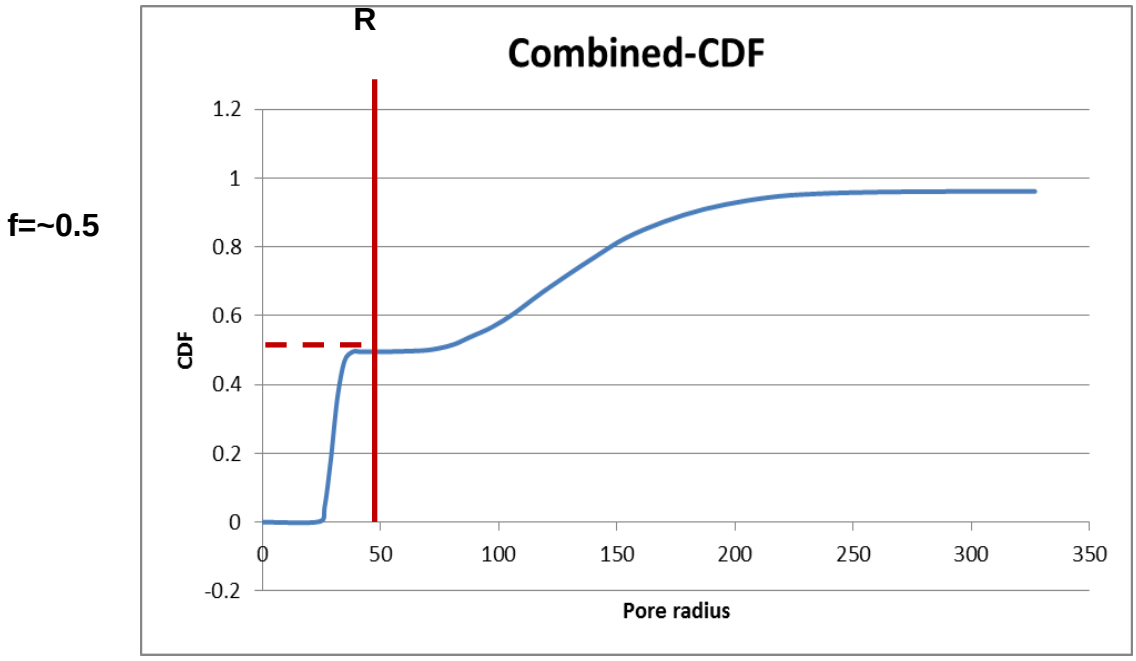

Figure 42: Schematic of Combined CDF

In a biporous wick, because of the interconnectivity of the clusters, liquid can be transferred anywhere clusters are touching, just as vapor can flow in the spaces between them. This increased flow area leads to a higher liquid flow rate supplying liquid to the heater surface over a wider range of input power. To pattern a biporous wick, one could simply use larger clusters in regions where vapor permeability was the dominant resistance and smaller clusters or particles where capillary pressure is dominant. If monoporous material was applied to the heater

interface, that would raise capillary pressure where liquid is needed the most but not needlessly restrict the vapor permeability elsewhere in the wick. So long as the monoporous layer was relatively thin, it would not have a significant impact on the overall permeability of the wick and the resistance to liquid and vapor counterflow would be minimal. By using larger clusters outside of the immediate surface area, high vapor permeability could be maintained while the interconnectivity of the clusters would provide liquid flow from the condenser to the heater surface. Another potential area for improvement would be wetting of the surface of the clusters. Prior to the complete dry out of the large pores, it is theorized that there are "secondary menisci formed around the contact area between clusters. A schematic of this situation is seen in Figure 43.

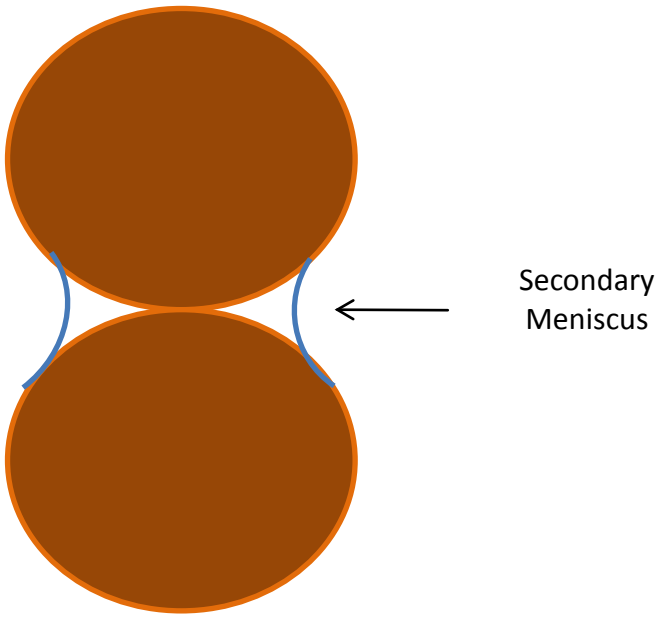

Figure 43: Schematic Secondary Meniscus between Clusters

The traditional concepts of heat transfer in a biporous structure would lead one to delay dry out by increasing the number of small pores as this would effectively raise the capillary pressure. Within the Kovalev model, this would manifest as a shift of the "cliff" in the pore size distribution to the left, meaning the critical R* value would be made smaller. However, simply adding more small pores everywhere does not affect the capillary pressure in a partial vacuum. If more, smaller pores were added everywhere, it would necessarily increase the available capillary pressure but there would be a costly decrease in liquid permeability. This decrease in permeability would raise the needed pressure drop to supply liquid to the heater interface faster than the increasing capillary pressure could act to provide liquid.

Clearly, if adding more small pores throughout the wick was the solution, this would be observed in numerical studies. The numerical results from the model in this work showed that dryout tended to be most sensitive to cluster size and that two of the lowest estimates of dryout were seen (69_275_907.5 and 69_196_646) with the smallest particles (69 microns). The highest dry out estimate was obtained for the tested wick which had the largest cluster size (460 microns) which would indicate that dryout is, by extension, a strong function of vapor permeability.

The reasoning behind this is logical; the vapor will preferentially occupy the large pores between the clusters due to the capillary forces inside the clusters. Vapor, being much less dense than liquid water must travel faster as it exits the wick than the liquid in the clusters in order to maintain continuity. This makes drag forces dominant on the vapor as the pressure drop due to frictional loses goes as the square of velocity. As such, the vapor permeability is likely to be the limiting resistance to vapor flow exiting the wick. However, in the vicinity of the heater, where

the local heat flux is highest, there is a greater need to maintain an active liquid interface. As liquid is either evaporated or nucleated, one would want a very high pressure drop between the liquid and vapor phases to make sure that whenever a bubble of vapor leaves the heater surface, liquid immediately rewets the surface in order to maintain the surface temperature. Clearly, it is evident that a high capillary pressure be maintained on the heater surface in order to keep it wetted and at saturation by using smaller particles. However, throughout the remainder of the wick large clusters are needed in order to maintain high vapor permeability.

The solution for optimized wicks must then lie somewhere in between; different parts of the wick have different needs resulting in different parameter selections to improve performance. Attempts have been made to pattern monoporous wicks by Weibel [52] and Liter [21], with some success. In order to achieve higher vapor permeability, channels were carved in the monoporous material in order to facilitate vapor flow to the condenser. The drawback of this approach is that if the space is completely open, a secondary meniscus can only form in the corners of the patterned sections, as seen in Figure 44.

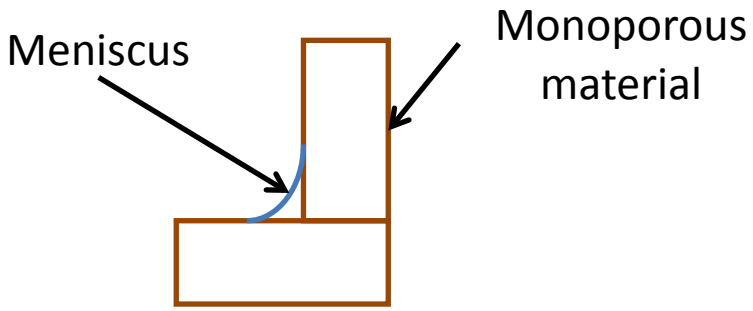

Figure 44: Schematic of secondary menisicus in a patterned wick

Theses secondary menisci can hold a significant amount of liquid to be transported throughout the wick. Increasing the wetting properties of the liquid could allow these secondary menisci to be able to transport liquid effectively across the surface of the clusters, from one secondary meniscus to another. There is the added benefit that increased wetting also allows the liquid to be heated more easily to saturation so there is less resistance to sensible heat transport. Research has been conducted on the addition of monoporous particles to the liquid to form hydrophilic structures on wicks [51] as well as oxidation schemes of the wick [44] in order to take advantage of this effect and has shown to be successful.

Depending on the type of surface modification used to achieve a more hydrophilic surface there would be varying effects of the pore size distribution. Structures would need to be deposited on the surface of the clusters and they could either be porous or non-porous. In both cases, these structures would likely decrease the size of all the pores by some margin, relative to the thickness of their coatings. This would act to shift the whole pore size distribution to the left as the pores would become smaller. Note that this effect would be more pronounced in the smallest pores as the thickness of the deposit comprises a much larger percentage of the overall pore size. In the case where the deposit is itself porous, the previous effect would still take place in conjunction with the addition of some pores which would likely be much smaller than any pore constructed by sintering the wick together. This would manifest as an extra “step” on the left hand side of the pore size distribution. A graphical representation of these effects is seen in Figure 45.

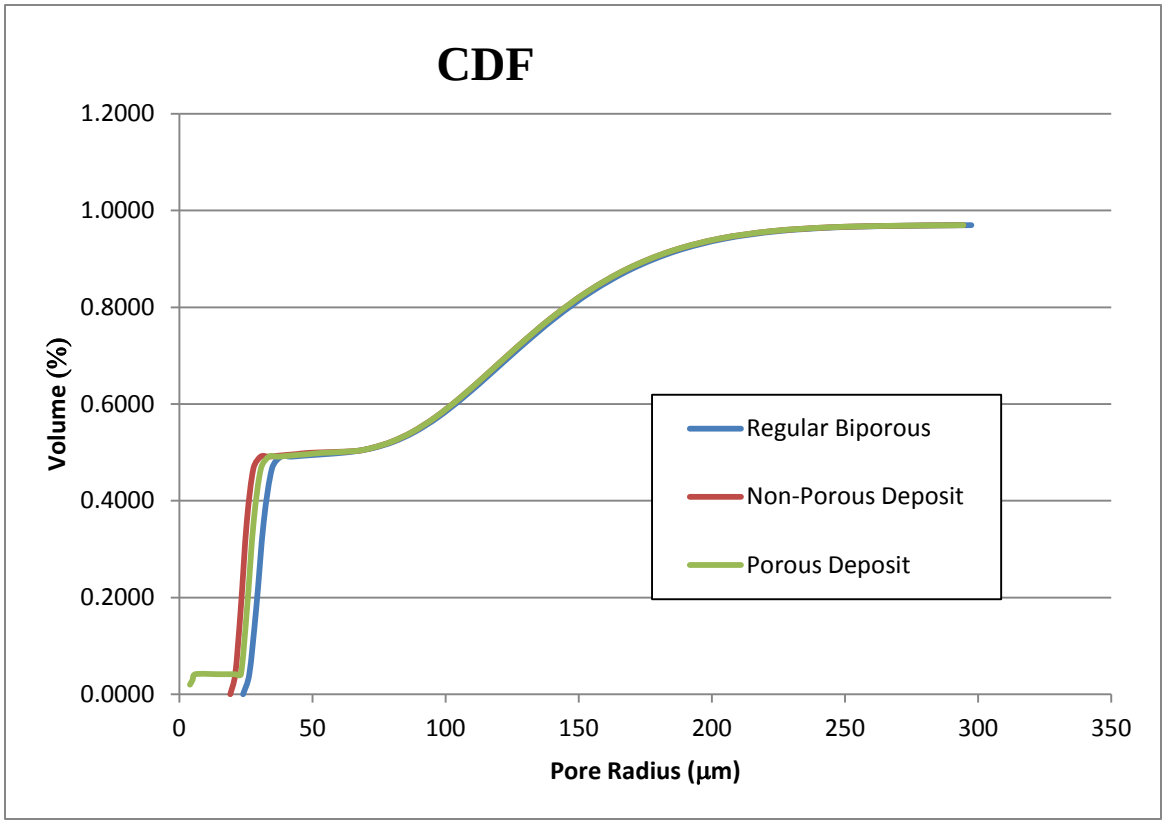

Figure 45: CDF changes due to surface modifcation

5.5 Summary

In summary, it has been shown that the Kovalev modeling technique can be effectively used to estimate the dry out of biporous material. Utilizing a statistical method to determine the maximum effective capillary pressure available from the wick and comparing it to the results of the required pressure drop calculated by the Kovalev model, estimations of dry out for five different wicks were presented. The results of these analysis showed an average error of the estimate in the range of 18%, which was deemed to be reasonably acceptable for the complex behavior of dry out in biporous material.

Analyzing the results of the dry out estimates as well as modeling efforts, two types of optimizations were inferred;

1. It was noted that through the majority of the wick, the dominating resistance was the vapor permeability but that in the immediate vicinity of the heater, capillary pressure was most important. In order to accommodate this effect, it was suggested that a smaller cluster size or only particles be used in the vicinity of the heater and larger clusters used throughout the remainder of the wick. Note that this observation was first suggested by Seminic in his thesis and is confirmed here using the Kovalev based model.
2. Further, to facilitate more efficient liquid transport, surface modifications to the clusters were suggested. The effect that these surface modifications would have on the pore size distribution was discussed.

In the following chapter, several experimental studies conducted by the author to investigate the modifications suggested here will be shown. Their successful improvement of dry out behavior will be assessed based on their performance relative to the previous biporous wicks tested by Seminic. The results of numerical study on these wicks will also be shown based on estimates of the augmented wicks pore size distributions. The basis of dry out postponement laid out in this chapter will be assessed in the following chapter to determine how well the Kovalev method can be used to optimize biporous wicks.

6.0 EXPERIMENTAL STUDIES

In this section, supporting experimental studies will be discussed. In the previous section, the Kovalev modeling technique was used as a method to both predict the thermal performance of a biporous material and as a method of estimating the dry out of same. This allowed insight into what is important to the performance of a biporous material and the benefits from manipulating the pore size distribution to increase capillary pressure and to modify the surface properties of the wick. This chapter discusses the validation of the modeling and its effectiveness as a predictor of optimized geometries.

6.1 Capillary Pressure through Geometric Manipulation

The experimental investigations were part of a DARPA sponsored research program referred to as "TGP", or thermal ground plane [32]. The goal of the TGP research effort was to develop a high efficiency heat spreader that was, among other things, very thin (~1-2mm). The UCLA effort focused on developing a vapor chamber with a sintered copper wick inside. The research team was to develop a wick that had a much higher effective thermal conductivity than solid copper while being less than 1mm thick. The wick also needed to be able to withstand 10x the acceleration of gravity and remain wetted which meant that high capillary pressure was needed. The thickness requirement necessitated a slightly different approach from that taken by Semenic [35], as his work primarily focused on finding the cluster and particle sizes that would yield the maximum heat flux. In the present case, the heat flux has to be high while the wick fit into the form factor. This drove the researchers to pay special attention to overall geometry while

obtaining the maximum heat transfer performance. A reliable model would have made it possible to accurately predict the performance of the wicks in a TGP and reduce the cost of development.

Without the mathematical model, the TGP program required an experimental effort to optimize the biporous material for particular applications. A picture of a TGP can be seen in Figure 47. The primary experimental apparatus used to optimize biporous wicks for these goals is referred to as a “Boiling Chamber” (BC). The BC was designed and built by Semenic [35] and modified to suit the needs of this work. The BC and its operation will be discussed followed by a presentation of the results of individual experimental investigations.

First, the efficacy of the BC as a method to predict the performance of biporous wicks in actual TGPs is explored. As a BC is not an actual heat spreader device, it is necessary to show the conditions under which it was an accurate predictor of en situ performance in a TGP.

Second, the investigations of different geometries will be detailed. Experimental efforts focused on three variations; annular, tri-layer and double layer wicks. These wicks represented an effort to pattern the cluster and particle sizes across the wick and schematics of their layouts can be seen in Figure 46.

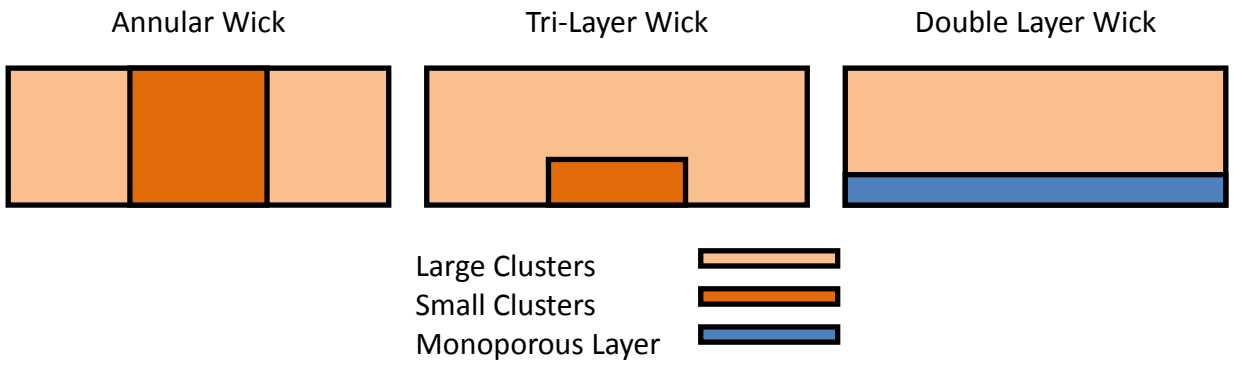

Figure 46: Schematic of Patterned Biporous Wicks

In both the annular wick and the Tri-layer wick, a smaller cluster size was used over the heater area, but in a tri-layer it was only a small amount above the heater whereas in the annular case it extended from the heater surface to the upper boundary of the wick. In a double layer wick, a monoporous layer was sintered between the heater interface with the biporous layer above it. In both cases the goal was to raise the capillary pressure at the heater in order to maintain wetting over a wider range of heat fluxes. Following discussion of the experimental results, their relationship to the overall goal of optimizing biporous wicks will be detailed.

6.1.1 TGP Testing Method

The tested TGPs were produced at Advanced Cooling Technologies (ACT), a small high technology company in Pennsylvania and are 3" by 5" troughs that are roughly 3 millimeters in depth, see Figure 47. On the back side of the trough, a small raised section was added for use as a heater interface. The interface had a small hole in it for the introduction of a thermocouple between the heater and the TGP itself. The trough was filled with the desired wick and then the upper surface was sealed with a plate. Each TGP has two 1 mm diameter copper tubes inserted into it. One bisects a corner of the TGP and another is inserted into the middle of the narrow

side of the TGP. The layout of a TGP is shown in Figure 47. The corner tube is used in the filling and desiccation process while the tube in the middle of the narrow side is used to insert a thermocouple for measuring the vapor temperature inside the chamber.

Once the TGP was constructed, it was charged with a given amount of fluid based on the porosity of the wick inside the device with some extra in order to help clear the TGP. Once the fluid was injected, the TGP was placed in a special mount that oriented the corner tube straight up and down. The TGP was then heated in order to evaporate excess fluid from the interior of the device as well as purge any air that was left inside. Once the fluid charge was reduced to the desired level (measured by mass) the corner tube was closed off to seal the interior of the chamber.

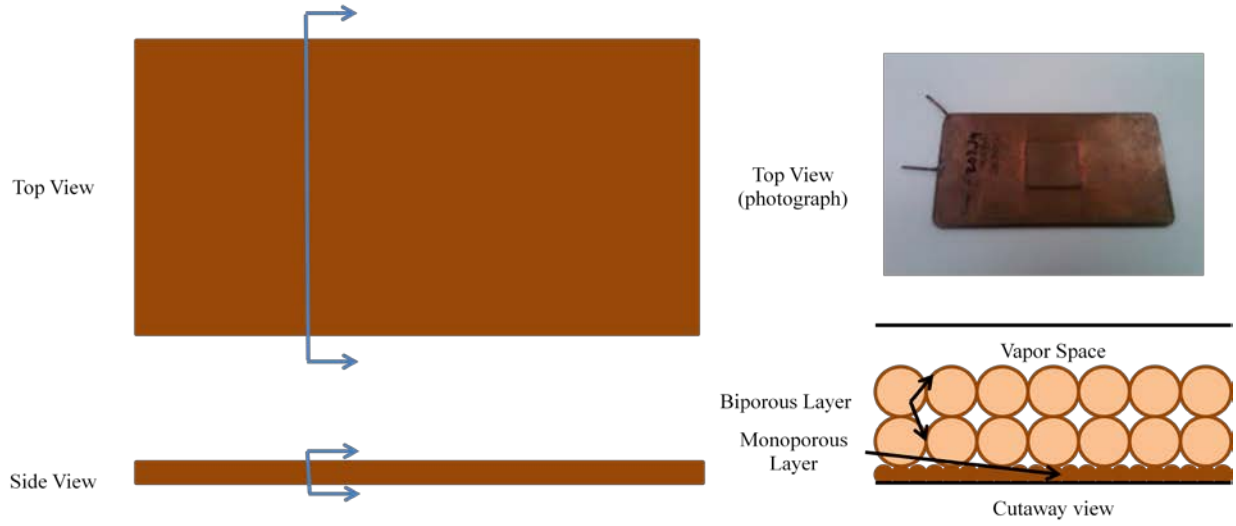

Figure 47: Schematic of TGP Layout

For testing, the TGP was placed in a vertical orientation along one if its longer sides with the bottom of the trough perpendicular to the ground. The heater was applied at the back of the

TGP on the interface plate (seen as the raised section of the TGP above in Figure 47) and a thermocouple was inserted into the hole under the interface plate. A schematic and photo of the test setup can be seen in Figure 48.

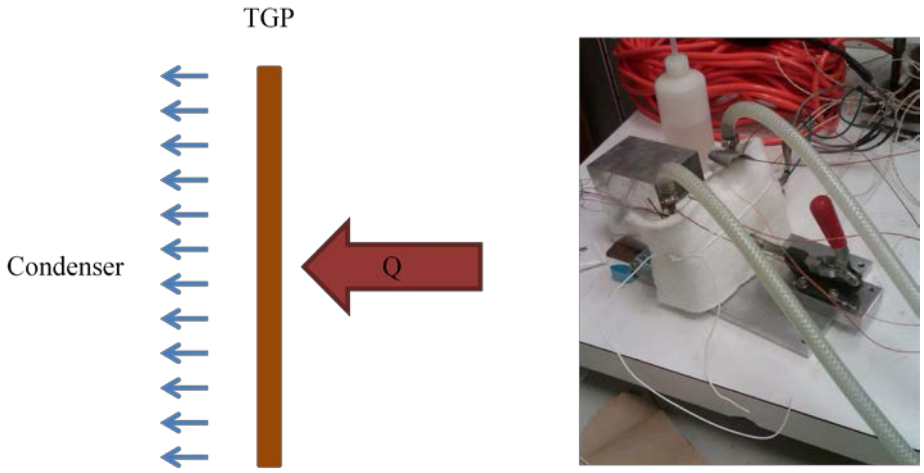

Figure 48:Schematic and Photo of TGP test setup

A condenser plate was attached on the top of the trough with a network of thermocouples. The entirety of the TGP was coated in insulation before the experiment was started. Once the heater and the cooling plate were activated data was collected at steady state for various heat fluxes.

6.1.2 Boiling Chamber Experimental Method

In this section, the procedure used to operate the BC experiment is detailed. This experiment was vital to the evaluation of the performance of biporous wicks. The BC experiment simulated conditions inside of a heat pipe by evacuating the chamber to a negative pressure in order to

lower the saturation temperature. The wicks tested were affixed to a mounting referred to as a boiling target, which was inserted into the base of the BC for testing, see Fig 47. Heat flux was provided by cartridge heaters and steady state measurements of temperatures were taken at various heat fluxes.

The wick was sintered at an industry partner, ACT, to the requested specifications of cluster and particle size before testing. The sample (with wick attached) was prepared for testing by first attaching 13 thermocouples to allow calculation of the heat flux into the wick as well as radial losses across the wick's lower surface. The thermocouples marked "TS" were placed on the outer ring of the collar of the sample and the ones marked "TC" were placed around the perimeter of the neck, or stem, of the sample. The thermocouples marked T1-T5 were placed into pre-drilled holes in the neck of the sample with T1 being the highest point and T5 is the hole closest to the base of the sample/heater block.

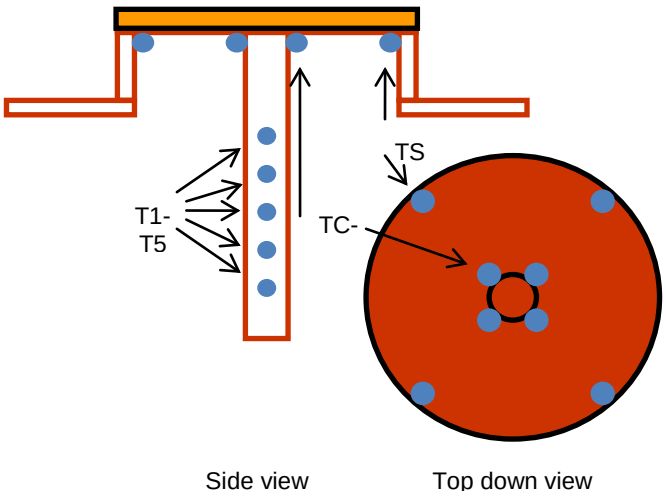

Figure 49: Boiling Target Sample

The wick to be tested was placed inside the boiling chamber shown in Figure 50; which was then closed, evacuated, and charged with working fluid until the wick was covered with a thin layer of fluid. Heat was supplied to the wick with three 750W cartridge heaters embedded in a block of copper labeled “heater” in Figure 50. This block was soldered to the base of the sample and conducted heat from the heater into the sample and wick.

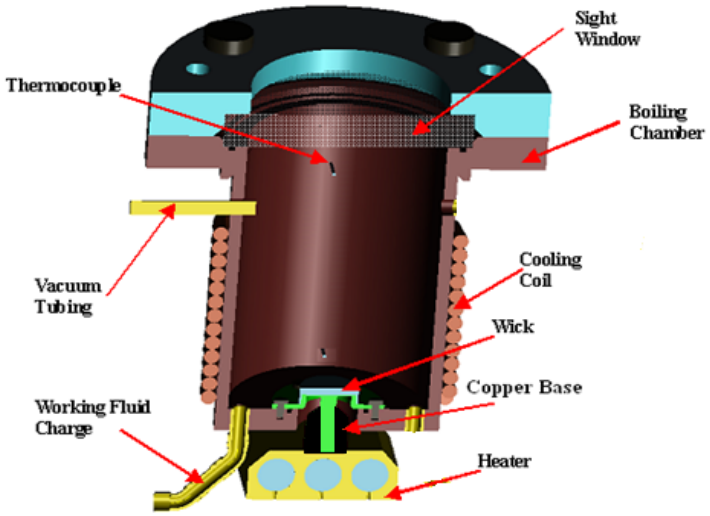

Figure 50: Boiling Target Test Chamber

The next stage of preparation was to saturate the wick with fluid and remove all the air from the wick and the chamber. The heater was set to a medium heat flux (below dry out) and allowed to run for approximately one hour. Water vapor was removed from the chamber using a vacuum pump until the water level was below the top surface of the wick but contacted the sides of the sample. The pressure was reduced to about 0.08 bar within the chamber so that most of the air was removed from the chamber. At this point the heater and vacuum pump were

deactivated and the chamber and sample were allowed to cool while sealed in a vacuum. The water supplied to the cooling coil was set to (40±0.5) C and kept constant during the experiment. When the chamber cooled, a check was performed to ensure the thermocouple inside the chamber read close to the wall temperature (temperature under the wick to ±0.1°C) so it could be assumed that an insignificant amount of air remains in the chamber. The vapor pressure of the water under these conditions was taken to be approximately 0.08 atmospheres.

In the case of an experiment conducted without vapor space restriction, the wick was now prepared for experimentation. The methodology behind the restrictor plate and its use are explained later. However, if restriction was to be tested, an additional step of inserting the plate was required and will now be detailed. The differences in the restricted and unrestricted cases can be seen in Figure 51.

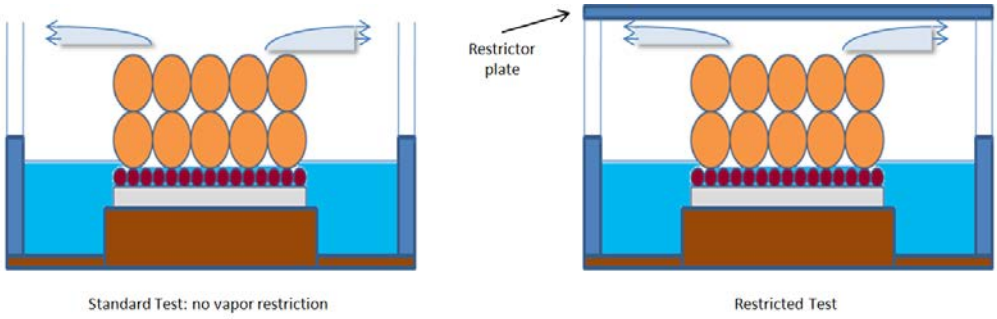

Figure 51: Comparison of Unrestricted and Restricted BC testing

Once the sample was adequately saturated, a vapor restrictor plate was inserted. Since the plate makes it impossible to tell how much water has evacuated from the wick and removed from the chamber by the vacuum pump, the wick was saturated without the plate present. There

were several iterations of a restrictor developed for use in this experiment. Eventually it was settled to use a cylindrical restrictor plate with telescoping legs to adjust its height. The telescoping legs were made out of long screws. The height of the restrictor was carefully adjusted outside of the boiling chamber using knowledge of the interior dimensions. This served two purposes; one was to avoid having to adjust the restrictor in the tight confines of the BC and the other was so that the plate could be quickly inserted into the BC to minimize the wicks exposure to oxidation or air reentering the wick. A schematic of the restrictor plate is seen in Figure 52.

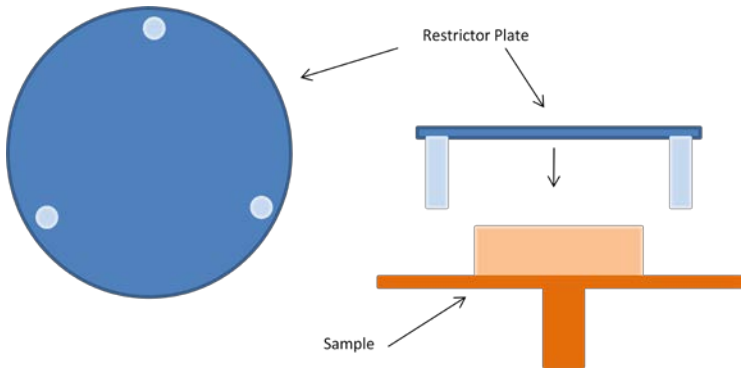

Figure 52: Schematic of Restrictor Plate

After the restrictor was inserted, the chamber was then quickly pressurized and the chamber was re-evacuated back to a high vacuum state. Care was taken so that this process was performed as quickly as possible to reduce air from entering the saturated wick.

At this stage the heater was reactivated and the power being supplied to the heater was gradually increased. Data was taken at several steady state power levels, increasing the power until the heaters could no longer safely provide heat flux to the experiment. Steady state was

achieved in about 20 minutes at each heat flux. Temperatures were recorded continuously throughout the experiment, but the data collection program noted when the experiment had entered steady state. The data collection program interpreted steady state to be when the temperature within the stem of the sample did not change by more than ±1°C for five minutes. Temperatures T1 through T4 (see Fig. 3) were used in a linear regression model to extrapolate the heat flux from the heaters to the wall/wick interface temperature. Thermocouple readings T_C and T_S were used to estimate radial heat flux inside the copper collar of the boiling target. Radial heat flux losses through the solid copper surface below the wick were calculated using T_C and T_S using a steady conduction equation for a solid disk.

The net heat flux supplied to the heat input region of the wick was calculated using a linear regression of Fourier's law with the temperature readings $T1$ through $T4$ and subtracting the radial heat flux into the collar. To calculate the flux through the stem of the sample, the gradients between each of the thermocouples were calculated and checked for linearity and then averaged to determine the flux. The thermal conductivity of copper was taken to be 401 at 300 K and 393 at 400 K.

The radial heat flux inside the wick was neglected due to a much lower thermal conductivity of the wick material compared to pure copper (on the order of 20 W/m/^{o}K) as determined by Seminic [36]. The linearity of the temperatures T_1–T_4 was checked at each heat flux to ensure validity of the calculated values. These values were then used in the analysis of the wick performance. Radial heat losses within the base plate were accounted for by a geometric formula suggested by Seminic [35] which includes the error introduced due to the spacing between T_c and T_s. The average gradients between T_c and T_s were used for the loss calculation to mitigate

uncertainties. These losses were subtracted from the heat flux calculated in the stem of the sample before presentation of the data. The equation for the calculation of radial loss is seen below in Eq. (60).

$$q_{loss} = \frac{2\pi k \delta_{base} (T_{c_{avg}} - T_{s_{avg}})}{\ln(D_{T_c} / d_e) \pi d_e^2 / 4} \quad \textbf{(62)}$$

D_{Tc} is the diameter for the ring of T_C measurements, δ_{base} is the thickness of the base plate and d_e is the diameter of the evaporator. Calculation of thermal conductivity was done by solving a 1D Fourier equation. We divided the heat flux through the wick by the difference between T_w and T_{vap}. The value of δ was taken as the thickness of the wick plus the vapor space

6.1.3 TGP Boiling Chamber Comparison

The first major difference between the BC experiment and an actual TGP is the restriction of the vapor space above the wick in an actual TGP. The BC experiment was originally designed to characterize porous wicks without having to deal with other effects due either to vapor escape restrictions or resistances associated with the condenser. As such, the condenser area and vapor space above the wick was considerably larger than what would be seen during operation in an actual device. In order to make comparisons between the BC and TGP's a method of restricting the vapor space by insertion of a plate was employed.

The restrictor plate consisted of a cylindrical disk that was fitted with adjustable legs around the periphery in order to investigate different vapor space thicknesses. The primary thicknesses of interest were 0 mm, 1 mm, and open (absence of the restriction plate). As the goal of the TGP program was to produce as thin of a device as possible 1 mm was considered the upper limit for an acceptable vapor space.

The first set of data, seen in Figure 53, shows the results of tests performed at UCLA to investigate the effect of the vapor flow restriction on wick performance. It is believed that by restricting the upper surface of the wick, the BC experiment would more closely represent the operating conditions inside of a TGP. Figure 53 shows that the restriction of vapor flow from the wick increases the super heat required to drive a given heat flux. In general, vapor is produced over the heater in the wick and is expelled upward and out of the wick where it is eventually cooled by the condenser region of the BC.

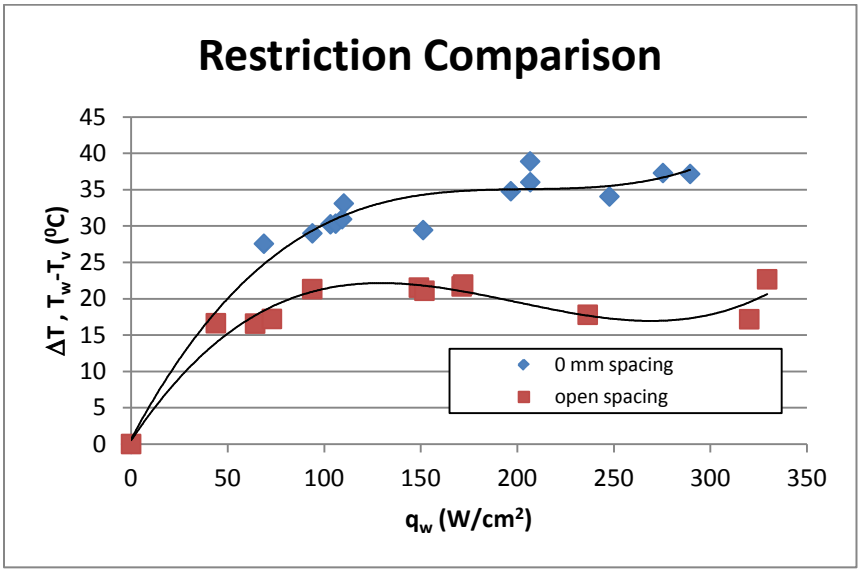

Figure 53: The impact of spacing above the wick on superheat,DT.

In the 0 mm configuration, vapor has to be forced through the large pores in the wick and out to the condenser. This results in considerably more frictional losses due to vapor only being able to pass through the large pores in the wick, which as previously mentioned, are quiet tortuous .

In order to compare the experimental data obtained from the UCLA vapor chamber with data from the ACT testing of a TGP, an electrical analog technique was used. The wick itself can be represented as a hydraulic resistance, R1 which is a function of primarily heat flux. Hence, the behavior of R1 was initially quantified as a function of current (heat flux) from an analog configuration of the open wick using the experimental data.

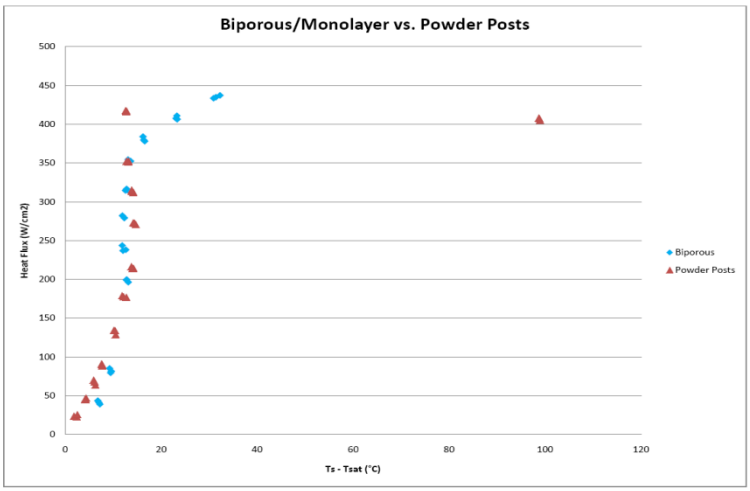

Figure 54: Comparison of Biporous Wick (BC) compared to TGP (ACT)

The network configuration for the cases in which the open space is restricted would be the resistance R1 and a second resistor R2 in series. This is similar to the analysis performed by Vadakkan [42] in that the vapor flow through the wick and available vapor space are coupled. This implies that a higher pressure gradient is required for the flow when the wick is more restricted. Figure 55 demonstrates that as the heat flux increases the required pressure gradient to maintain the vapor out flow rate increases till the dry-out of the large pores initiates. Since the large pores are considered as the primary vapor passages, when their dry out starts to occur, the vapor permeability increases and the required pressure gradient declines.

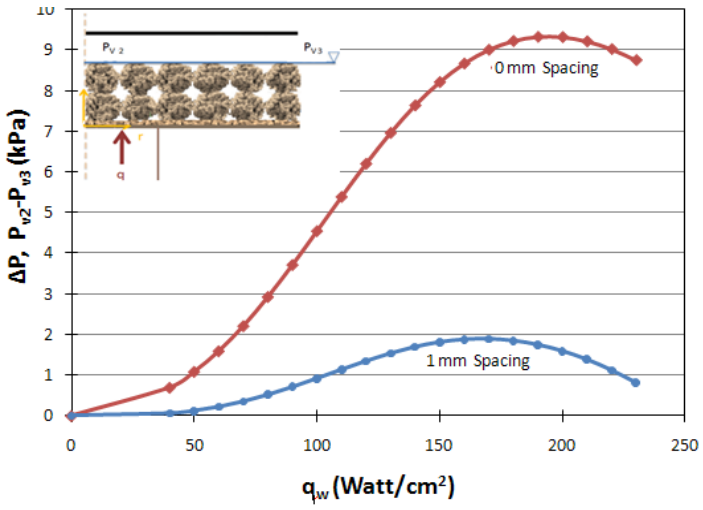

Figure 55: A comparison of the pressure drop with a 1 mm spacing with a fully restricted case [1]

The TGP and boiling chambers were treated as thermal circuits and the results were improved such that the two sets of experiments could be compared against each other. This was done by taking the wick resistance calculated with each experiment and putting them into the

circuit representing the other experiment. This was used this to obtain new wall heat fluxes and then plot them against the original data.

The TGP prototypes used for comparison had an approximate vapor spacing of 1mm; this is in addition to the space taken up by the wick and the outer walls of the TGP. In order to compare the resistances of the TGP to those found in a 1mm restricted BC experiment, the resistances associated with the vapor space in the BC were used with the heat flux from the TGP experiments in order to predict the TGP performance. Figure 55 shows the results of testing a BC wick with 1mm spacing compared to the results obtained by a TGP with a similarly sized wick. It can be seen that the data for each curve falls very close to each other though the UCLA estimate dries out slightly earlier. It should be noted that there is some experimental uncertainty associated with the vapor restriction being exactly 1mm as the plate had to be rapidly inserted into the chamber for testing. Furthermore, the vapor temperature measurement in the TGP's was from a tube that was inserted into the side of the TGP. With only 3mm of thickness it is difficult to know that the tube was only exposed to the vapor temperature. However, despite these possible sources of variance, the data appeared to validate the claim that the BC could be used to predict TGP performance.

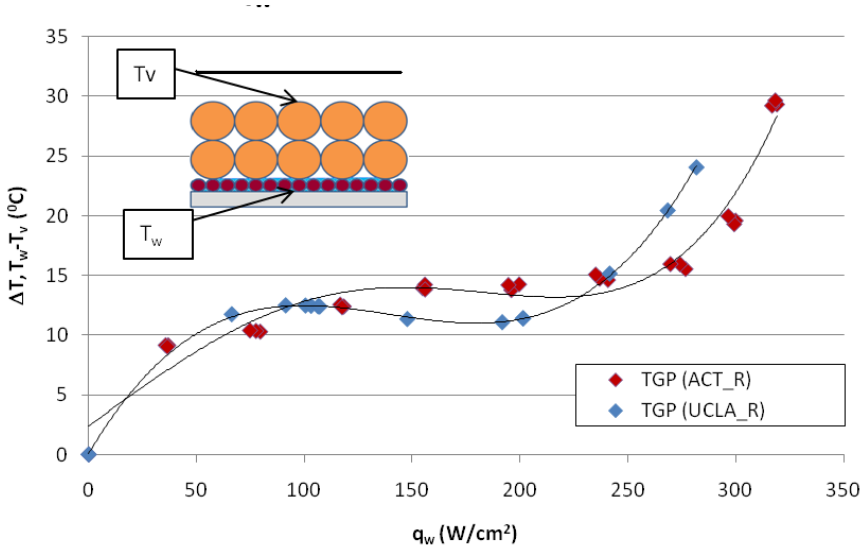

Figure 56 Comparison of ACT and UCLA values of the derived ΔT for 60_120/60_300_800, at 1 mm restriction

Variances in the data itself could be the result of differences in the general testing methods between the two experiments. At ACT, the fluid charge inside the TGP is closely regulated as it is well known that fluid charge has a significant impact on heat pipe performance. Empirically this has proven to be true true with the TGP's constructed at ACT. However, at UCLA the fluid reservoir surrounding the boiling target sample is very large relative to the TGP case. Also, when testing for a restricted case at UCLA, some air could enter the wick when the restrictor plate is introduced into the experiment. This is because the wick clearing process requires that the experimenter observe the fluid level inside the chamber, which is impossible to do accurately if the plate is already in the chamber (this phenomenon is shown in Figure 51 and Figure 52). So, after the wick has been cleared, the chamber must be breifly repressurized in order to insert the plate. While care is taken to make sure this is done quickly and efficiently, some error could be introduced.

Experiments involving the vapor restrictor wick have been repeated various times with several different wicks. In general, the trend that decreasing the available vapor space above the wick increases the superheat required to drive a particular heat flux remains prevalent. Successive tests have shown that data points collected in separate experiments fall within temperature measurement uncertainties. However, in general, over time the performance of the wick tends to degrade. It is postulated that this is due to repeated exposures to air which could be oxidizing the wick and reducing the liquid permeability.

In summary, by restricting the vapor escape pathway from a wick in the BC experiment, it has been shown that it is possible to accurately predict the en situ performance of a biporous wick in a TGP. Tests were conducted with TGP's and BC wicks which had an available vapor space of approximately 1mm. The results were reasonably accurate, though the restricted BC wick dried out slightly sooner. While this variance is attributed to experimental uncertainty, the fact that it dried out slightly before a TGP reinforces the statement that it is a conservative estimate. Armed with the ability to make justified claims as to the performance of various advanced wick geometries in TGP's, experiments aimed at augmenting the geometry to improve performance will now be discussed.

6.1.4 Tri-layer and Annular Wicks

The results of testing both the tri-layer and annular wicks are displayed in Figure 57. Again, a tri-layer wick is defined as a biporous wick in which small amount of biporous material, with smaller characteristic diameter than the predominant cluster size is placed directly over the heater. An annular wick is one which cylinder of clusters is placed over top of the heater and the surrounding annular volume of wick has a larger cluster size. The logic being that this would

help increase the capillary pressure immediately over the heater while still maintaining relatively high vapor permeability outside of the heater.

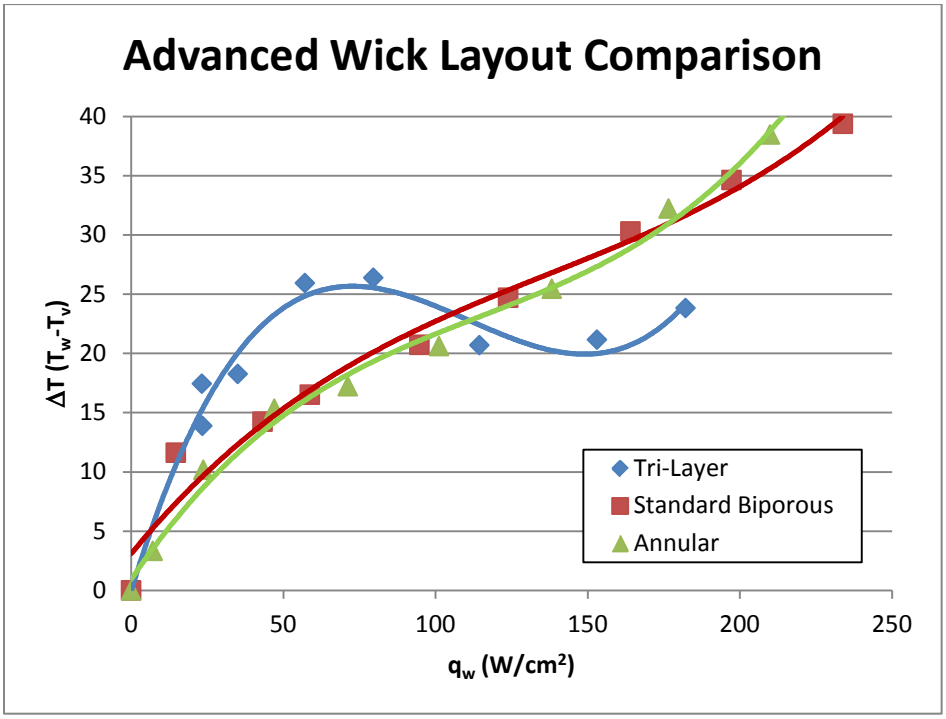

Figure 57: Advanced Wick Comparisons

As shown in Figure 57, it is clear that the annular wick performed almost identically to that of a standard biporous wick of similar dimensions. The tri-layer wick, despite initially having worse performance in terms of the wall superheat, showed improved performance after approximately 100 W/cm^2. It should be noted that in each of the advanced wick configurations, additional sintering is required beyond that which is used to initially create the biporous wicks. This added "soak" time in the furnace carries with it an increased risk of fusing particles

together. This is because each section must be sintered separately in order to guarantee definite boundaries between porous media phases.

In the case of the cylindrical wick, it is believed that any gain in performance afforded as a result of the increased capillary pressure over top of the wick was negated by the fact that vapor permeability was effectively reduced there, as well. This would serve to add an additional hydrodynamic resistance to vapor flow right at the point where it is generated as it would take additional vapor pressure drop in order to clear liquid from the spaces between clusters. This additional pressure drop would reduce the flow rate of vapor exiting the wick and raise evaporator temperatures, thereby reducing performance. It is also possible that additional sintering steps may have affected bonding between the various regions. If for instance the cylinder clusters were not properly bonded to the annular clusters, it would make it more difficult for liquid to be wicked from the outside of the wick into the center for evaporation.

The tri-layer wick, on the other hand, while the goal was the same, had a significantly smaller volume of smaller clusters was used over the heater relative to the cylindrical wick. In this case, many of the problems suggested with the cylindrical wick have been minimized. It is believed that there was still a significant resistance to clearing liquid out of the smaller clusters in the region immediately above the heater, as evidenced by the higher super-heat at lower heat fluxes, but this was overcome as heat flux was increased. As to why this resistance was larger for the tri-layer than the annular wick, is not known. It is the author's opinion that based on the techniques used to form the sintered wicks it would have been more difficult to form a small discrete region of smaller clusters over the heater than in the annular case. For this reason, it is

possible that the tri-layer region likely spread wider across the heater than in the annular case, which would temporarily amplify the vapor flow resistance.

Once the liquid was cleared between the smaller clusters, the increase in capillary pressure in the region over the heater, the increase in capillary pressure would have acted to keep the heater region wet for longer than a standard biporous wick. The smaller clusters would have created more secondary menisci, which would have supplied ample liquid and improved performance. However, once these secondary menisci dried out, the performance would likely have been similar to that of a standard biporous wick, as the permeability of the liquid inside the clusters would be the limiting resistance and would be the same for both the tri-layer and standard. Even though the results of testing the tri-layer were somewhat positive, the fact that the annular wicks were not effective led the research to pursue other geometric configurations. There were simply too many unknowns to work out in terms of how to effectively construct these wicks without significant problems especially once testing was started on the double layer wicks.

6.1.5 Addition of a Monoporous Layer

The addition of a monoporous interface layer between the heater interface and the biporous material was first suggested by Seminic [35] in his thesis (shown schematically in Figure 58) although not tested. Increasing the capillary pressure in the vicinity of the heater would maintain wetting of the heater surface to higher fluxes than the biporous wick alone would. Furthermore, this monoporous layer would be fed with liquid from the biporous material above it wherever the cluster rested on the monoporous layer. Further, the thin layer would significantly reduce the temperature difference needed to accomplish the heat transfer leading to much better performance.

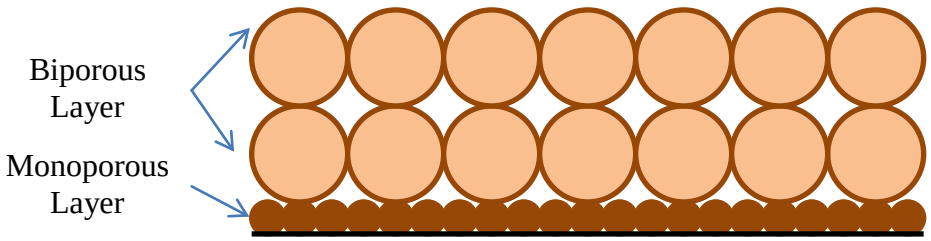

Figure 58: Schematic of double layer wick

The feed length of the liquid is determined by the clusters in the biporous material. Assuming a well an idealized layout of spherical clusters, the longest distance between the surface of the monoporous layer and the center of the cluster (the point at which the cluster interfaces with the monoporous surface) is the radius of the cluster. This distance is the maximum length that liquid must be pumped in order to wet the monoporous layer surface. It stands to reason that minimizing this distance would reduce the frictional losses associated with maintaining a wetted condition on the monoporous layer. However, as this would reduce the cluster sizes, there would be a penalty paid in the form of reduced vapor permeability if the cluster sizes were reduced indefinitely. So there exists a balance between this resistance and adequate vapor permeability in the biporous layer. A schematic of the feed length situation can be seen in Figure 59.

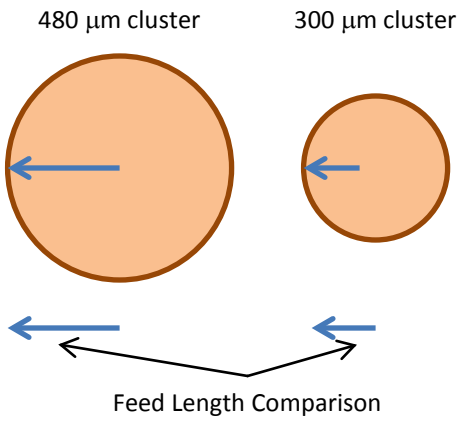

Figure 59: Feed Length Comparison

It is believed that the additional monoporous layer has two primary effects on the heater interface. First, the addition of many small pores at the heater interface where there was only solid surface before effectively raises the effective capillary pressure at the interface which helps to feed liquid to the heater interface more efficiently, relative to the clusters. This is because when there is only a biporous wick, after nucleation begins the clusters can only feed liquid to the heater interface by way of the secondary meniscus formed between the exterior of the cluster and the heater surface. Once nucleation begins, local dry-out points will form at the midpoints between the clusters as these regions are furthest from the liquid supply. With a monoporous layer underneath the cluster, the secondary meniscus is capable of filling all the pores between the clusters, resisting the formation of local dry-out points.

Secondly, it has been shown rigorously that monoporous layer aids in evaporation and boiling heat transfer by way of increasing surface area at the interface. However, a common limitation of monoporous material is the limited vapor permeability and liquid permeability. In the case of a double layer wick, monoporous wick is intentionally kept thin so that vapor can

easily escape through the monoporous layer and the relatively high permeability of the biporous material has the same effect. Also, as mentioned earlier, the double layer wick bypasses the monoporous material's lack of liquid permeability by being fed vertically from the biporous material, rather than laterally from itself.

In order to test the efficacy of this geometric layout, wicks were constructed with identical biporous layers with and without monoporous interface layers. The monoporous layers all had the same geometry; 60 μm particles and a thickness of 120 μm. Two wicks were tested; one with a biporous layer consisting of 300 μm clusters and one consisting of 480 μm clusters. Both of the wicks had 60 μm particles throughout and a biporous layer thickness of 800 μm. Note that all wicks are referred to by the size of the structures that they are comprised of; the dimensions of the monoporous layer (if one exists) are listed to the left of the "/" and the dimensions of the biporous layer are listed after. The monoporous layer lists the particle size then thickness and the biporous designation lists the particle size, cluster size, and finally the thickness. All dimensions are in microns (μm).

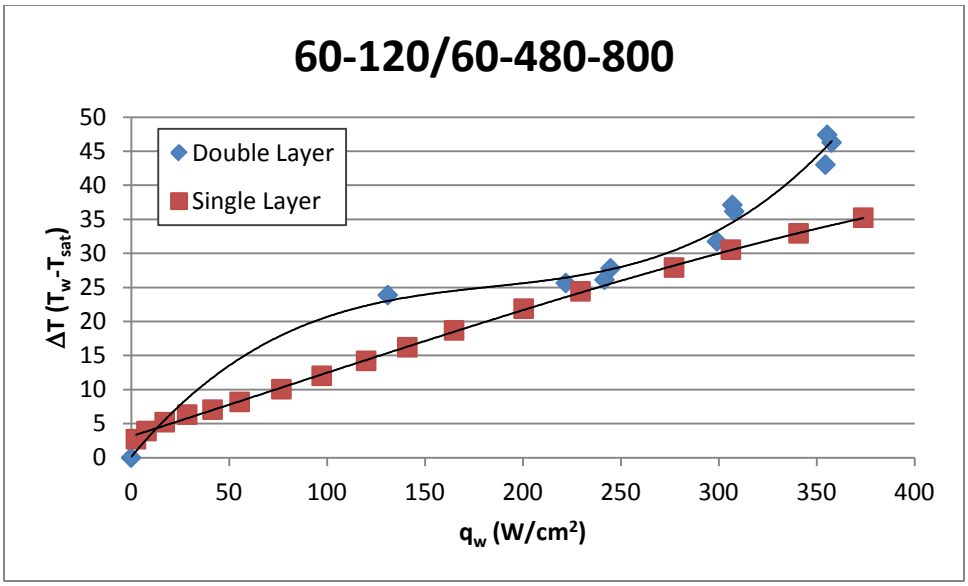

Figure 60: Single and Double Layer Comparison for 60_480_800 wick

The results presented in Figure 60 show the results for the double layer wick with 480 μm clusters tested at UCLA. For reference, data from a single layer biporous wick of 60μm particle size, 480 μm cluster size and 800 μm thickness is shown on the graph. The double layer sample has a 60μm particle size 120μm thick monolayer underneath the previously mentioned biporous wick, henceforth known as 60_120/60_480_800. It should be noted that the overall thickness of the double layer wick was 920 μm due to the addition of the 120 μm thick monolayer making the double layer wick slightly thicker than the regular biporous wick.

In the 480 μm case, the monoporous layer did not improve performance, and in some cases actually degraded it. There is also some scatter in the data that is most likely due to measurement uncertainty. The fact that performance was not increased was unexpected in this case as the 480 μm cluster size biporous wick was one of the most effective biporous wicks. Outside of mechanical errors, it is also possible that the large distance between cluster centers

relative to wicks with smaller clusters (i.e. 300 µm) could contribute to the lack of improvement. This is because the feed distance is longer contributing to a higher hydrodynamic resistance.

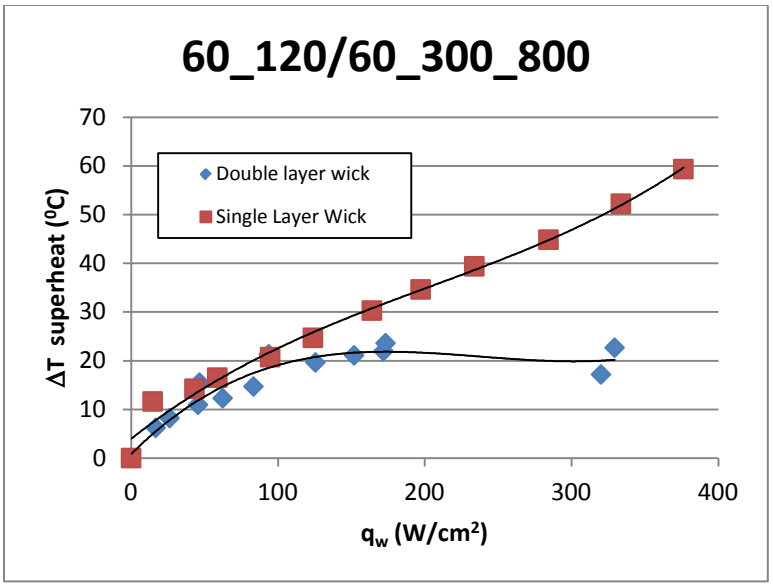

Figure 61: Single and Double Layer Comparison for 60_300_800 wick

The second test was performed on a wick with 300 µm cluster size and shows clearly that the addition of the monoporous layer to the wick improves the performance of this particular wick when the heat flux is greater than about 125 W/cm^2. The addition of the monoporous layer reduced the superheat required for a given flux in comparison to its respective single layer wick.

The reason for the dramatic difference in performance characteristics between the two cluster sizes is most likely a function of the feed length differences. The idealized feed length is 60% larger in the 480 µm cluster case. However, the nature of the biporous wick is clearly not idealized. In general, as cluster size is decreased the standard deviation of cluster diameters

increases noticeably (this fact will be discussed in detail later in this dissertation). This leads to the belief that the 480 μm clusters are much more irregularly shaped than the 300 μm clusters and therefore it would be reasonable to assume that the feed lengths could be even longer than the idealized 60%. These increased lengths would contribute to more rapid dry out in the monoporous layer. Furthermore, the improvement noted in the 300 μm case was not considered to be anomalous due to repeated tests on several different wicks of the same geometry, all of which showed improvement.

In summary, the double layer wick showed promise as an effective means of geometrically augmenting a standard biporous wick in order to increase performance in wicks with smaller cluster sizes. The impact of adding a monoporous layer seems to be a strong function of the of the biporous wick cluster size. Larger cluster sizes tend to not adequately maintain a wetted condition in the monoporous layer relative to smaller cluster sizes. It is clear that the most effective means of manipulating the pore size distribution to increase heat transfer performance is the addition of a monoporous layer and that the resulting cluster size, particle diameter and monolayer thickness can only be found through an optimization study. The fact that the monoporous layer was so effective demonstrates that the suggestions from Semenic [35] and the Kovalev model will be useful in optimizing performance.

6.2 Biporous Wick Surface Modification

There have been many efforts to modify water as a heat transfer fluid with the intent of improving the liquid/surface interface. Wasekar [49] investigated the addition of anionic surfactants to the working fluid which resulted in increased bubble incipience and an increase in heat transfer coefficient. Wen [50] studied nanoparticles in suspension in the fluid to positively affect the heat transfer properties of the liquid by showing an increased boiling heat transfer

coefficient. These studies proved successful in improving the general performance of these fluids by altering their thermophysical properties. However, it has also been shown that overloading the water with additives can have a negative effect. Das [11] showed that significant loading of nano-scale particles to working fluids can negatively impact boiling performance as concentration of particulates at the evaporative surface is increased.

In order to modify the surface properties of the wick in this work, a proprietary fluid, referred to as IAS was used. The Inorganic Aqueous Solution (IAS) is a complex mix of approximately 9 chemical constituents in water, see Table 5 for the results of chromatography performed on the fluid. The IAS has been tested extensively at UCLA for use an enhanced heat transfer fluid and was used in conjunction with biporous material in order to optimize performance.

Table 5: Ions present in IAS

<table>
<tr><td colspan="2">Solution</td><td rowspan="2">Suspension</td></tr>
<tr><td>Positive ions</td><td>Negative ions</td></tr>
<tr><td>Na^+</td><td rowspan="2">MnO_4^-</td><td rowspan="3">$MgCrO_4$</td></tr>
<tr><td>K^+</td></tr>
<tr><td>Mg^{2+}</td><td rowspan="2">$Cr_2O_7^{2-}$</td></tr>
<tr><td>Ca^{2+}</td><td rowspan="2">MnO_2

Only after long time storage</td></tr>
<tr><td>Sr^{2+}</td><td rowspan="2">CrO_4^{2-}</td></tr>
<tr><td>Ag^+</td></tr>
</table>

The fluid itself was originally believed to be a solid-state, hyper-conductive surface treatment for copper tubing as it was originally proposed by Professor Qu, in China [30]. These so called “Qu Tubes” or “Super tubes” generated significant interest in the United States as a result of several favorable performance claims. Performance of delivered devices was inconsistent, though, especially when tested assuming that the device was performing in a solid state mode.

The significant presence of chromates might suggest that the fluid was originally inspired by chromate passivation schemes, popular for use with aluminum alloy. Rocco [33] compared

two different methods of chromate coatings on Al/Zn alloys which were designed to discourage corrosion and allow increased adherence of paint. The increased corrosion resistance might permit water to be in constant contact with an aluminum surface and actively resist oxidation.

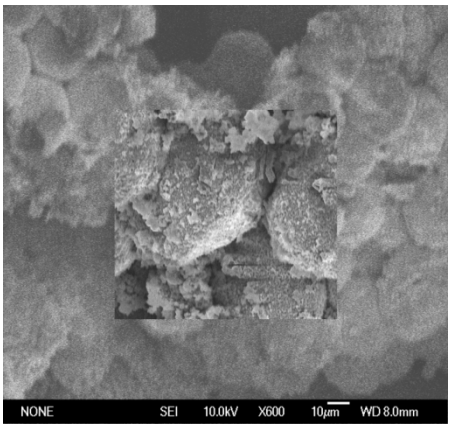

Figure 62: SEM of IAS Treated Copper Porous Media

SEM photographs were taken showing many ligature shaped deposits in the interstitial spaces between particles and clusters within the wick. It was speculated at the time that these deposits might not only have an effect on the physical structure and hydrodynamic properties of the wick, but also might affect the surface interactions and reactions. This hypothesis was inspired in part due to testing on the IAS performed at the Naval Research Lab which showed that IAS formed 100x less hydrogen in a reaction test with aluminum as compared to water.

Thermophsyical Property testing performed by researchers at UCLA showed that the properties of the IAS varied very little from water. Enthalpy of vaporization and surface tension were virtually identical to that of water, despite generally improved performance in comparison with that of water. However, significant reduction of contact angle was noted between liquid

water and surfaces that had been treated by IAS. The origin of this performance gain is the focus of future work.

When trying to understand the impact of IAS on biporous material, there are many things to consider. First, the structures that form on the surface of the particles and clusters clearly have an impact on the heat transfer, but from a purely physical standpoint, they must also contribute to restricting the pores to flow. It follows then that the IAS has competing influences on the performance of sintered copper material. The restriction of the pores decreases the permeability while increasing the capillary pressure. The surface coating formed by IAS also increases the wetting of the surface to the liquid IAS and the structures that grow raise the overall surface area per unit volume. In this section, a modeling technique used to predict performance of biporous material is used to try to understand the forces at work powering the performance changes seen with IAS. The model relates the pore size distribution to the fluid flow and heat transfer in the wick. The impact of IAS on the pore size distribution and heat transfer will be discussed and their effects on the modeling technique outlined. The results of this modeling will then be presented, estimating the change to the evaporation heat transfer coefficient.

6.2.1 Reduction in pore sizes

Using IAS in copper deposits two distinct layers. The first layer is a passivation layer, which is very compact and tends to coat all surfaces. The second layer is more disperse and forms the familiar structures, seen in SEM's of biporous material. These structures tend to form in areas where the IAS is evaporated and though these structures are not continuous they tend to form in a periodic fashion and are of a uniform thickness. With respect to a biporous wick, since most of the evaporation is taking place at the heater surface and in the small pores, these structures will primarily form in the small pores. This means that the small pores are most likely

to experience a change in size in shape. There are several important implications of this supposition.

Making the small pores smaller will reduce the liquid permeability of the wick. This will act to increase the pressure drop required to pump liquid to the heater, decreasing the capillary limit of the wick. This will have a negative effect on the performance of the wick because it will act to decrease the dry-out heat flux as defined as the point at which the capillary pressure drop is exceeded by the mass flow rate of vapor exiting the wick. On the other hand, decreasing the pore size will increase the available capillary pressure in the wick as determined by the Young-Laplace equation. Raising the capillary pressure makes it harder to deplete the pores of liquid. This is clearly a competing influence with the decreased permeability. However, if liquid is flowing around the outside of the clusters, there would be a meniscus which forms in the necking area of the wick. This meniscus would be able to supply the smaller pores on the outside of the wick to keep them wet. It is possible that this effect could counterbalance the loss of permeability. The effect of shrinking the sizes of the small pores on the current modeling effort would be to reduce the small pore sizes 15% (based off inspection of SEM images) in the pore size distribution.

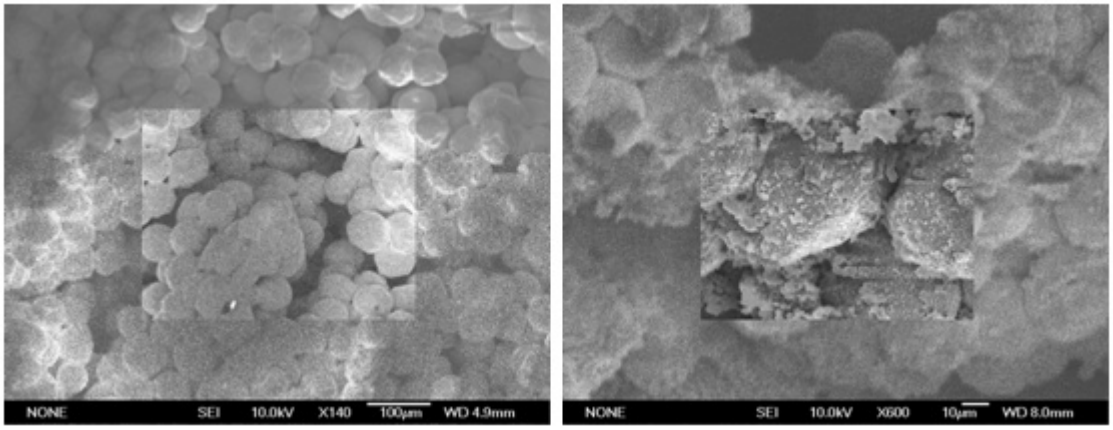

Figure 63: IAS effect on biporous material

The secondary structures formed by the IAS are themselves porous and have many small pores on them. These pores on the IAS substructure may not be interconnected and as their formation is periodic and not continuous, they would have to be externally supplied with liquid. Furthermore, as they are very small, their permeability and capillary pressure would be much lower and higher, respectively, relative to the existing small pores in the biporous material. They would likely not be involved in the supplying of liquid to the heater interface but would contribute to maintaining a wetted surface on the structure of the particles. As it is difficult to ascertain the connectivity of these additive small pores, no change to the pore size distribution was made.

6.2.2 Effect on Heat Transfer

There has been a great deal of work in the area of enhancement of heat transfer from porous surfaces. Many have tried to augment the particle surfaces with artificial structures, such as carbon nano-tubes (CNT's), see Ranjan [28]. Many of the principles associated with the

enhancement of heat transfer by the addition of CNT's are the same that can be applied to IAS treated wicks. In increasing heat transfer, increasing both the effective surface area and wetting are both important.

It is clear from the SEM's discussed in the above section that the IAS secondary structures provide additional surface area to the wick. The enhanced surface area provides more area across the surface of the particles for evaporation as well as providing an increase in capillary pressure which will keep the surfaces of the particles wet. It is believed that one of the reasons that biporous material is so effective is that the irregular shape of the clusters provides more surface area per unit volume than a similarly sized patterned wick, constructed of monoporous material. Taking the irregular shape of the biporous clusters and augmenting them by adding surface area on the particles that construct them will magnify this effect. In Ranjan's work, it was clearly shown that the addition of CNT's to the surface of particles increased the maximum effective heat transfer coefficient of the wick. In the original biporous modeling effort, the heat transfer coefficient was determined from kinetics and then corrected for an increase in surface area per unit volume. The effect on the modeling, when looking at IAS, is to further adjust the heat transfer coefficient to a higher value which will fit the experimental data for IAS treated wicks.

Another effect of using IAS is its impact on the liquid wetting of the surface. Much work has been conducted by UCLA to show that the contact angle for IAS is reduced, relative to water, and that the structures themselves play a large role in this effect. This increased wetting is likely the vehicle by which the surface of the particles stays wet through evaporation. The wetting action fills the small pores of the secondary structures and reduces the resistance to fluid

flow in the wick. Copper is naturally hydrophobic as are its common oxides that form in air but the IAS is able to effectively counteract this effect. In relation to CNT's, the CNT's thermal conductivity is very high but a limiting factor on their performance is that they are naturally super hydrophobic. A common method for counteracting this effect is to coat the CNT's with a microscopic layer of copper, which is again, still prone to hydrophobic oxide formation. Being that the IAS does not suffer from these hydrophobicity problems, it is clear that this effect will contribute to further increasing the effective heat transfer coefficient.

To summarize, the formation of secondary structures by an IAS has the effect of forming more small pore sizes, adding micro-pores to the surfaces of the particles and small pores, and augmenting the effective heat transfer coefficient. The results of adjusting these parameters to fit to experimental data will now be discussed.

6.2.3 Results

The results of the modeling and experimental efforts will now are discussed. The particular wick that was studied with both water and IAS was comprised of 60 μm particles, 400 μm clusters, and a thickness of 800 μm. The experimental data from a run with water and IAS performed on this wick are displayed in Figure 64.

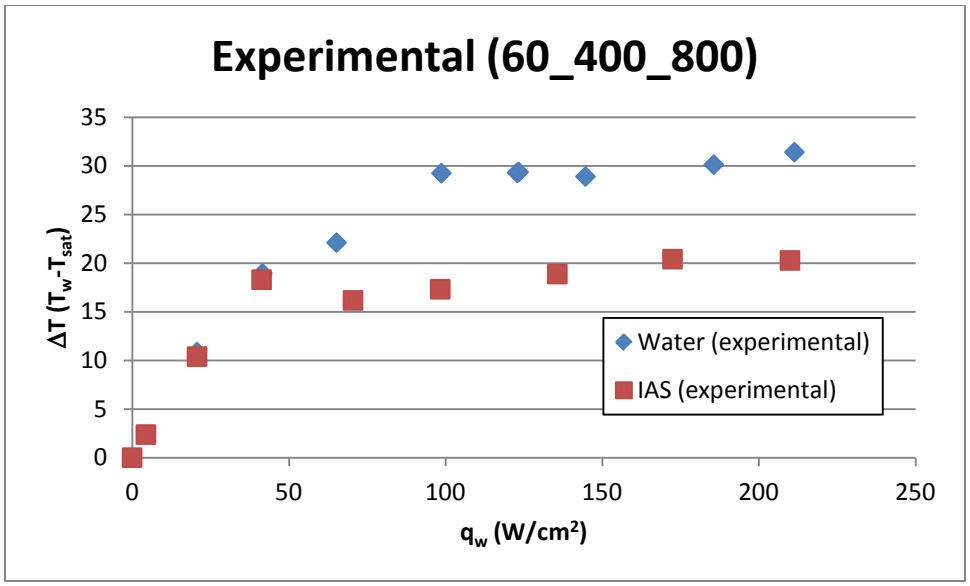

Figure 64: Experimental IAS comparison

Note that the IAS and Water values are basically coincident until approximately 50 W/cm^2, and then diverge. This is likely the point at which nucleation begins in the wick; at this point the hydrodynamic properties of each working fluid with respect to evaporation become dominant. The IAS reduces the superheat value by approximately 30%-40% and is fairly linear after nucleation, as is the water. The tests were not run to higher heat fluxes as the experiment was not configured in such a way to establish dryout. The main result of this investigation is that it was possible to show that IAS effectively reduced the superheat of the biporous copper evaporator wick after nucleation was begun.

As stated before, in order to apply the previous biporous modeling effort to the IAS, several changes were made. First, the small pore sizes were reduced by 15%. This reduction was an estimate based on examining SEM's of biporous wicks and observing that the deposits were most likely to form in the small pores where the majority of evaporation took place. In

order to match the results seen in the 60_400_800 wick, the effective heat transfer coefficient was adjusted in order to achieve the desired effect. The results of this modeling effort are seen in Figure 65.

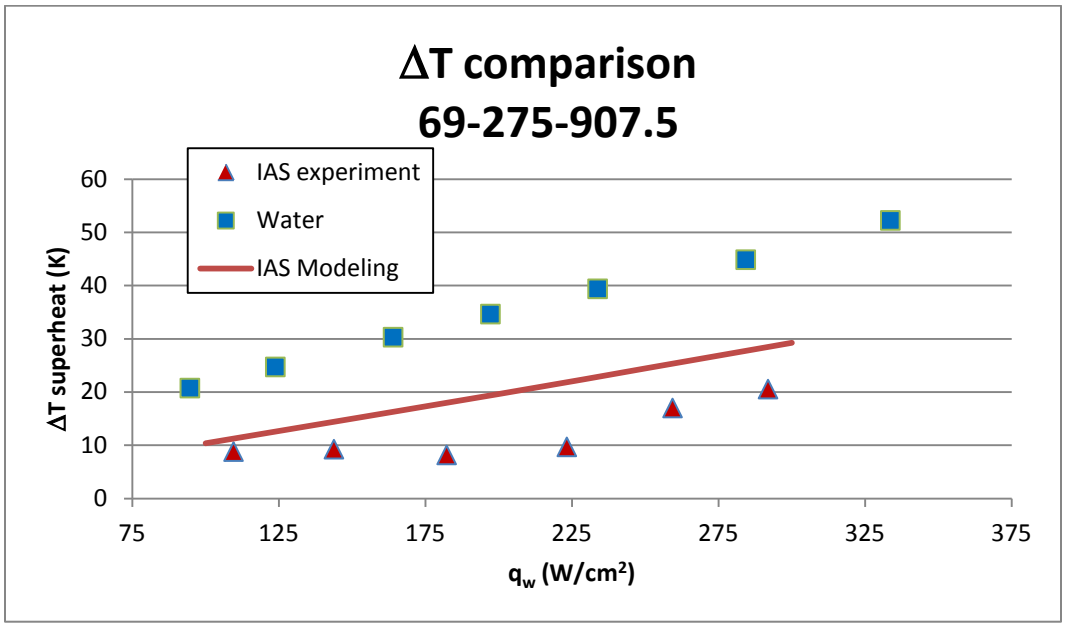

Figure 65: Modeling IAS Comparison

Clearly the results in this case are not as linear in the region following nucleation but the noted increase in performance is consistent. The IAS showed an increase in performance of approximately 30% @ 200 W/cm^2 heat flux, which is slightly less than what was observed in the experimental investigation. It should also be noted that the mean average error between the IAS modeling and experimental data was approximately ~34%. This error is larger than was noted for the biporous material but this is to be expected with regards to the much more complicated physics.

The IAS increased the heat transfer coefficient increased by 3x relative to water. This seems large, but since it is an approximation that incorporates the kinetics estimate of the heat transfer coefficient and effective surface area increase, as well as increased wetting, it is not altogether unexpected. However, it is evident that this significant increase cannot be entirely attributed to an increase in surface area per unit volume and that a significant contribution must come from meniscus level heat transport. Since as pore size decreases, the percentage of thin film evaporation can increase to over 50% of the total heat transport [27], future work must look at determining the amount that the meniscus contributes to the evaporation heat transfer coefficient.

Furthermore, it is worth noting that the effect that the IAS has is very similar in nature to the improvement afforded by utilizing the previously mentioned double layer wicks have. This seems to indicate that perhaps a similar effect is the cause of performance increase; small pores are formed near the heater interface which increases capillary pressure, maintaining surface wetting for a wider range of heat fluxes.

Another parameter whose augmentation by the IAS relative to water that needs to be compared is the capillary pressure. The results of this comparison are shown in Figure 66.

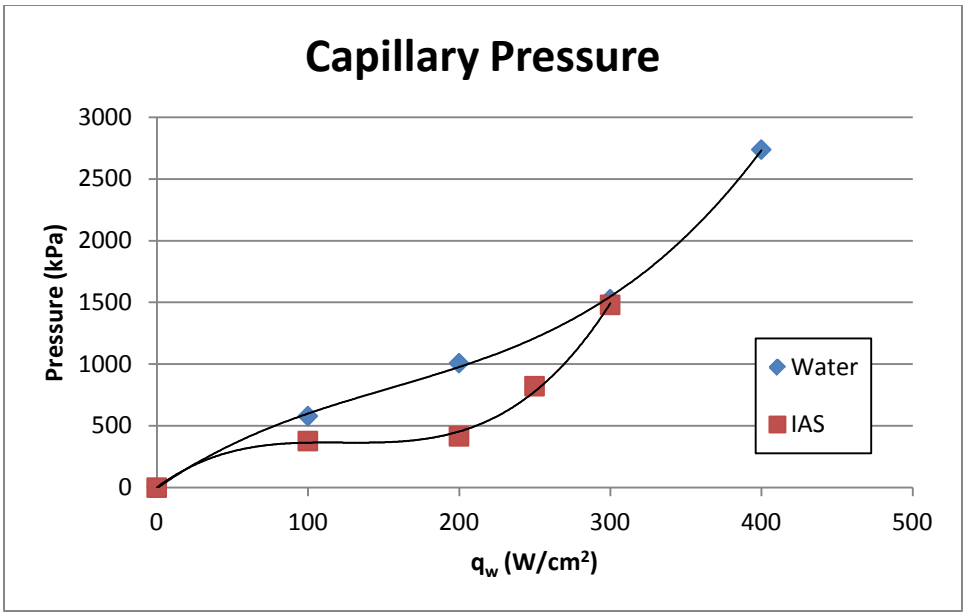

Figure 66: Required Capillary pressure Comparison

Note that, in this case capillary pressure is referred to as the necessary pressure head required to supply liquid to the heater surface. The IAS was found to require less capillary pressure at lower heat fluxes but began to rise quickly after 200 W/cm^2 of heat input. This does not mean that the overall capillary pressure of a wick treated with IAS has decreased; this is simply an indication of how much of the available capillary pressure is being used to supply liquid to the surface. Since the IAS restricts the pore sizes, the potential capillary pressure is raised while the liquid permeability is decreased.

These results are consistent with typical utilization of CNT's on microstructured wicks [51]. In Weibel's work, it was observed that the application of CNT's to patterned sintered wick tended to cause boiling incipience earlier than a bare wick, but slightly decreased the dryout heat flux. This seems to suggest that the increase in capillary pressure and surface wetting properties are effective at reducing the resistance to liquid flow when there is liquid outside the clusters,

where the reduction in liquid permeability as a result of small pore atrophy is less pronounced. This is likely because of a secondary meniscus forming in the necking area between clusters.

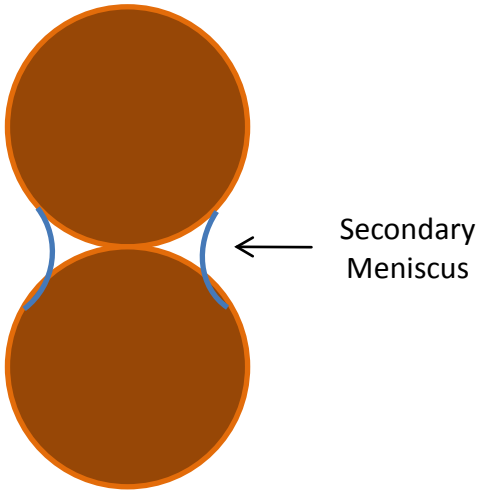

Figure 67: Schematic of Secondary Meniscus

However, as heat flux is increased, the small pores become the primary mode by which liquid is transported, and the reduction in permeability tends to increase the required capillary pressure faster than if the wick had not been treated with IAS. Thus, the maximum overall effective heat transfer coefficient will increase but the critical heat flux at which dryout will occur, will be reduced somewhat. This makes physical sense but further experimental study is needed in order to determine the validity of this claim.

6.2.4 Summary of surface modification efforts

In summary, the effects of using IAS on sintered copper biporous wick surfaces are discussed. The primary effects are on the pore size distribution and the heat transfer. Primarily, the small

pores are reduced by approximately 15% and the effective heat transfer coefficient is increased. Previous modeling efforts focused on developing an effective method of predicting dryout in biporous wicks with water was applied to those having used the IAS. Experimental data isolating this effect in biporous material was used to estimate the reduction in superheat temperatures and the model was used to replicate this effect. The results showed that the increased wetting and effective surface area increased the evaporative heat transfer coefficient by approximately 3x, if this method is used. Furthermore, the capillary pressure behavior is consistent with previous application of surface nano-structures to sintered material in that, an increase of maximum overall effective heat transfer coefficient was observed in conjunction with a reduction in the predicted dry-out heat flux. While these results are promising, more experimental study is needed to confirm these theories.

6.3 Summary

In this section, the several experimental studies designed to investigate effective means of predicting TGP performance and increasing biporous wick performance have been presented. First, experiments were conducted to show that an experimental apparatus in use at UCLA which was used to characterize biporous wicks was an effective means of predicting how those wicks would perform in actual heat spreader (TGP) devices. This was done by restricting the vapor space available to the wicks in a similar manner to an actual TGP and was shown to be effective.

Second, three geometric variations on standard biporous wicks were shown which were used to manipulate the pore size distribution. In all cases, the primary goal of geometric optimization to increase the wick's ability to keep the heater interface wetted. Tri-layer and

annular wicks were first discussed as these aimed to concentrate smaller cluster sizes near the heater interface. While the annular wicks tended not to improve performance, the tri-layer wicks tended to increase performance after nucleation by some degree. By far, the best performer was the addition of a monoporous interface layer between the biporous material and heater interface. This was shown to significantly decrease the superheat required for given heat fluxes relative to a standard biporous wicks with smaller cluster sizes. The primary result of these experimental studies was the determination that the most effective means of optimizing a biporous wick through geometric means was the addition of a monoporous interface layer assuming that a cluster size of 300 μm was appropriate.

Finally, modifications of the surface of the biporous material in order to increase wetting were discussed. This was done through the use of a proprietary fluid referred to as IAS. The IAS had the effect of constricting the small pore sizes somewhat but also drastically increasing the wetting properties of the surface. There was also an increase in surface area per unit volume which is instrumental in increasing heat transfer performance. This increase in effectiveness of the surface wetting in conjunction with a slight change in the pore size distribution was able to significantly improve performance of biporous material.

To tie all these experimental studies together, the goal of this chapter was to show that insights gained from the Kovalev modeling technique could be used to optimize the performance of a biporous wick. The suggestions carried over from the previous chapter were to increase the surface wetting of the wicks while also manipulating the pore size distribution to create more favorable conditions for heat transport. Both methods were successful, within the limits of being able to construct the wicks effectively. Furthermore, the Kovalev modeling technique was used

to emulate the performance of a biporous wick using IAS and achieved reasonable success. Thus, the Kovalev method has been shown not only to be an effective method of modeling a biporous wick but has shown to be a tool that can be used to optimize a biporous material on the basis of heat transfer. In the following chapter, some future work will be suggested to refine and extend the capabilities of this particular technique.

7.0 FUTURE WORK

In this section, the suggested future work will be detailed. This dissertation has outlined efforts to develop a method of optimizing sintered copper biporous material using a Kovalev modeling method. While this method was successful, there are many opportunities for improving the flexibility of the model and accuracy of its results. These opportunities fall into two major categories; improvements to the base model and improvements in the ways the model is used to develop optimized wicks.

7.1 Base Model

While the Kovalev method proved to be very useful in predicting the performance of sintered copper material tested at UCLA, there are some specific things that would lead to a more effective modeling effort. There were many things about the model that had be assumed along the way in order to get the model to work as there was not ample time to explore each parameter completely. In what follows, some aspects of the model that could be improved are discussed. .

As mentioned earlier, the accuracy of the estimates provided by the Kovalev technique are strongly tied to the accuracy of the pore size distribution used to make the estimates. In this work, the distribution was constructed from particle analyzer data and the pore sizes were inferred based on previous mathematical estimates based on an empirical bed of spheres model. Due to the highly irregular shape and packing orientation of sintered copper material, the pore sizes are not necessarily so well behaved as to be regularly arranged. A more rigorous investigation of the relationship between particle size, cluster size, and pore size would help to better understand this relationship. A more refined pore size distribution would also help answer

the question of what the relative number of pores is, i.e., how many small pores to large pores there are. Furthermore, a more rigorous definition of what constitutes a large pore could be established. As the large pores are comprised of the spaces between the clusters, it is sometimes difficult to establish the typical shape of a large pore, as can be seen in Figure 68.

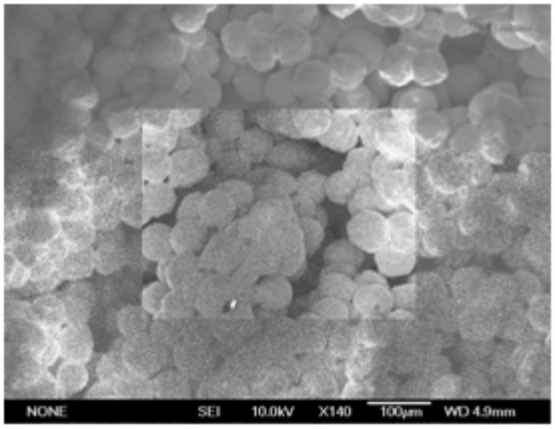

Figure 68: SEM of sintered Copper Material

The shape of the clusters has a significant impact on many facets of biporous material performance, not limited to the shape of pores or the pore size distribution itself. Another assumption that was used to develop the model was that the volumetric heat transfer coefficient was a strong function of the surface area per unit volume of the wick. For the cluster sizes investigated in this work (approx. 200μm-600μm), this methodology led to the volumetric heat transfer coefficient increasing as a function of cluster size. This is likely due to the fact that the surface area per unit volume actually increases as a function of nominal cluster diameter indicating that clusters tend to more irregularly shaped as they are sieved to larger sizes. This is supported by the fact that the standard deviation of the clusters is a strong direct function of size, increasing almost linearly with cluster size. While it is believed that the heat transfer coefficient is a function of surface area per unit volume and the data shows this, more rigorous investigation

of this specific phenomena is needed to completely affirm it. Similar to the pore size distribution, very careful measurement of the geometric parameters of a wick that had been tested would serve to verify this observation.

The model described in this work is 1-D and it is natural to suggest that in the future the model be taken to two dimensions so as to help increase its flexibility. As most of the wicks that were investigated in this work and tested at UCLA were radially symmetric, moving from 1-D to 2-D cylindrical coordinates would capture a large portion of the data and allow for greater insight into the behavior of these biporous wicks. Furthermore, this would make the Kovalev modeling technique easier to apply to more varied and complex biporous wicks. For instance, modeling studies could be carried out on the annular wicks that were tested as part of this dissertation to see if there was any phenomenological basis for why they did not show performance improvements. It would also be helpful in taking a closer look at the double layer wicks that had performed so well.

It would also be desirable to carry out modeling investigations on more varied types of wicks than those listed here. The wicks investigated in this work were all sintered copper and all but one were biporous. While that was the focus of this work, there are many and varied types of porous and biporous material. For instance, there is biporous material made from chemically etched post arrays. As this more simplistic geometry is extremely well defined relative to the sintered material, this would be an opportunity to do more validation to verify the validity of the Kovalev technique. Developing a library of wicks that had been investigated using this modeling technique would sharpen it even further as a tool for optimizing porous materials.

7.2 Extension to Optimization

Whereas the previous part of this chapter discussed the potential improvements to the base model for prediction of the performance of biporous material, in this section the ways in which the model could be used to optimize sintered material is discussed. In this dissertation, two main methods of improving performance were suggested; 1) changing the geometry to manipulate the pore size distribution and 2) improving the surface wetting properties of the biporous material. These optimizations were inferred from results of modeling the biporous wick performance and the relationship between dry out and capillary pressure. The former was investigated by modifying the biporous wick through the use of monoporous material in specific regions where capillary pressure was most important and the latter was investigated using a designer working fluid in place of water. Some of the potential for future work for each of these optimization paths are discussed.

One of the biggest problems with investigating geometric changes in the wick is maintaining some level of consistency regarding the construction of these wicks. That is to say, that constructing a sintered copper wick with different types of porous material is a complicated task. The simplest form of an advanced biporous wick discussed in this work is the double layer wick, where monoporous material is laid down underneath biporous material. The sintering must take place in multiple steps to create this arrangement and each step increases the chance of failure. Failure in this case meaning that adequate porosity is not maintained in the monoporous material due to over sintering, which causes the particles to fuse to one another, forming low porosity material. In looking at either the triporous or annular wicks, these construction methods are even more complex.

In order to remedy this, future work could be done on the sintering process itself in order to see if there is an easier way to form these wicks without having to go through so many risky sintering steps. Furthermore, anything that would result in a more consistent process for producing biporous wicks with similar parameters would greatly help in the investigation of their behavior. This could also be extended to the way in which the biporous material itself is constructed. It is believed that the irregular shape of the biporous material is critical to its performance, but it also makes it difficult to mass produce. The current process is very labor intensive and low yield with regards to producing a desired cluster size and so could be improved. Having greater confidence in the specific geometry of the wicks would help to further validate the claims made in this thesis regarding estimating the dryout point of different biporous materials.

Furthermore, more sophisticated methods of optimization would drastically help the search for optimized wicks. The optimization done in this work was primitive in that only a few optimized designs were inferred from modeling data. In the future, coupling the model to advanced numerical methods such as genetic algorithms or to design of experiment (DOE) software would be beneficial to take a more targeted approach to optimization.

With regards to the surface modification of the wick, this work focused on the use of a replacement working fluid, IAS, in place of water. This fluid was used to increase the wetting properties on the surface of the biporous particles and clusters. The IAS is a very complex aqueous solution of several different ions and as such, an assumption was made that the IAS primarily impacted the performance by increasing the surface area on the surface of the clusters

and increased the wetting of the liquid on the copper surface, similar to an oxidation coating [44]. The growth of secondary structures on sintered is shown again for emphasis in Figure 69.

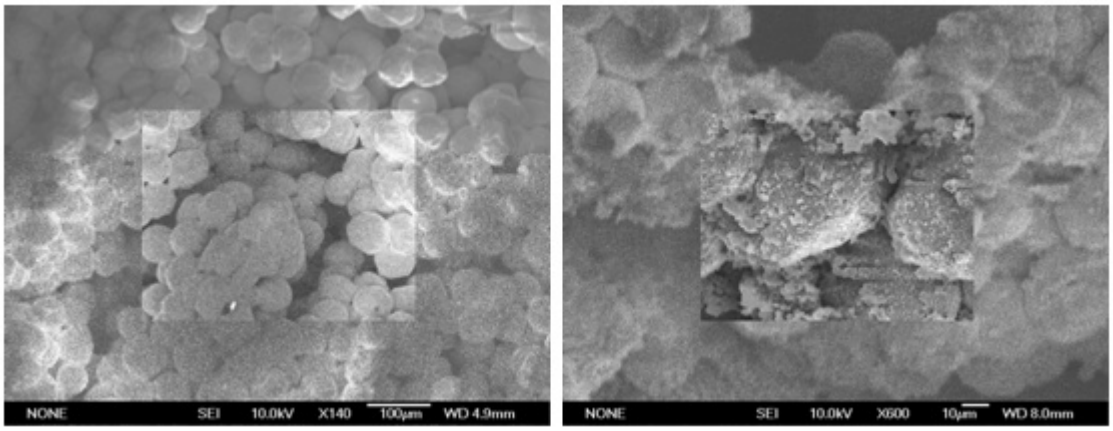

Figure 69: IAS effect on sintered material

As far as the model in this work is concerned, the use of IAS only impacted the formulation of the volumetric heat transfer coefficient and in the pore size distribution. Clearly, the deposition of secondary structures by ions in suspension has a much more complex effect on the heat transfer of evaporating liquid. In the future it is advisable to conduct research regarding the exact nature of the evaporation of IAS from copper surfaces at the microscopic meniscus level. This includes accounting for the change in disjoining pressure and physics involved with evaporation from the interline, or thin film contact region. The current understanding is that the IAS increases evaporation capacity by stretching the thin film evaporation region of the meniscus through enhance wetting.

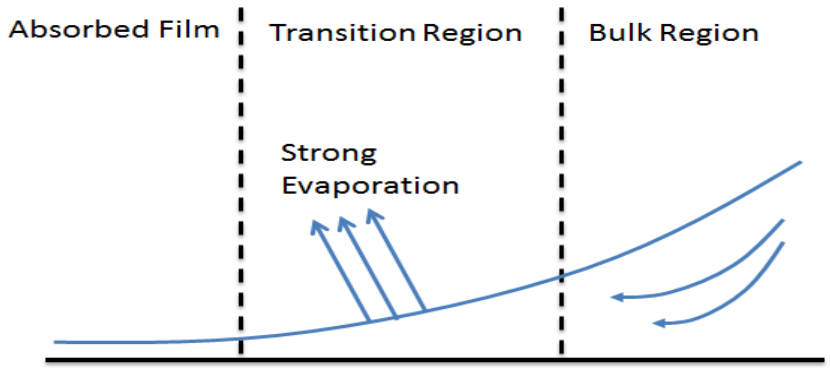

Figure 70: Schematic of interline region

A more complete investigation of this phenomenon is currently under way at UCLA by Suppowit [39]. The information gleaned from the microscale could be coupled to the macroscale Kovalev model to refine the parameters associated with evaporation. Namely, if an accurate portrayal of evaporation at the meniscus is achieved, this can be integrated across many similar menisci to acvhieve a true contact angle and increase in heat transfer coefficient.

Future work needs to be done to more rigorously determine the true effect of IAS on the local pore size distribution. In this work, it was assumed that the effect was primarily on the small pores and that it was typically uniform. However, this does not take into account the deposition as a function of ion concentration or exposure time nor does it account for the fact that deposition could be more pronounced at the liquid reservoir/porous medium boundary. There could be a filtering effect where more deposition occurs at the periphery of the wick where it is adjacent to pooled fluid and this could lead to a gradient effect on the pore size distribution and small pore constriction as one moves away from the fluid reservoir and towards the heater. This effect needs careful further study for it to be incorporated better with the Kovalev model.

The suggestions for future work listed here are by no means comprehensive but are the most obvious ones arising during the development of the Kovalev based model. Clearly, there are many opportunities for improvement to the modeling and experimental work presented in this work. However, it is important to note that even with these opportunities the work presented here does provide a viable pathway forward to continued investigation into optimization of porous medium evaporators.

8.0 CONCLUSION

The stated goal of this thesis was to devise a way to optimize the performance of sintered copper biporous material for use as an evaporator. This goal was accomplished through utilization of a modeling technique based on the work of Kovalev [19] and was shown to be successful. While there have been many different attempts to model flow in porous media this is the first one to focus primarily on optimizing sintered biporous material and use it as a tool to improve biporous wick performance. In this dissertation, the following items were major results of the thesis work:

1. A derivation of the equations needed to construct a model from the work of Kovalev was presented. This included all relevant variables needed to predict evaporative heat transfer in two phase flow in a porous media as well as the technique used to close the equations and solve them over the computational domain
2. A technique used to derive the thermophysical properties needed to use the model was developed. This technique used statistical methods to not only derive a pore size distribution but also to estimate the liquid and vapor relative permeabilities as well as the heat transfer coefficient and capillary pressure. The estimated capillary pressure from the wick was estimated to within 10% of experimental measurements made by Semenic [35]. A secondary result of this part of the investigation was determining that the cluster size had a large effect on the thermophysical properties. It was found that the standard deviation of the cluster (and particle sizes) was also a strong function of the nominal diameter indicating that the larger the diameter, the more irregularly shaped the cluster will be. This led to the assumption that the surface area per unit volume actually increased within the range of cluster sizes tested as a function of cluster diameter.

3. The resulting model was validated against experimental data for one monoporous wick and 5 biporous wicks. The resulting mean average error between the model and experimental data was less than 15% and well within the estimated variance in Semenic's data [35] of 16.5 %. This validation of the model predictions of heat transfer performance against experimental data give confidence in the results obtained from the model for other performance properties, such as capillary pressure and liquid saturation. These secondary performance properties will be useful for later work in optimization.
4. The model was then used as a tool to help predict the dry out of the large pores in the wick, the condition thought to exist when the effective heat transfer coefficient reaches its peak. This was found to be a function of the capillary pressure estimates returned from the model and when compared to the maximum effective capillary pressure, derived from the pore size distribution, an estimate of the dry out point was made possible. These dry out points were compared with experimental data and resulted in a mean error of less than 18% for all wicks which improves upon the average error of Vadnjal [41] of 20%. The median is included because the maximum error encountered was 28% although a majority of the errors were less than 20%. Still, predicting the dry out point of the large pores to within an average error of 18% was unprecedented and allowed for the model to be used to help predict the performance and be used to optimized wicks. From observations of the wick performance obtained with the model, it was suggested that the best way to improve wick performance was through manipulation of the pore size distribution to increase capillary pressure over the heater interface and also to modify the surface wetting properties.

5. Finally, experimental studies carried out by the author were presented showing the results of wick optimization studies suggested by the model. Several different wick geometries were tested where there were two different regions in the same wick with finer structure used to increase capillary pressure over the heater area. The best performing of these geometries was the "double layer" wick; a wick where a thin monoporous layer of particles applied over the whole bottom (heated) surface of the wick and biporous material above as a liquid supply structure. Under the right geometric circumstances, this geometry was a vast improvement over regular biporous wicks of the same geometry, reducing thermal resistances by more than 30% in some cases. Secondly, a designer fluid was used in place of water in order to alter the surface wetting properties. This fluid, referred to as IAS, is a complex ionic mixture of several different chemicals. The IAS dramatically decreases the contact angle on copper relative to water while maintaining roughly the same specific heat and enthalpy of vaporization, making it an extremely attractive substitute for water in evaporative cooling devices. The IAS was shown to not only increase performance through surface wetting, but also it formed secondary porous structures on the surfaces of the wick. Again, under the right geometric circumstances, the IAS significantly decreased thermal resistance over a biporous wick of the same geometry using water. The Kovalev model was used in order to reinforce our belief that the effects came from increased surface wetting and internal surface area as well as the addition of small pores.

In summary, it was shown that the Kovalev model is an effective means to both predict and optimize the performance of sintered copper biporous wicks. The model presented in this work is a first attempt to tie statistical estimations of the pore size distribution directly to

the large pore dry out/maximum effective heat transfer coefficient and represents an important step to applying sintered copper biporous material to more complex wick designs. There is considerable potential for future expansion of this work to more varied wick types and wick arrangements.

APPENDIX

MATLAB Code

Solver:

```
%% ODE solve 3
tic;

clear all
close all
%% As of 3/15, this program determines the thermal performance for a chosen
%% heat flux by calculating the boundary conditions and domain values
%% simultaneously by way of an Euler in the domain and Newton Raphson about
%% the boundary conditions
dbl = 0;

 %% the following blocks are initial conditions for various wicks.  They
 %% call the appropriate pore size distributions ("wick ==..") and read in
 %% the experimental data from the appropriate text files.  "Validate" is
 %% simply the experimental data.  D is cluster size, d is particle size,
 %% and delta is the overall thickness of the wick

  %% experimental data txt files contain only one column, heat fluxes and
 %% then a zero indicating the next values are delta T's

%% 328_82_1082, verified ~ 0.93% error for q = 222.35, 1/11/2012, he =
%% 2e4,dependant on geometry
% validate = zeros(20,2);
% Tadej = textread('328_82_1082.txt');
% hn = 2e8; %% dpeendant on R, 7/16/2012
% validate(:,1) = Tadej(1:20,1); %% heat flux, 328_82_1082
% validate(:,2) = Tadej(21:40,1); %% delta T, 328_82_1082
% wick = 4;
% Rmax = 358e-6;
% D = 324e-6;
% d = 71e-6;
% delta = 1082e-6;

%% 82_460_1518, verified
%
% validate = zeros(19,2);
% Tadej = textread('82_460_1518.txt');
% hn= 7e8;
% validate(:,1) = Tadej(1:19,1); %% heat flux, 328_82_1082
% validate(:,2) = Tadej(20:38,1); %% delta T, 328_82_1082
% wick = 7;
% Rmax = 572.64;
```

```
% D = 460e-6;
% d = 82e-6;
% delta = 1518e-6; %% problem not here, somewhere else, 6/21/2012
% delta = 907.5e-6;
%% 69_196_646.8, verified
% validate = zeros(17,2);
% Tadej = textread('69_196_6468.txt');
%
% validate(:,1) = Tadej(1:17,1); %% heat flux, 328_82_1082
% validate(:,2) = Tadej(18:34,1); %% delta T, 328_82_1082
% wick = 5;
% hn=2.0e8;
% D = 196e-6;
% d = 69e-6;
% delta = 646.8e-6;
% Rmax = 244e-6;
%% 69_460_800
% validate = zeros(31,2);
% Tadej = textread('69_460_800.txt');
% hn = 9.0e8;
% validate(:,1) = Tadej(1:31,1); %% heat flux, 328_82_1082
% validate(:,2) = Tadej(32:62,1); %% delta T, 328_82_1082
% wick = 6;
% Rmax=520e-6;
% D = 449e-6;
% d = 61e-6;
% delta = 800e-6;
%% 58_330_800 (60_400_800) WATER
% validate = zeros(10,2);
% Tadej = textread('58_460_800_w.txt');
% hn = 2.0e8;
% validate(:,1) = Tadej(1:10,1); %% heat flux, 328_82_1082
% validate(:,2) = Tadej(11:20,1); %% delta T, 328_82_1082
% wick = 11;
% Rmax=716e-6;
% D = 324e-6;
% d = 57.47e-6;
% delta = 800e-6;

%% 58_460_800 (60_400_800) Water
% Set up for 69_275_907.5, 10.24.2012
% validate = zeros(9,2);
% Tadej = textread('58_460_800_IAS.txt');
% wick =2;
% hn =2e8;
% validate(:,1) = Tadej(1:9,1); %% heat flux, 328_82_1082
% validate(:,2) = Tadej(10:18,1); %% delta T, 328_82_1082
% Rmax=183e-6;
% D = 272e-6;
% d = 61e-6;
% delta = 907.5e-6;
%% 82_275_907.5, verified, ~ 22.24% error for q = 218, 1/11/2012, he = 2.0e4,
%% dependant on geometry
% validate = zeros(19,2);
% Tadej = textread('82_275_9075.txt');
% hn = 2.0e8;
```

```
% validate(:,1) = Tadej(1:19,1); %% heat flux, 328_82_1082
% validate(:,2) = Tadej(20:38,1); %% delta T, 328_82_1082
% wick = 3;
% Rmax=297e-6;
% D = 272e-6;
% d = 71e-6;
% delta = 907.5e-6;

%% 69_275_907.5, verified, %24.2 error, 200.46, he=2e6
validate = zeros(16,2);
Tadej = textread('69_275_9075.txt');
hn = 2.0e8;
validate(:,1) = Tadej(1:16,1); %% heat flux, 328_82_1082
validate(:,2) = Tadej(17:32,1); %% delta T, 328_82_1082
wick = 2;
% % qchf = 429.88 w/ 69.21 DT
Rmax=297e-6;
D = 272e-6;
d = 61e-6;
delta = 907.5e-6;
deltam = 120e-6;
Rmax1 = 41.94e-6;
dbl = 0;

%% 60_120/60_300_880
% validate = zeros(9,2);
% Tadej = textread('60_120_60_300_780.txt');
%
% validate(:,1) = Tadej(1:9,1); %% heat flux, 328_82_1082
% validate(:,2) = Tadej(10:18,1); %% delta T, 328_82_1082
% hn =5e8;%2.0e7;
% wick = 2;
% % qchf = 429.88 w/ 69.21 DT
% Rmax=297e-6;
% D = 272e-6;
% d = 61e-6;
% delta = 907.5e-6;
% deltam = 120e-6;
% Rmax1 = 41.94e-6;
% dbl = 1;
%
%% 69_460_2000
% validate = zeros(32,2);
% Tadej = textread('69_460_2000.txt');
% hn = 2.0e8;
% validate(:,1) = Tadej(1:32,1); %% heat flux,
% validate(:,2) = Tadej(33:64,1); %% delta T,
%
% % % qchf = 429.88 w/ 69.21 DT
% Rmax=570e-6;
% D = 460e-6;
% d = 69e-6;
% delta = 2000e-6;

%% 69_460_1400
```

```
% validate = zeros(31,2);
% Tadej = textread('69_460_1400.txt');
% hn = 9.0e8;
% validate(:,1) = Tadej(1:31,1); %% heat flux,
% validate(:,2) = Tadej(32:62,1); %% delta T,
%
% % % qchf = 429.88 w/ 69.21 DT
% Rmax=520e-6;
% D = 449e-6;
% d = 61e-6;
% delta = 1400e-6;
%% 60_900, monoporous
% validate = zeros(13,2);
% Tadej = textread('60_900.txt');
% hn = 5.0e8;
% validate(:,1) = Tadej(1:13,1); %% heat flux,
% validate(:,2) = Tadej(14:26,1); %% delta T,
%
% % % qchf = 429.88 w/ 69.21 DT
% Rmax=38e-6;
% D = 58e-6;
% d = 58e-6;
% delta = 900e-6;
% wick = 8;
%% 300_600, monoporous
% validate = zeros(12,2);
% Tadej = textread('300_600.txt');
% hn = 1.4e8;
% validate(:,1) = Tadej(1:12,1); %% heat flux,
% validate(:,2) = Tadej(13:24,1); %% delta T,
%
% % % qchf = 429.88 w/ 69.21 DT
% Rmax=124e-6;
%
% D = 275e-6;
% d = 61e-6;
% delta = 600e-6;
% wick = 9;
%%


IL = 100; %% smaller IL helps with stability, total number of steps in z
direction
IT = 100000; %% maximum number of time steps
IQ = 30;
relax = 1e-3;  %% relaxation parameter, lambda

%% various matrix intializations
qmax = zeros(1,IQ);
maxtheta = zeros(1,IQ);
Terr = zeros(1,IT);
z1 = linspace(0,delta,IL); %% z(one), z position, m
dz = z1(1,2)-z1(1,1);
drdz = zeros(1,IL);
Fn = zeros(6,4);
```

```
%% Properties
rhov = 0.0511; %% kg/m^3, density of water vapor
muv = 0.000013; %% Pa*s, viscosity liquid water
rhol = 1000; %% kg/m^3, density of liquid water
epsilon1 = 0.642; %% porosity
mul = 0.6531/100;  %% Pa*s, viscosity liquid water
Ar = 0.15; %% area ratio
Rgas = 461.5; %% Water vapor gas constant, J/kg/K
keff = 2987*(D*1e6)^-0.9 ; %% W/m/k, thermal conductivity from Seminic
Thesis, monoporous
keffm = 145; %% W/m/K Thermal Conductivity of monoporous material
kvapor = 0.016;
sigmaw = 72.3e-3; %% N/m
thetad = 0;
he = 0; %%2.0e6; %% heat transfer coefficient, Aleks' thesis v11
g = 9.81; %%m/s^2
hfg = 2257000; %% j/kg
% Sw =6*(1-epsilon1)/D; %% specific surface area of bed of spheres



%% do loops

ptmax = 1e5;
% compare = zeros(ptmax,2);

%% PCmax calculator, calculates max capillary pressure
% Pcmax = (-0.2*(d/1e-6)+27.81)*1000; %%Pa, translate a velocity to determine
Jl,from tadej
% yp11 = 12;
% xp11 = 59;
% yp21 = 10;
% xp21 = 72.5;
%
% slope1 = (yp21-yp11)/(xp21-xp11);
% yo1 = yp11-slope1*xp11;
%
% Pcmax = (slope1*d/1e-6+yo1)*1000;
% kl = 4.1083e-012;
% kv = 1.4003e-011;

%% kl calculator, permeability calculator
kl = (0.04*(d/1e-6)-0.83)*10^-12; %% From Semenic
% kl = 5.84e-12;
% yp12 = 0.8;
% xp12 = 58.5;
% yp22 = 1.9;
% xp22 = 83;
%
% slope2 = (yp22-yp12)/(xp22-xp12);
% yo2 = yp12-slope2*xp12;
%
```

```
% kl = (slope2*d/1e-6+yo2)*10^-12;
% kv2 = 1.788e-10;
% kv = 1.788e-10;
%% kv calculator, vapor permeability
kv = (1.2*(D/1e-6)-190.1)*10^-12; %% From Semenic
% kv = 1.59e-10;
% yp13 = 200;
% xp13 = 302;
% yp23 = 900;
% xp23 = 892;
%
% slope3 = (yp23-yp13)/(xp23-xp13);
% yo3 = yp13-slope3*xp13;
%
% kv = (slope3*D/1e-6+yo3)*10^-12;
%%  Modeling comparison to Amouzegar, not necessary for performance
%%  calculations but left for legacy

dPc = 2*sigmaw/d ;
nul = mul/rhol;
nuv = muv/rhov;
Re = 0.0032;
%
% x1 = dPc*kl/mul/nul*delta/Re;
% x2 = nuv*kl/nul/kv*(delta/Re)^2;
% qcl = mul*hfg/Re*(2.1534*x1^0.4526/(1+0.5399*x2^1.029));
%% Other constants and variable matricies

Tsat = 40;
[rhol,rhov,Psat] = SaturationTEMPtable(Tsat);
aph = sqrt(2/pi)*(1/Rgas)^(3/2)*Psat*hfg^2/(Tsat+273.15)^(5/2);
%         avol = 5.6*epsilon1^2*sqrt(aph*kl)*(pi/2-
atan(sqrt(aph*delta/kl)))*phi/sqrt(Y(1,j))*avolint;
phicheck=zeros(1,IL);
hv = zeros(1,IL);
Y = zeros(6,IL);
Vv = zeros(1,IL);
Rev = zeros(1,IL);
YEr = zeros(4,ptmax);
Po = 15000;  %% vapor pressure in vapor space
err = zeros(1,ptmax);
Er = zeros(3,3);
Yn = zeros(3,3);
DER = zeros(4,4);

lmax =50;
out = zeros(length(validate),5);

F = zeros(6,IL);
hsafety = 0;
emergency = 0;

fluxlimit = 40; %% sets maximum flux, typically set equal to q so that only
one point is run, if greater than q, multiple fluxes will be looked at in a
```

```
single run but this causes problems with the intial conditions from one heat
flux to the next
q =40; %% sets intial flux, typically set equal to fluxlimit, note q*10 =
W/cm^2

%% Kovalev based permeability calculator
% [phi kl kv] = CDF_3_22(250e-6,D,d);
% phi = 0.9999;
%% Loops
emergencyR = 0; %% emergency exit parameter
%  phi = 0.8;
%  kv = 0;4
 for l = 1:1 %% heat flux loop
    Y(1,1) = 40e-6;  %% intial guess for R*
%     if dbl ==0
        Y(2,1) = 10; %% intial guess for delta T
%     elseif dbl == 1
%         Y(2,1) = 1;
%     end
    Y(5,1) = 15000*1.001;%1.0001*1.5e4; %% initial vapor pressure at wall
    Y(6,1) = 15000*0.999;%0.9999*1.5e4; %% initial liquid pressure at wall
    Yi = Y(:,1);
% phi = 0.8;
%% DID YOU CHECK TO MAKE SURE CDF IS ON THE RIGHT DISTRIBUTION?


    if q>fluxlimit%length(validate)
        break
    end

    qw = -10*q*1e4; %% conversion from W/cm^2 to W/m^2 for computational
purposes

%

    Y(3,1) = qw/keff;
    Y(4,1) = 0;

    for h = 1:1   %% evaporation check loop

%         [phit kl kv ] = CDF_5_9(2*Y(1,1)); %% stable
%         phi = 0.75;
        for i = 1:ptmax;%%ptmax %% iteration loop
            if emergency ==1
                fprintf('emergency exit') %% emergency exit in case of
runaway error
                break
            end

            for j = 1:IL-1 %% z loop


                [rhov rhol Tsat] = saturationPRESStable(Y(5,1)); %% variable
property call out
```

```
            if dbl == 1 %% double layer wick calculations
                if z1(j)<deltam
                    wick = 1;
                    keff = keffm;
                else
                    wick = 2;
                    keff = 2987*(D*1e6)^-0.9 ; %% W/m/k, thermal conductivity
from Seminic Thesis, monoporous
                end
            end
            [phi kl1 kv1 ] = CDF_5_9(2*Y(1,j),wick); %% stable, calculates
liquid sat, porosities from pore size distribution
            if phi <0.3
                phi = 0.3; %% safety sdo phi doesn't go negative
            end
% %                 %             end
                phistore(j) = phi; %% collects and stores liquid saturaitons
                %                          [phi kl kv] = CDF_3_22(Y(1,j));
%                 [phi kl kv] = CDF_3_22(Y(1,j));

    A = (muv/kv/rhov/(1-phi)+mul/kl/rhol/phi); %% constant from equations
% end
%% Begin calculations for Euler Method
                F(1,j) = Y(1,j)^2*Y(4,j)*A/2/sigmaw/cosd(thetad);
                F(2,j) = Y(3,j);
                F(3,j) = hn*Y(2,j)/keff;%*(1-phi)*(epsilon1/(1-epsilon1));
                F(4,j) = hn*Y(2,j)/hfg*epsilon1*(1-phi);
                F(5,j) = -muv/kv*Y(4,j)/rhov/(1-phi);
                F(6,j) = mul/kl*Y(4,j)/rhol/phi;
                %
                %         Yt(:,j+1) = Yt(:,j)+dz.*F(:,j);
                Y(:,j+1) = Y(:,j)+dz.*F(:,j); %% Euler Method


                %% 2_28_2012 - trying to re work solution method, with
rederivation
                %% of equations


                if isnan(Y(1,j+1))==1 || isinf(Y(1,j+1))==1
                    emergency = 1;
                    emergencyR = 20;
                    fprintf(' R is nan')
                    break
                end


            end %% z loop


            Yn(1,i) = Y(1,1);
            Yn(2,i) = Y(2,1);
```

```
            Yn(3,i) = Y(5,1);
            YEr(1,i) = (Rmax-Y(1,IL)); %% far side
            YEr(2,i) = Y(2,IL);
            YEr(3,i) = (Po-Y(5,IL));
            YEr(4,i) = (Po-Y(6,IL));
            Ynom = [1/Rmax 1 1/Po 1/Po]';

            if i>=2
%% construction of Jacobian in order to use shooting method, referenced as
%% closure method.
                DER = [  -1     0     0     0
                          0     1     0     0
                          0     0    -1     0
                          0     0     0    -1];
%                 DER(1,1) = (YEr(1,i)-YEr(1,i-1))/(Y(1,1)-Yi(1));
%                 DER(2,2) = (YEr(2,i)-YEr(2,i-1))/(Y(2,1)-Yi(2));
%                 DER(3,3) = (YEr(3,i)-YEr(3,i-1))/(Y(5,1)-Yi(5));
%                 DER(4,4) = (YEr(4,i)-YEr(4,i-1))/(Y(6,1)-Yi(6));


                del = -relax.*(YEr(:,i))'/DER; %% NEwton Raphson, followed by
determination of new guesses for unkown boundary conditions
                Yi = Y(:,1);
                Y(1,1) = Y(1,1) +del(1);
                Y(2,1) = Y(2,1) +del(2);
                Y(5,1) = Y(5,1) +del(3);
                Y(6,1) = Y(6,1) +del(4);

            end

            %% evaporation evaluations and error calculations
            if i>2



                err(:,i) = max(abs(YEr(:,i)).*Ynom);
                %             err(i) = 1-(abs(Y(2,1))-
abs(Y(2,IL)))/abs(Y(2,1));
                errout = err(i)
                %% below commands are generally safety precautions to
                %% prevent unnecessary calculations when major error
                %% discovered

                if errout< 1
%                     relax = 0.001;
                end
                %             if i>10
                if isnan(errout)==1
                    fprintf('NaN problem') %% exits if NaN found, prevents
unnecessary calculations if errors discovered
                    emergency = 1;
                    break
                end
                if (err(i-1)-err(i))<0
```

```
                    %                       emergency =1;
                    %
                    %                       break
                end
                if isnan(Y(1,1))==1
                    %                       fprintf('R* == NaN')
                    emergencyR = emergencyR+1;
                    Y(1,1) = 100e-6;
                    %                       continue
                end
                %             end
                if errout <=1e-1
%                     if dbl == 1
%                         Yout1= Y;
%                         dbl = 0;
%                         qw = Y(3,IL)*keff;
%                         break
%                     elseif dbl == 0
%                         break
%                     end
                    break
                end
            end


            %         [phi kl kv] = CDF_3_22(Y(1,j),D,d);


        end %iteration loop
    end
    %% storage of major global variables for plotting and comparison
    %         hn = 2*10^(8*(1-1/(q*5)));
    out(q,1) = -qw/1e4; %% heat flux
    out(q,2) = Y(2,1); %% delta T
    out(q,3) = Y(5,1)-Y(6,1); %% PC
    out(q,4) = min(Y(1,:));
    out(q,5) = phi;


%     q = q+1;
%     averagetime=toc
    %         fprintf('convergence stored')




end
% plot(1:IL,Y(4,:))


% Y(2,IL-1)-Y(2,IL)
%% plotting of variables
figure (1)
```

```
plot(z1,Y(2,:))
title('theta')
xlabel('z position, m')
ylabel('dtemperature, K')
%
% % % %
% figure(2)
% plot(z1,-Y(3,:)/1e4*keff)
% title('dtheta/dz')
% xlabel('z position, m')
% ylabel('heat flux, W/cm^2')
% %
figure(3)
plot(z1,Y(1,:))
title('R*')
xlabel('z position, m')
ylabel('cutoff pore size, m')
% % % % % %
% figure(4)
% plot(z1,Y(4,:))
% title('G, vapor mass flux')
% xlabel('z position, m')
% ylabel('vapor mass flux, kg/m^2/s')
%
% figure(5)
% plot(z1,Y(5,:))
% title('Vapor Pressure')
% xlabel('z position, m')
% ylabel('Pressure, Pa')
% %
% figure(10)
% plot(z1,Y(6,:))
% title('liquid Pressure')
% xlabel('z position, m')
% ylabel('Pressure, Pa')
%
% figure(6)
% plot(z1,Vv)
% title('Vapor Velocity')
% xlabel('z position, m')
% ylabel('Velocity, m/s')
%
% figure(7)
% plot(z1,Rev)
% title('Reynolds number')
% xlabel('z position, m')
% ylabel('Reynolds number, #')
%
% figure(8)
% plot(z1,hv)
% title('Heat Transfer Coefficient')
% xlabel('z position, m')
% ylabel('Heat Transfer Coefficient, W/m^2')

% figure(9)
% plot(z1,phicheck)
```

```
% title('area ratio')
% xlabel('z position, m')
% ylabel('area ratio, #')

figure(200)
plot(out(:,1),out(:,2),'b-')
hold on
plot(validate(:,1),validate(:,2),'ro')
title('Numerical/Experimental comparison, 69-275-907.5 wick')
xlabel('heat flux, W/cm^2')
ylabel('Delta T, deg. K')
legend('Computation','Seminic(2007)','Location','Northwest')
% plot(validate2(:,1),validate2(:,2),'go')

figure(300)
plot(z1(1:99),phistore)
title('Liquid saturation, 60-120/69-275-907.5')
xlabel('z location in wick')
ylabel('liquid saturation (fraction from 0 to 1)')
legend('phi','Location','southeast')

% figure(600)
% plot(validate(1:15,2),validate(1:15,2),'r-')
% hold on
% plot(validate(7:15,2),out(7:15,2),'bo')
% title('Error Comparison, 69-275-907.5 wick')
% xlabel('experimental delta T')
% ylabel('computational delta T')
% legend('experimental data','computational results','Location', 'Northwest')
% for i = 7:15
% errorp(i) = abs(out(i,2)-validate(i,2))/validate(i,2);
% end
% axis square

% figure(400)
% plot(out(:,1),out(:,3)-Pcmax,'ro')
% % hold on
% % plot(-1*out(:,1),Pcmax,'b-')
% title('Capillary pressure')
% xlabel('heat flux, W/cm^2')
% ylabel('Required Capillary pressure, Pa')
%
%
% figure(300)
% plot(validate(:,2),out(1:length(validate),2),'bo')
% hold on
% plot(validate(:,2),validate(:,2),'r')
% title('Comparison of Model to Experimental Data')
% xlabel('Delta T, Model')
% ylabel('Delta T, Model')
% legend('Model data','experimental data')
% figure(100)
% plot(1:i,err(1:i))
% title('Convergence History')
% xlabel('iteration number')
```

```
% ylabel('err')
% manual = [11.75199 22.6205 32.9693 42.9444 52.6271 62.0696; 100 200 300%
400 500 600]; %% 462_69, he = 2e4
% manual = [9.0645 17.277 25.0326 32.4692 39.6618; 100 200 300 400 500]; %%%
275_69, he = 2e4
% manual = [10.1635 19.6382 28.6927 37.4399; 100 200 300 400]; %%
382_82_1082, , he = 2e4
%
% compare(l+1,1) = Y(2,IL);
% compare(l+1,2) = qw/10000;
% Yn = Y(2,1);
% end

% figure(10)
% plot(validate(:,1),validate(:,2))
% hold on
% plot(compare(:,2),compare(:,1),'ro')
% title('Tadej vs. Model')
% xlabel('qw W/cm^2')
% ylabel('DT, deg. K')
averagetime=toc %% timer to determine total time to run program
```

```
%% The comments in this file are generally setup for the purpose of
%% debugging the function as an independant script file.  As such, the
%% function comand can be commented, and then uncomment the variables
%% needed for comparison/plotting to investigate the CDF and PMF plots
%% individually without having to go through the primary solver

% clear all
% close all
% wick =2;
%
function [phi kl kv ] = CDF_5_9(Dg,wick)
% D = 272e-6;
% d = 61e-6;
% % phistore = zeros(25);
% klt = (0.04*(d/1e-6)-0.83)*10^-12; %% Tadej
% kvt = (1.2*(D/1e-6)-190.1)*10^-12; %% Tadej
%% This function has a stepwise, delta function for the pore size
%% distribution and therefore returns both liquid and vapor permeability
%% and phi, which corresponds to the open space percentage occupied with
%% liquid

%% the declaration of "wick" in the solver program determines which pore
%% size CDF is pulled up

%% "dist" text files contain 3 columns; pore size, CDF, PMF
if wick == 1
    A=textread('69_dist.txt');
elseif wick ==2
    A=textread('69_275_9075_dist.txt');
elseif wick ==3
    A=textread('82_275_9075_dist.txt');
elseif wick ==4
    A=textread('82_328_1018_dist.txt');
elseif wick ==5
    A=textread('69_196_6468_dist.txt');
elseif wick ==6
    A=textread('69_460_800_dist.txt');
elseif wick ==7
    A=textread('82_460_1500_dist.txt');
elseif wick ==8
    A = textread('58_dist.txt');
elseif wick == 9
    A = textread('275_dist.txt');
elseif wick == 10
    A = textread('58_460_800_dist.txt');
elseif wick == 11
    A = textread('58_330_800_dist.txt');
elseif wick ==12
    A=textread('69_275_9075_IAS_dist.txt');
end
% % % A = [r/1e-6 phi f(r)]
r = (A(:,1))*0.5e-6;
```

```
IL = length(r);
% C =200; %% STABLE
% sigmaw = 72.3e-3; %% N/m
C = 1;
% if Rg > max(r)
%     phi = 0.9999;
%     q = length(A);
%     kint = C*r(:,1).^2.*A(:,3);
%     kl = trapz(r(1:q),kint(1:q))/phi;
%     kv = 0;
%     flag = 1;  %% if Rg>rmax, then this indicates that evaporation is not
taking place
% else
% % Rg = 3.6e-3;
% for l = 1:25
%     Dg = (25*1e-6)*l; %% Diameter Guess

% Dg = 160e-6;

%% Permeability Calculation
diff = abs(A(:,1).*1e-6-Dg);
position = min(diff);
q = 1;
for i = 1:length(A)
    if diff(i) == position %% this determines where R* is in the pore size
distrubtion
        q = i;
        break
    else
        q = q+1;
    end
end

phi = A(q,2);

%% position is used as the differentiation point for calculation of liquid
%% and vapor permeabilities, liquid saturation

kint = C*(A(:,1).*5e-7).^2.*A(:,3);
klmult = 460;
kvmult = 440;
if q ==1
    q = 2;
    kl = (trapz(r(1:q),kint(1:q)))*klmult/phi; %% good for 69_275
    kv = (trapz(r(q:IL),kint(q:IL)))*kvmult/phi; %% good for 69_275
elseif q == length(A)
    q = length(A)-1;
    kl = (trapz(r(1:q),kint(1:q)))*klmult/phi; %% good for 69_275
    kv = (trapz(r(q:IL),kint(q:IL)))*kvmult/phi; %% good for 69_275
else
    kl = (trapz(r(1:q),kint(1:q)))*klmult/phi; %% good for 69_275
    kv = (trapz(r(q:IL),kint(q:IL)))*kvmult/phi; %% good for 69_275
end
%% Debugging
% klstore(l) = kl;
```

```
% kvstore(l) = kv;
% phistore(l) = phi;
% Dgstore(l) = Dg;
end

%% All below comments are plotting used for debugging of CDF's


% % % kint = C*r(:,1).^2.*A(:,3);
% % figure(1)
% % plot(A(:,1),A(:,2))
% % title('CDF')
% % xlabel('pore size, micrometers')
% % ylabel('phi(R*), CDF(R*)')
% % legend('69-275-907.5','Location','NorthWest')
% %
% % figure(2)
% % plot(A(:,1),A(:,3))
% % title('PDF')
% % xlabel('pore size, micrometers')
% % ylabel('f(r)(R*), PDF(R*)')
% % legend('69-275-907.5')
% kltstore = zeros(1,length(Dgstore));
% kltstore(1,:) = klt;
%
% kvtstore = zeros(1,length(Dgstore));
% kvtstore(1,:) = kvt;
%
%
% figure(3)
% plot(Dgstore,klstore)
% hold on
% plot(Dgstore,kltstore(1,:),'r')
% title('kl')
% xlabel('pore radius (meters)')
% ylabel('permeability (m^2)')
% legend('Model','Seminic (2007)','location','southeast')
%
% figure(4)
% plot(Dgstore./2,kvstore)
% hold on
% plot(Dgstore./2,kvtstore(1,:),'r')
% title('kv')
% xlabel('pore pore radius (meters)')
% ylabel('permeability (m^2)')
% legend('Model','Seminic (2007)','location','northeast')
%
% figure(5)
% plot(Dgstore./2,phistore(1,:))
% hold on
% plot(A(:,1).*5e-7,A(:,2),'r')
% title('phi')
% legend('Model','excel')
% xlabel('pore pore radius (meters)')
% ylabel('vol. %')
```

REFERENCES

[1] Amouzegar, L., Reilly, S., Catton, I. 2010. "Investigating the Performance of Bi-Porous Disk-Shaped Wick with the Restricted Vapor Space Via Developing an Electric Analogue Method". Proceedings of the ASME/JSME 2011 Joint Heat Transfer Conference, Honolulu, HI.

[2] Annapragada, S., Murthy, J., Garimella, S., 2008. "Permeability and Thermal transport in Compressed Open-Celled Foams". Numerical Heat Transfer, Vol. 54, issue 1, 2008.

[3] Baliga, B., Patankar, S., 1983. "A Control Volume Finite-Element Method for Two-Dimensional Fluid Flow and Heat Transfer". Numerical Heat Transfer, vol. 6, pp. 245-261.

[4] Bau, H., Torrance, K., 1982. "Thermal Convection and Boiling in a Porous Medium". Letters in Heat and Mass Transfer, Vol. 9, pp. 431-441.

[5] Brinkman, H., "A calculation of the viscous force exerted by a flowing fluid on a dense swarm of particles". Appl. Sci. Res., Vol. A1, 1947

[6] Burdine, N., 1953. "Relative Permeability Calculations from Pore Size Distributions Data". AIME Journal of Petroleum Technology, Vol. 198, pp. 71-77.

[7] V. P. Carey, 1992, "Liquid-vapor phase-change phenomena", Hemisphere, New York, NY, USA

[8] Chang, J., You, S., 1997. "Boiling heat transfer phenomena from micro-porous and porous surfaces in saturated FC-72". International Journal of Heat and Mass Transfer. Vol. 40, No. 18, pp. 4437-4447.

[9] Chernysheva, M. a., and Y. F. Maydanik. 2009. “Heat and Mass Transfer in Evaporator of Loop Heat Pipe.” Journal of Thermophysics and Heat Transfer, Vol. 23 (4)

[10] Coso, D., et al, 2012. “Enhanced Heat Transfer in Biporous Wicks in the Thin Liquid Film Evaporation and Boiling Regimes”. ASME Journal of Heat Transfer, Vol. 134, no. 101501-1.

[11] Das, S., 2003. “Pool boiling characteristics of nano-fluids”. International Journal of Heat and Mass Transfer 46, no. 5 (February): 851-862.

[12] Dhir, V., 1972. “Viscous Hydrodynami Instability Theory of the Peak and Minimum Pool Boiling Heat Fluxes”. PhD dissertation, University of Kentucky.

[13] Dullien, F., “Porous Media: Fluid Transport and Pore Structure”. Academic Press, San Diego CA, 1992.

[14] Ghiaasiaan, S., 1983, “On Multi-Dimensional Thermal-Hydraulic and Two-Phase Phenomena During Reflooding of Nuclear Reactor Cores”. PhD dissertation, Department of Mechanical Engineering, UCLA.

[15] Hanlon, M., and Ma, H.. 2003. “Evaporation Heat Transfer in Sintered Porous Media.” Journal of Heat Transfer, Vol. 125 (4)

[16] Katto, Y., Masuoka, T., 1966. “Criterion for the Onset of Convective Flow in a Fluid in a Porous Medium”. International Journal of Heat and Mass Transfer, Vol. 10 pp. 297-309.

[17] Kaya, T, and J Goldak. 2006. “Numerical analysis of heat and mass transfer in the capillary structure of a loop heat pipe.” International Journal of Heat and Mass Transfer, Vol. 49 (17-18), pp. 3211-3220.

[18] Kendig, M., Buchheit, R., 2003. "Corrosion Inhibition of Aluminum and Aluminum Alloys by Soluable Chromates,Chromate Coatings, and Chromate-Free Coatings". Corrosion, Vol. 59, No. 5.

[19] Kovalev, S., Solov'ev, S. 1984. "Model of Heat Transfer in the Boiling of Liquid at a Porous Surface". Translated from Teplozika Vysokikn Temperatur, Vol. 22, No. 6, pp. 1166-1171, November-December.

[20] Kovalev S.A. 1987. "Liquid boiling on porous surfaces". HEAT TRANSFER – Soviet Research, Vol. 19, No. 3 May-June 1987

[21] Liter S. and Kaviany M. 2001. "Pool boiling CHF enhancement by modulated porous layer coating: theory and experiment". International Journal of Heat and Mass Transfer, Vol. 44 (2001), pp. 4287-4311

[22] Lin, F., et al, 2011. "Evaporative heat transfer model of a loop heat pipe with a bidisperse wick structure". Interanational Journal of Heat and Mass Transfer, vol. 54, pp. 4621-4629.

[23] Liu, H., Patil, P., Narusawa, U, 2007. "On Darcy-Brinkman Equation: Viscous Flow Between Two Parallel Plates Packed with Regular Square Arrays of Cylinders". Entropy, vol. 9, pp. 118-131.

[24] Miscevic, M, O Rahli, L Tadrist, and F Topin. 2006. "Experiments on flows, boiling and heat transfer in porous media: Emphasis on bottom injection." Nuclear Engineering and Design, Vol. 236, (19-21), pp. 2084-2103.

[25] Ojha, M., et al, 2010. "Role of solid surface structure on evaporative phase change from a completely wetting corner meniscus". Phys. Fluids 22 052101.

[26] Polezhaev, Y., Kovalev, S., 1990. "Modeling heat transfer with boiling on porous structures". Thermal Engineering, Vol 37, No. 12, pp. 617-620.

[27] Ranjan, R., Murthy, J., Garimella, S., 2011. "A microscale model for thin-film evaporation in capillary wick structures". International Journal of Heat and Mass Transfer, vol. 54, pp. 169-179.

[28] Ranjan, R., et al, 2011. "A numerical model for transport in flat heat pipes considering wick microstructure effects". International Journal of Heat and Mass Transfer, vol. 54, pp. 153-168.

[29] Rao, S., Balakrishnan, A., 1997. "Analysis of pool boiling heat transfer over porous surfaces". Journal of Heat and Mass Transfer, vol. 32, pp. 463-469.

[30] Rao, P.R., Wessling, F.C. 2010. "Thermal characterization tests of the Qu Tube heat pipe". Masters Thesis, University of Alabama, Huntsville.

[31] Reilly, S., Catton, I. 2011. " Utilization of Advanced Working Fluids in Heat Pipes", Proc. of the ASME/JSME Joint heat Transfer Conference, AJTEC2011-44360.

[32] Reilly, S., and I. Catton, 2009. "Improving Biporous Heat Transfer by Addition of Monoporous Interface Layer". ASME Summer Heat Transfer Conference 2009, San Francisco, CA.

[33] Rocco, A.M. et al, 2004. "Evaluation of chromate passivation and chromate conversion coating on 55% Al-Zn coated Steel", Surface and Coatings Technology , vol. 179, , pp. 135-144.

[34] Rosenfeld, J., North, M., 1995. "Porous media heat exchangers for cooling of high-power optical components". Optical Engineering, Vol. 34, No. 2, pp. 335-341.

[35] Semenic T., et al., 2007. "High Heat Flux Removal Using Biporous heat Pipe Evaporators". PhD dissertation, UCLA Mechanical Engineering.

[36] Semenic, T., Lin, Y. and Catton, I., 2008. "Thermophysical Properties of Biporous Heat Pipe Evaporators". Journal of Heat Transfer, Vol. 130, no. 2.

[37] Smirnov, H., 2010, *Transport Phenomena in Capillary-Porous Structures and Heat Pipes*, Taylor and Francis Group, FL, USA.

[38] Smirnov, H., 2001. "Boiling on Coated Surfaces and in Porous Structures". Journal of Porous Media, Vol. 4, No. 1, pp. 33-52

[39] Suppowit, J., 2012, Graduate Student Researcher at UCLA. Personal Communication

[40] Uhle, J. 1991. "Boiling Heat Transfer Characteristics of Steam Generator U-tube Fouling Deposits." PhD dissertation, Department of Nuclear Engineering, MIT.

[41] Vadnjal, A., 2007, "High Heat flux Evaporator". PhD dissertation, Department of Mechanical Engineering, UCLA.

[42] Vadakkan, U., Garimella, S., Murthy, J., 2004. "Transport in Flat heat Pipes at High Heat Fluxes From Multiple Discrete Sources". ASME Journal of Heat Transfer, Vol. 126, pp.347-354.

[43] Vasiliev, L., 2008. "Micro and miniature heat pipes – Electronic component coolers". Journal of Applied Thermal Engineering, Vol. 28, pp. 266-273.

[44] Vityaz, P., et al, 1984. "Heat pipe with bidispersed capillary structures". Proceedings of the 5th International Heat Pipe Conference, Tsukuba Japan, Vol. 1, pp. 127-135.

[45] Wang J. and Catton I., 2001. "Biporous heat pipes for high power electronic device cooling" Seventeenth IEEE SEMI-THERM Symposium 2001, San Jose CA

[46] Wang, J., Catton, I., 2001. "Evaporation heat transfer in thin biporous media". ASME Journal of Heat and Mass Transfer 37 (2001) 275-281

[47] Wang, J., Catton, I., 2001. "Biporous Heat Pipes for High Power Electronic Device Cooling". Proceedings of Seventeenth IEEE SEMI-THERM Symposium, pp. 211-218.

[48] Wang, H., Garimella, S., Murthy, J., 2007. "Characteristics of an evaporating thin film in a microchannel". International Journal of Heat and Mass Transfer, No. 50, pp. 3933-3942.

[49] Wasekar, V. M., and R. M. Manglik. 2000. "Pool Boiling Heat Transfer in Aqueous Solutions of an Anionic Surfactant". Journal of Heat Transfer 122, no. 4: 708.

[50] Wen, D., and Ding, Y., 2005. "Experimental investigation into the pool boiling heat transfer of aqueous based γ-alumina nanofluids". Journal of Nanoparticle Research 7, no. 2-3, 265-274.

[51] Weibel, J., Garimella, S., 2012. "Visualization of vapor formation regimes during capillary-fed boiling in sintered-powder heat pipe wicks". International Journal of Heat and Mass Transfer, Vol. 55, pp.3498-3510.

[52] Weibel, J., Garimella, S., North, M. 2010. "Characterization of evaporation and boiling forom sintered powder wicks fed by capillary action". International Journal of Heat and Mass Transfer, Vol. 53, pp. 4204-4215.

[53] Wojcik, T., 2008. "Improved Model of Boiling Heat Transfer Hysteresis of Metal, Fibrous, Capillary, Porous Structures". 5th European Thermal-Sciences Conference, The Netherlands.

[54] Yagov, V., Buyanov, A., Nemtsev, V., 2005. "Modeling of Two-Phase Flow Patterns in a Bed of Spherical Fuel Microelements". VI Minsk International Seminar "Heat Pipes, Heat Pumps, Refrigerators".

[55] Yeh, C., Chen, C., Chen, Y., 2009. "Heat transfer analysis of a loop heat pipe with biporous wicks". International Journal of Heat and Mass Transfer, vol. 54, pp. 4426-4434.

[56] Zuber, N., 1959. “Hydrodynamic Aspectcs of Boiling Heat Transfer”. PhD Thesis dissertation, University of California at Los Angeles.